Ecology and Development Series
No. 8, 2003

Mohammad Mohsin Hafeez

Water Accounting and Productivity at Different Spatial Scales in a Rice Irrigation System:

A Remote Sensing Approach

Zentrum für Entwicklungsforschung
Center for Development Research
University of Bonn
ZEF Bonn

Ecology and Development Series No. 8, 2003

Mohammad Mohsin Hafeez

Water Accounting and Productivity at Different Spatial Scales in a Rice Irrigation System: A Remote Sensing Approach

Cuvillier Verlag Göttingen

Bibliografische Information Der Deutschen Bibliothek
Die Deutsche Bibliothek verzeichnet diese Publikation in der Deutschen Nationalbibliografie; detaillierte bibliografische Daten sind im Internet über http://dnb.ddb.de abrufbar.
1. Aufl. - Göttingen : Cuvillier, 2003
Zugl.: Bonn, Univ., Diss., 2003
ISBN 3-89873-769-1

D 98

Vorsitzender : Prof. Dr. Armin Skowronek

1. Referent : Prof. Dr.–Ing. Helmut Eggers

2. Referent : Prof. Dr. Paul L.G. Vlek

Tag der Promotion: 06.12.2002

Angefertigt mit Genehmigung der Hohen Landwirtschaftlichen Fakultät der Rheinischen Friedrich-Wilhelms-Universität Bonn

Gedruckt mit Unterstützung des Deutschen Akademischen Austauschdienstes

Nonnenstieg 8, 37075 Göttingen
Telefon: 0551-54724-0
Telefax: 0551-54724-21
www.cuvillier.de

1. Auflage, 2003
Gedruckt auf säurefreiem Papier

ISBN 3-89873-769-1

ABSTRACT

Asia's food security relies largely on 75 million ha of irrigated rice, which accounts for 75% of the annual world rice supply and a high proportion of the freshwater used in irrigated agriculture. To improve water-use efficiency in irrigated rice, a number of water saving technologies at field level have been developed. However, the possibility of re-use of water at a higher scale level leads to the important issue of finding "real" water saving possibilities at the irrigation system level.

This study aimed to measure water productivity in the rice-based irrigation system of District 1 of the Upper Pampanga River Integrated Irrigation System (UPRIIS), Philippines, through water accounting. In particular, it quantified current water use, re-use, and water productivity, and estimated seasonal actual evapotranspiration (ET_a) through the Surface Energy Balance Algorithm (SEBAL) using different satellite sensors, i.e., Landsat 7, ASTER and MODIS, for the dry season 2001. District 1 was divided into 10 different spatial scales, ranging from 1,513 ha to 18,003 ha, to examine the scaling-up effect on water productivity. All water accounting components, i.e., surface inflow and outflow, rainfall, water pumped for re-use, storage change, actual evapotranspiration (ET_a) (rice and non-rice), percolation, and rice yields were measured at each spatial scale.

The ET_a values estimated from SEBAL were compared with the measured pan evaporation (E_{pan}), and with crop evapotranspiration (ET_c) calculated with the modified Penman-Monteith method from two meteorological stations. The estimated ET_a values using 6 MODIS images acquired on different dates differed strongly from the E_{pan} values. Compared with the ET_c values, however, ET_a values were within the range. With the ASTER image, the estimated ET_a values were close to the E_{pan} values, but were 2.5% lower than the ET_c values. Finally, using 3 Landsat 7 images, ET_a values were, on average, 6% lower than the ET_c values. It was noted that there are differences in ET_a values between the sub-regions of District 1 when the area is not uniformly planted with a rice crop (i.e., at the beginning and end of the growing season). Seasonal ET_a values were estimated on the basis of temporal integration of 6 MODIS and 3 Landsat images. By comparing these with the E_{pan}, and ET_c values, the seasonal ET_a estimates were shown to be accurate and usable for water accounting in District 1.

The combination of ASTER, Landsat and MODIS images was examined and results showed a non-significant variation for ET_a estimation in the case of the ASTER and Landsat images. However, there is significant variation for ET_a estimation in case of MODIS images. The crop-water deficit was assessed using MODIS and Landsat images on the same overpass day. The volume of water consumption and deficit were compared for different pixel sizes, which showed that 59.4% (11,800 ha) of the 20,000 ha command area were in good condition (water deficit of -0.75 to +0.75mm/day) on 18 May 2001.

Three types of water accounting indicators were applied to provide relevant information on water productivity at different spatial scales. The first indicator, the Process Fraction of gross inflow (PF_{gross} = ET of rice crop / (rain + irrigation + groundwater pumping)) ranged from 0.07 at (1,513 ha) scale to 0.21 at the (District scale). PF_{gross} showed an upward trend over increasing scales. The second indicator, the Depleted Fraction of gross inflow (DF_{gross} = rice and non-rice ET_a / gross inflow) ranged from 0.09 (1,513 ha scale) to 0.26 (18,003 ha scale), also show an upward trend with

scale. At the District scale, DF_{gross} was 0.26, indicating that 74% of the gross inflow (irrigation, rainfall, and groundwater pumping) was flowing out of District 1, and that there is a wide scope for increasing water productivity. The third indicator is Water Productivity "WP", which is further divided as into WP of gross inflow (WP_{gross} = rice yield / gross inflow), WP of irrigation water ($WP_{irrigation}$ = rice yield / irrigation) and WP of rice evapotranspiration (WP_{ETric} = rice yield / rice evapotranspiration). WP_{gross} showed a similar upward trend, with values ranging from 0.05 kg/m^3 (1,513 ha scale) to 0.18 kg/m^3 (18,003 ha scale). This increase can be explained by the large volume of re-used water from 15 small check dams, hundreds small farm ponds and 1451 pumps installed in District 1. $WP_{irrigation}$ values also showed an upward trend with scale, and $WP_{irrigation}$ at District 1 scale being almost three to four times higher than at the three smallest scales of the study area. WP_{ETrice} (crop-water use efficiency) values for the three smallest scales (1,513 ha to 3,011 ha) of the study area were around 0.75 kg/m^3 and around 0.90 kg/m^3 for the other scales of District 1. One reason for the low WP_{ETrice} values for the smallest downstream areas was a lower rice yield as compared to upstream areas.

The study showed that many farmers are depending on the re-used water in the system. This is indicated by the estimated total amount of water re-used through pumping (equivalent to 30 % of the water lost through seasonal ET_a of rice). Water can be saved by reducing the high water losses from non-process depletion (32 %) in the downstream areas (3,011 ha). There is also a high volume of utilizable uncommitted water (12 % of gross inflow) leaving the upstream scale (11,239 ha), which can be saved by better management of the De-Leon check dam. Overall, the findings of the study showed that water productivity increases as the scale goes up due to increased water re-use opportunities and that scale effects are important for understanding and planning for water saving and water productivity and for planning appropriate measures.

Wasserbilanzierung und -produktivität auf verschiedenen räumlichen Ebenen im bewässerten Reisanbau: ein Fernerkundungsansatz

KURZFASSUNG

Die Nahrungsmittelversorgung Asiens wird zum Großteil durch 75 Mill. Hektar (ha) Bewässerungsreisanbau gesichert, der 75% des jährlichen globalen Reisbedarfs deckt und einen hohen Anteil am landwirtschaftlichen Süßwasserverbrauch ausmacht. Um den Wirkungsgrad der Wassernutzung zu verbessern, wurden mehrere Technologien zur Wassereinsparung auf Feldebene entwickelt. Die Möglichkeiten der Wasserwiederverwertung auf höherer Ebene führt dabei zu der wichtigen Fragestellung hinsichtlich der Ermittlung „realer" Wassereinsparungen auf der Ebene von Bewässerungssystemen.

Ziel der vorliegenden Studie war es, die Wasserproduktivität im Distrikt 1 des „Upper Pampamga River Integrated Irrigation System" (UPRIIS), Philippinen, über detaillierte Wasserbilanzierungen zu bestimmen. Insbesondere wurde der derzeitige Wasserverbrauch, die Wasserwiederverwertung und die Wasserproduktivität quantifiziert. Die saisonale aktuelle Evapotranspiration (ET_a) während der Trockenzeit 2001 wurde mit Hilfe des „Surface Energy Balance Algorithmus" (SEBAL) mit Daten verschiedener Satellitensensoren wie Landsat 7 ETM+, TERRA/ASTER und TERRA/MODIS abgeschätzt. Um die Wasserproduktivität auf unterschiedlichen Maßstabsebenen zu untersuchen, wurde der Distrikt 1 in zehn verschiedene räumliche Skalen (von 1,513 ha bis 18.003 ha) aufgeteilt. Alle relevanten Wasserbilanzierungskomponenten, d.h. Wasserzufluss und -abfluss, Niederschlag, zur Wiederverwertung gepumptes Wasser, Veränderungen im Grundwasserspeicher, aktuelle Evapotranspiration (ET_a) (auf Flächen mit und ohne Reisanbau) sowie Perkolation und Reiserträge wurden für jede Maßstabsebene ermittelt.

Die mittels SEBAL ermittelten ET_a-Werte wurden sowohl gemessenen als auch berechneten Verdunstungswerten gegenübergestellt. Zur direkten Messung wurden normierte Tanks verwendet (E_{pan}) (Class-A Pan), die Berechnung der Verdunstung erfolgte auf der Datenbasis von zwei meteorologischen Stationen und Anwendung der modifizierten Penman-Monteith Methode, die als Resultat standardisierte Evapotranspirationsraten agrarischer Kulturpflanzen (ET_c) liefert. Im Vergleich zeigten die auf Basis der MODIS Bilder (6 Szenen verschiedener Tage) geschätzten ET_a-Werte erhebliche Unterschiede zu den gemessenen E_{pan}-Werten. Verglichen mit den ET_c-Werten lagen die ET_a-Werte jedoch innerhalb dieser Bandbreite. Die auf Grundlage des ASTER Bilds ermittelten ET_a-Werte stimmten nahezu mit den E_{pan}-Werten überein. Sie waren jedoch um 2.5% niedriger als die ET_c-Werte. Schließlich waren die auf Basis von drei Landsat 7 ETM+ Bildern ermittelten ET_a-Werte im Durchschnitt 6% niedriger als die ET_c-Werte. Auffallend waren vor allem die Differenzen in den ET_a-Werten innerhalb der Subregionen in Distrikt 1, wenn das Gebiet nicht einheitlich mit Reis bedeckt war (d.h. am Anfang und Ende der Anbausaison). Die saisonale Evapotranspiration (ET_s) wurde durch die zeitliche Integration von sechs MODIS und drei Landsat Bildern bestimmt. Durch den Vergleich mit den E_{pan}- und ET_c-Werten wurde der Nachweis der Genauigkeit der ET_a-Werte erbracht. Diese können daher für die Wasserbilanzierung in Distrikt 1 eingesetzt werden.

Die Kombination von ASTER, Landsat und MODIS Bildern wurde untersucht. Die Ergebnisse zeigen eine nicht signifikante Variation für die ET_a-Berechnung mittels ASTER und Landsat Bildern. Jedoch wurde eine signifikante Variation bei der ET_a-Abschätzung mit MODIS Bildern beobachtet. Das Defizit des pflanzenverfügbaren Wassers wurde anhand von MODIS und Landsat Bildern des gleichen Überflugtages ermittelt, wobei die Menge des verbrauchten Wassers und das Wasserdefizit für verschiedene Pixelgrößen bestimmt wurden. Die Ergebnisse zeigen, dass sich am 18. Mai 2001 59.4% (11.800 ha) von insgesamt 20.000 ha landwirtschaftlicher Fläche in sehr gutem Bewässerungszustand befanden (Wasserdefizit zwischen -0.75 und +0.75mm/Tag).

Drei verschiedene Wasserbilanzierungsindikatoren wurden eingesetzt, um relevante Information über die Wasserproduktivität auf verschiedenen Maßstabsebenen zu erhalten. Die Werte des ersten Indikators, Prozessanteile des Bruttozuflusses (PA_{brutto} = ET des Reisanbaues / (Niederschlag + Bewässerung + gepumptes Grundwasser), lagen zwischen 0.07 (1,513 ha Maßstab) und 0.21 (Distrikt-Maßstab) und zeigen einen Aufwärtstrend bei zunehmendem Maßstab. Die Werte des zweiten Indikators, Verlustanteile des Bruttozuflusses (VA_{brutto} = mit und ohne Reis / ET_a / Bruttozufluss), betrugen zwischen 0.09 (1,513 ha Maßstab) und 0.26 (18,003 Maßstab) und zeigen ebenfalls eine Zunahme mit steigendem Maßstab. Auf Distrikt-Ebene betrug der VA_{brutto} 0,26. Dies deutet darauf hin, dass 74% des Zuflusses (Bewässerung, Niederschlag und gepumptes Grundwasser) aus Distrikt 1 abfliesst und, dass ein großes Potential hinsichtlich der Erhöhung der Wasserproduktivität vorhanden ist. Der dritte Indikator, die Wasserproduktivität (WP), wurde weiter unterteilt in WP des Bruttozuflusses (WP_{brutto} = Reisertrag / Bruttozufluss), WP des Bewässerungswassers ($WP_{Bewässerung}$ = Reisertrag / Bewässerung) und WP der Reisevapotranspiration ($WP_{ET\text{-}Reis}$ = Reisertrag / Reisevapotranspiration). Die WP_{brutto}-Werte zwischen 0.05 kg/m^3 (1,513 ha Maßstab) und 0.18 kg/m^3 zeigten einen ähnlichen Aufwärtstrend. Diese Zunahme kann durch die große Menge wieder verwertbaren Wassers aufgrund der 15 kleinen Sperrdämme, Hunderten von kleinen bäuerlichen Stauflächen und 1451 Pumpanlagen in Distrikt 1 erklärt werden. Die $WP_{Bewässerung}$-Werte zeigen ebenfalls einen Aufwärtstrend mit zunehmendem Maßstab, d.h. die Werte der $WP_{Bewässerung}$ in Distrikt 1 waren fast drei- bis viermal so hoch wie die Werte der drei kleinsten Maßstabsebenen im Untersuchungsgebiet. Die $WP_{ET\text{-}Reis}$-Werte (Wassernutzungseffizienz des Reisanbaues) der drei kleinsten Maßstabsebenen (1,513 ha bis 3,011 ha) betrugen ca. 0,75 kg/m^3 und ca. 0,90 kg/m^3 auf höheren Maßstabsebenen in Distrikt 1. Im Vergleich zu den größeren, stromaufwärts liegenden Bereichen sind die niedrigen $WP_{ET\text{-}Reis}$-Werte in den kleinsten, stromabwärts liegenden Bereichen auf den geringeren Reisertrag zurückzuführen.

Die Studie zeigt, dass viele Reisbauern auf die Wiederverwertung des Wassers im Bewässerungssystem angewiesen sind. Dies wurde deutlich durch die ermittelte Gesamtwassermenge, die über Pumpen wieder in den Kreislauf zurück geführt wird (entspricht 30% des Wasserverlustes durch saisonale Evapotranspiration der Reisanbauflächen). In den stromabwärts gelegenen Bereichen (3,011 ha) können beträchtliche Wassermengen durch die Reduzierung der hohen, jedoch nicht beim Bewässerungsprozess auftretenden Wasserverluste (32 %) eingespart werden. In den stromaufwärts liegenden Gebieten (11,239 ha) existiert ebenfalls ein hohes Potential nutzbarer, nicht zweckgebundener Wasserressourcen, da 12% des Bruttozuflusses diesen Bereich ungenutzt verlassen, ein Betrag, der durch ein effizienteres Management

des De-Leon-Staudammes eingespart werden könnte. Insgesamt zeigen die Ergebnisse einerseits, dass die Wasserproduktivität bei ansteigenden räumlichen Maßstabsebenen aufgrund besserer Möglichkeiten zur Wasserwiederverwertung zunimmt sowie andererseits, dass dieser Effekt eine überaus wichtige Komponente darstellt, die bei entsprechenden Planungen ressourcenschonender- und -produktivitätssteigernder Maßnahmen berücksichtigt werden muss.

TABLE OF CONTENTS

LIST OF ABBREVIATIONS

ANOVA	Analysis of Variance
ASTER	Advanced Spaceborne Thermal Emission and Reflection Radiometer
AWMTs	Assistant Water Management Technicians
A-x	A-Extra
DA	Department of Agriculture
DEM	Digital elevation model
$DF_{available}$	Depleted fraction per unit of available water
DF_{gross}	Depleted fraction per unit of gross inflow
DF_{net}	Depleted fraction per unit of net inflow
District 1	Area of TRIS-L and SDA
E_{pan}	Evaporation from Class A-pan
ERSDAC	Earth Remote Sensing Data Analysis Center
ET	Evapotranspiration
ET_{24}	Daily actual evapotranspiration
ET_a	Actual evapotranspiration
ET_c	Crop evapotranspiration
ETM+	Enhanced Thematic Mapper Plus
ET_o	Reference evapotranspiration
$ET_{potential}$	Potential evapotranspiration
ET_{rice}	Evapotranspiration of rice crop
ET_s	Seasonal actual evapotranspiration
E-X	E-Extra
FAO	Food and Agriculture Organization
FCC	False color composite
FFIA	Federation of farmer-irrigators associations
FIA's	Farmer-irrigators associations
FIG	Farmer Irrigators Group
Ftppull	File transfer protocol
G_0	Soil heat flux (W/m^2)
GCP	Ground control points
GIS	Geographic information system
GPS	Global positioning system
H	Sensible heat flux (W/m^2)
HDF	Hierarchical data format
IRRI	International Rice Research Institute
IWMI	International Water Management Institute
K_c	Crop coefficient
K_m	Multiplier for ET for the representative period
L	Monin-Obukov Length
L1B	Level 1B
L1G	Level 1G
LP	Land preparation
LS	Land soaking
MODIS	Moderate Resolution Imaging Spectroradiometer

NDVI	Normalized difference vegetation index
NIA	National Irrigation Administration
OE	Operations Engineer
PAGASA	the Philippines Atmospheric Geophysical and Astronomical Services Administration
$PF_{available}$	Process fraction per unit of available water
$PF_{depleted}$	Process fraction per unit of depleted water
PF_{gross}	Process fraction per unit of gross inflow
PF_{net}	Process fraction per unit of net inflow
R^2	R-squared
R_{n24}	Averaged daily net radiation (W/m^2)
RMSE	Root mean square error
Rn	Net radiation (W/m^2)
RUG	Rotation Unit Group
SAE	San Augustin Extension
SD	Santo Domingo
SDA	Area of SDA-A, SDA-B & SDA-C
SDA	Santo Domingo Area
SDA-(A+B)	Area of SDA-A and SDA-B
SDA-(B+C)	Area of SDA-B & SDA-C
SDA-A	Santo Domingo Area-A
SDA-B	Santo Domingo Area-B
SDA-C	Santo Domingo Area-C
SDA-D	Santo Domingo Area-D
SEBAL	Surface Energy Balance Algorithm for Land
SP	Seepage and Percolation
Swir	Shortwave infrared
TES	Temperature Emissivity Separation
TIR	Thermal Infrared
TP	Transplanting
TRIS	Talavera River Irrigation System
TRIS-L	Talavera River Irrigation System-Lower
TRIS-L + SDA-A	Area of TRIS-L and SDA-A
TRIS-L+SDA-(A+B)	Area of TRIS-L, SDA-A and SDA-B
TRIS-U	Talavera River Irrigation System-Upper
UPRB	Upper Pampanga River Basin
UPRIIS	Upper Pampanga River Integrated Irrigation System
USDA	United States Department of Agriculture
Vnir	Visible near infrared
WCCC	Water Control Coordinating Council
WP_{Etrice}	Water productivity per unit of rice evapotranspiration(kg/m^3)
WP_{gross}	Water productivity per unit of gross inflow (kg/m^3)
$WP_{irrigation}$	Water productivity per unit of irrigation (kg/m^3)
WP_{net}	Water productivity per unit of net inflow (kg/m^3)
ZE	Zone Engineers
ZIS	Zhangua Irrigation System

LIST OF FREQUENTLY USED SYMBOLS

Symbol	Representation	Dimension
λE	Latent heat flux, or the energy necessary to vaporize water	W/m^2
$K^{\downarrow}$	Incoming short-wave solar radiation	W/m^2
$L^{\downarrow}$	Incoming broadband long-wave radiation	W/m^2
ε_0	Surface emissivity	-
σ	Stefan-Boltzman constant	$W/m^2/K^4$
T_0	Surface temperature	K
ρ_0	Surface albedo	-
r_0	Average daytime surface reflectance	-
ρ_{air}	Atmospheric air density	Kg/m^3
C_p	Air specific heat at constant pressure	J/Kg/K
dT_{air}	Near surface air temperature difference	K
R_{ah}	Aerodynamic resistance to heat transport	s/m
T_0_dem	DEM adjusted soil surface temperature	K
ψ_h	Psychometric buoyancy parameters for heat transport	
ψ_m	Psychometric buoyancy parameters for momentum transport	
Λ	Evaporative fraction	-

1. INTRODUCTION

1.1 Background

The world's thirst for water is likely to stay as one of the most pressing resource issues of the 21st century. Considering the population growth, increasing urbanization, industrial development and intensive agricultural production, global demand for water has continued to increase by roughly 2.4 % annually since 1970. Global water withdrawal is even expected to increase by 35 % by the year 2020, with growth in demand rising fastest in developing countries (Rosegrant et al. 1997). This high water demand, however, is characterized by the problem of water availability. In many Asian countries, for instance, per capita availability of water resources declined by 40-60 % between 1955 and 1990, and is expected to decline further by 15-54 % over the next 35 years (Gleick 1993). There are various reasons for this decline, which could be location-specific. These include decreasing resources (e.g., falling groundwater tables, silting of reservoirs), decreasing quality (e.g., chemical pollution, salinization), and increased competition among agricultural, urban and industrial uses.

Water for agriculture claims the largest share of water consumption worldwide, but particularly in the Asian region where it accounts for 86 % of total annual water withdrawal there (compared with 49 % in North and Central America, and 38 % in Europe). This is not surprising considering the significance of the sector in the economy. However, bearing in mind the present state of water consumption and availability, it is deemed necessary to look at possible ways to improve the efficiency of water use in the sector, particularly in rice production, which is very important for most developing countries but where water-use efficiency is unfortunately very low. To illustrate this, about two to three Olympic-sized swimming pools full of water are required to produce just one ton of rice (IRRI 2001).

Rice being its major staple food, Asia produces and consumes about 92 % of the world's rice (IRRI 1997). Of the total world rice supply, more than 75 % comes from 79 million hectares (ha) of irrigated land in Asia. It should be noted that 90 % of the total diverted fresh water in Asia is used for irrigated agriculture, of which more than 50 % goes to rice irrigation (Tabbal et al. 2002). To keep up with the population growth and income-induced demand for food in most low-income Asian countries

(Hossain 1997), it is estimated that rice production has to increase by 56 % over the next 30 years (IRRI 1997). In 2025, in South and Southeast Asia approximately 17 million ha irrigated rice areas will suffer "physical water scarcity" and 22 million ha "economic water scarcity" in the dry season (Tuong and Bouman 2002). Against this background, measures to increase water-use efficiency are deemed critical for achieving food security. In addition, Klemm (1999) noted that a reduction of 10 % in water used for irrigating rice would free up to 180,000 million m^3, which is equivalent to about 25 % of all fresh water used globally for non-agricultural purposes. Thus, improvement in water-use efficiency in the agriculture sector could also lessen the impacts of water scarcity-related problems on other sectors.

1.2 Problem statement

Irrigation efficiency is the most commonly used term to describe how well water is being used within a system (Molden and Sakthivadivel 1999). However, many scientists caution on possible misconceptions on irrigation efficiency within the basin context. Bagley (1965) noted that failure to recognize the boundary characteristics when describing irrigation efficiencies can lead to erroneous conclusions. He pointed out, for example, that water lost due to low efficiencies of one system, such as in a farmer's field, may not be lost to a larger system, such as an irrigation system. In the same way, water lost from an irrigation system may not necessarily be considered as an inefficiency loss if this water is re-used within the water basin.

This argument has been corroborated by a number of studies. Bos (1979) identified several flow paths of water entering and leaving an irrigation project, clearly identifying water that returns to the basin and is available for downstream use. Bos and Wolters (1989) reiterated that the portion of water diverted to an irrigation project that is not consumed, is not necessarily lost from a river basin, because much of it is being re-used downstream. Van Vuren (1993) listed several constraints on the use of irrigation efficiency and identified situations when lower efficiencies are tolerable. Palacios Velez (1994) also argued that water that is lost is not always necessarily wasted. Inasmuch as water losses from one field may be re-used in downstream fields, any gains from reducing losses in a particular field may negatively affect the water balance of those other fields (Seckler 1996, Keller et al. 1996). However, whether local water savings

affect the water productivity at higher scale levels depends on whether local water "losses" are being re-used elsewhere, and on the possibilities to effectively use water savings at one point in the system at another point in the system (Solomon and Davidoff 1999).

Whether or not the water saved at the field level will increase efficiency at the irrigation system level depends on where the water that was delivered to the field is drained. For example, water that eventually drains into oceans or deep saline aquifers is considered permanently lost from the irrigation system so that reduction in this type of drained water can lead to real water saving or increase in water-use efficiency. On the other hand, water that flows out of a field into creeks, groundwater, or downstream areas can possibly be re-used, i.e. by blocking creeks and diverting the water into new irrigation canals, by directly pumping from creeks and drains, or by pumping from the (shallow) groundwater. In this way, one farmer's water loss may be another farmer's water gain (Seckler 1996).

The possibility for re-use of irrigation water has led some people to advocate that water savings at the field scale are only false savings that do not really contribute to increased water-use efficiency. In view of this possibility, water-use efficiency at the system level is deemed higher than at the individual field level. It is noted, however, that recapture and re-use of water that is "lost" upstream mostly involve additional investments and operation costs, such as pumping or the building of dams downstream (Guerra et al. 1998). Moreover, the potentials for water re-use depend on a number of factors, such as topography (e.g. can a creek be converted to a dam), sub-surface hydrology (e.g., does percolated water re-charge a shallow groundwater reservoir that can subsequently be pumped), quality issues (e.g., water may be too polluted with agrochemicals or salts) and costs of pumping. Eventually, a complete cost-benefit analysis for water savings at different scales is asked for. Here, the focus is on the benefit side of the re-use of water downstream from where losses occur. Therefore, the crucial issue for this thesis is finding "real" water saving, that is, the reduction of water flows to sinks from which it cannot be recovered any more, i.e., the sea and atmosphere. In this regard, the components of water inflows and outflows, which describe water balance in the system, will have to be analyzed to determine current levels of efficiency and to develop strategies to improve efficiency.

Molden (1997), having pointed out several weaknesses in using efficiency terms and scale effects in shifting analysis from the field to irrigation systems and river basins, presented a common framework to describe water use within a basin, i.e., water accounting. Water accounting, which is based on a water balance approach, quantifies the amount of water entering a system (i.e., through surface flows, groundwater flows by pumping, and rainfall) and the amount of water leaving a system (i.e., through evapotranspiration, surface outflow and groundwater flows). Water accounting classifies the amount of depleted water within an irrigation system based on uses, intended use or not, beneficial or not. It also classifies outflow water as committed water for downstream uses and non-committed water. Water accounting performance indicators were developed as an alternative to the classical irrigation efficiencies used in irrigation engineering. Water accounting identifies the available water, its potential development, and its distribution among different users within an irrigation system.

A number of researches have been done to evaluate irrigation-water-use efficiency and productivity, but mostly at a farmer field level scale. Very few studies on the effects of water saving at the field level on overall water saving and water productivity of the rice-based irrigation system level have been undertaken, especially in the Southeast Asian region (Guerra et al. 1998). Thus, this study examines water-use efficiency and productivity through water accounting at different spatial scales.

Water accounting techniques have been tested and applied to identify opportunities for water saving and improving productivity in irrigation systems and river basins like Bhakra in India, Chistian in Pakistan, and Kirindi Oya and Huruluwewa in Sri Lanka. However, these studies mainly involve upland crops such as wheat, cotton and sugar cane. It is noted that there has been a study at the basin level in the Zhangua Irrigation System (ZIS) of China that also applied water accounting techniques to determine whether the on-farm water management practice of alternate wetting and drying in paddy rice translates into water saving. The results showed that secondary storage and re-use of water are of crucial importance in the overall ZIS system-water productivity (Dong Bin et al. 2001; Loeve et al. 2002). Nevertheless, more case studies are necessary to fully understand water use and productivity at different spatial scale levels in rice-irrigated systems. This study focuses on irrigated rice system of the Philippines, where irrigated rice accounts for about 61 % of the 3.4

million hectares utilized for rice production. The study area, the Upper Pampanga River Integrated Irrigation System (UPRIIS) was designed to cover 102,500 hectares of agricultural land. As a major rice producer of the country, the area would benefit much from improvement in water-use efficiency.

Finally, it should be noted that an important component of the water balance is evapotranspiration (ET), because this amount is lost to the system and cannot be recycled (unlike runoff, seepage and percolation losses). However, its physical measurement is not a simple task at large spatial scales. In this study, the spatial distribution of ET was measured using different remote-sensing techniques to obtain more accurate ET estimates.

1.3 Research objectives

The main objective of this study is to measure water productivity at ten different spatial scales in District 1 of UPRIIS through the water accounting procedure. Specifically, the study aims to:

1 estimate seasonal actual evapotranspiration using different public sensors like Landsat 7 ETM+, TERRA/ASTER and TERRA/MODIS data at different spatial scales in District 1 for the dry season 2001; and

2 quantify the current water use, water re-use, and water productivity at different spatial scales in the rice-based irrigation system of District 1.

In view of these objectives, the following research questions are posed:

a) How much current water is flowing into the system?
b) How much water is flowing from the system?
c) How much water is lost through beneficial evapotranspiration (rice crop)?
d) How much water is lost through non-beneficial evapotranspiration?
e) How much water is lost through seepage and percolation?
f) What are the current levels of water re-use?
g) What are the current water-use efficiencies at various spatial scale levels within the irrigation system?
h) What are potentials for water re-use at different scale levels in the system?
i) What are the potentials for true water savings?

1.4 Outline of the study

Chapter 2 describes the important features of the irrigation system in the study area including, among other things, the properties and location of sub-systems, water delivery schedule, present conditions of the irrigation system, climate, soil types, land uses, and cropping calendar.

Chapter 3 deals with the water flux measurement methodology and results of different spatial scales of District 1. The different water-balance components like rainfall, surface inflow, surface outflow, groundwater fluctuation, seepage and percolation, and evapotranspiration from different spatial scales are discussed in detail. The amount of re-used water from various sources like pumps, creeks and check dams is quantified and discussed. Lastly, this chapter discusses the current on-farm water-management practices of farmers in District 1.

Chapter 4 deals with the remote sensing methodology and results for land-use classes and spatially distributed actual evapotranspiration in the study area. Rice growing areas monitored by the National Irrigation Administration (NIA) are compared with the Landsat 7 classifications on April 16 and May 18, 2001. It gives the evaluation of the performance of the Surface Energy Balance Algorithm (SEBAL) model for spatially distributed seasonal actual evapotranspiration using different sensors like MODIS, ASTER and Landsat 7 ETM of different processing levels, and as well as the results of the comparison with the potential crop evapotranspiration derived from two meteorological stations during the dry season of 2001 in District 1. Finally, the interchange ability of high spatial resolution sensors with temporal resolution sensors is discussed, and crop water deficit using two sensors at the same over pass day is also examined.

Chapter 5 discusses the water accounting and productivity approach at ten different spatial scales in District 1. Different water accounting indicators are applied to pinpoint water saving opportunities by describing the paths of water flow, how much water is being depleted and which use is depleting the water at each spatial scale. The scaling-up effects on water productivity are also examined to assess the hypothesis whether water productivity increases due to high water re-use opportunities at higher scales. This chapter also deals with the accuracy analysis of different water balance

components like surface flow (in-out), percolation, rainfall, pumped groundwater and actual evapotranspiration at each spatial scale.

Chapter 6 provides the general discussion and conclusions across ten different spatial scales in the study area.

2. THE STUDY AREA

2.1 Introduction

Like most of the developing countries, the Philippines is still an agricultural economy. Its agricultural sector accounts for about 19 % of the gross domestic product (GDP) and 40 % of employment (DA 2001). However, the area devoted to agriculture has been decreasing due to the pressures of urbanization and industrialization. The need to optimize productivity in the available agricultural land is, therefore, imperative. Optimizing productivity, however, includes not only land aspects but also other scarce resource inputs to production like water.

Irrigated rice comprises about 61 % of the 3.4 million hectares (ha) utilized for rice production, the majority of which comes from Central Luzon, which is considered as the country's rice bowl (IRRI 1997). Rice production in Central Luzon is of strategic importance to food security and poverty alleviation because of the area's dense population and close proximity to the capital city, Manila. Irrigation plays an important role in the economy of Central Luzon where rice is the major source of employment and income. Located in the area is the Upper Pampanga River Basin (UPRB), which has a total drainage area of 374, 250 ha and is relatively well-endowed with water, with per capita water availability exceeding 3500 m^3. Irrigation is mainly from a large reservoir, supported by communal irrigation schemes and shallow tube wells in the UPRB. The UPRB provides a stable food requirement of 25-30% of the total population of the Philippines. The growing scarcity of good quality water in most river basins results in intense inter-sectoral competition of water. The increase in non-agricultural demand will have to be met from new resource development or inter-sectoral transfers of water. The availability of water is being threatened by various sources over the last decade: water from the Angat reservoir in Bulacan Province is being increasingly diverted toward Greater Manila at the expense of irrigation (Pingali et al. 1997); water in the Agno River in Pangasinan Province is polluted with sediments and chemicals from mining activities upstream (Castaneda and Bhuiyan 1993); and many irrigation systems were destroyed and clogged by the earthquakes of 1990 and the Mount Pinatubo eruption in 1991 (NIA 1996). Water is always scarce in the dry season of Central Luzon, where the lack of rainfall makes cropping impossible without irrigation.

Within the Basin, the Upper Pumpanga River Integrated Irrigation System (UPRIIS) was established in 1975 and designed to irrigate 102,500 hectares, which produce an average of 63.22 million metric tons of rice every year. UPRIIS gets its water from a combination of run-of-the-river flows and the Pantabangan reservoir (largest watershed in the Philippines) with a storage capacity of 3 billion cubic meters. The Pantabangan dam is owned and operated by NIA. UPRIIS is divided into four (4) districts. The study area is in District 1.

2.2 Irrigation system of District 1

District 1 has a total area of 34,000 ha including rice fields, upland crops, vegetables, roads, settlements and water bodies. It comprises San Augustin Extension (SAE), Talavera River Irrigation System (TRIS), Upper and Lower; and Santo Domingo Area (SDA). SDA was divided into four (4) scales: SDA-A, SDA-B, SDA-C and SDA-D using existing roads as criteria for subdivision. The area of SAE, TRIS-Upper and SDA-D were excluded from the study area because it was not possible to measure the numerous inflow/outflow points in these areas.

District 1 is bounded by the Talavera River on the east and the Ilog Baliwag River in the west, and consists of an upper part, called TRIS-L with main city Munoz, and a lower part, the SDA, with main city Santo Domingo. There are two major sources of water such as the Pantabangan dam through the diversion Canal No. 1 and the Talavera diversion dam through TRIS main canal for District 1. The irrigation system is designed in such a way that the water from the main diversion canal is diverted into the big creek “Sapang Kawayan” and the check dam “De Babuyan,” which is built on the Sapang Kawayan creek in the lower part of TRIS-L and is the origin of the Santo Domingo main canal. NIA tries to divert water into the Sapang Kawayan creek from main diversion canal one week before releasing water to the sub-laterals of TRIS-L. All re-used water in the upstream area (TRIS-L) of District 1 is recaptured through interceptor drains that divert water into creeks. These creeks serve as major sources of water for the southern part (or SDA) of District 1.

For the multi-scale analysis, the study area of District 1 was divided into four scales: TRIS-L, SDA-A, SDA-B, and SDA-C as shown in Figure 2.1. The boundary of sub-areas was established on the basis of existing roads.

Figure 2.1: District 1 and the different Irrigation Sections in the study area

2.2.1 Talavera River Irrigation System-Lower (TRIS-L)

The diversion Canal 1 and the creeks (source of re-used water from TRIS-Upper) are the main source of water for TRIS-L. The gross area of TRIS-L is 11, 239 ha (including fields, roads, woodlands, water bodies and settlements) while 78% of the area is under rice during the dry season 2001. The TRIS- L area is divided into 48 farmer-irrigators associations (FIAs) with an average size of 233 ha. There are 11 small check dams located within TRIS-L, which capture the re-used water from the rice fields through small creeks and then supplement additional irrigation water in the laterals and sub-laterals of downstream areas of TRIS-L. The majority of the farmers depend entirely on irrigation water due to the good network of laterals and sub-laterals, but at the same time a large number of farmers use pumps as an additional source of water in the TRIS-L area. Only a few farmers located at the tail end of Lateral F could not grow rice crops

due to severe water shortage, and during dry the season 2001, these farmers only produced upland crops through groundwater pumping.

2.2.2 Santo Domingo Area-A (SDA-A)

The main source of water for SDA-A (southernmost part of District 1) is Lateral A (through SD main canal) and 2 big creeks (Baloc and Lamboy) carrying re-used water from the TRIS-L area. The gross area is 1,513 ha (consisting of roads, settlements, woodlands, rice fields and water bodies), while 78% is covered by rice crops during the dry season 2001. The only check dam is "Bausao", which is the origin of Lateral A-Extra (A-x); lateral A-x is the source of water for the lower parts of SDA-A and SDA-D. Most of the farmers have installed pumps, which provide an alternative source of water for irrigation in case of a water shortage.

2.2.3 Santo Domingo Area-B (SDA-B)

The major source of water is Lateral B & C of the SD main canal, and two creeks, which get their water from the Ilog Baliwag River. The gross area is 2,240 ha (consisting of settlements and different land-use types), while 76% of the area is under rice crops. It is divided into six (6) FIAs, each with an average size of 373 ha. The 2 check dams Swa (upstream) and Pajo (downstream) play a critical role in capturing water from the rice fields and later serving water to downstream SDA-B and SDA-C areas. The severe water shortage has forced farmers to get additional water either from groundwater through pumps or from illegal pipes buried along the Santo Domingo main canal (more than 100 illegal outlets in a 2 km area) to sustain the rice crops. Every farmer depends on pumps for additional sources of water for activities in the dry season ranging from land preparation to harvesting.

2.2.4 Santo Domingo Area-C (SDA-C)

SDA-C is the tail end of the main canal covers a gross area of 3,011 ha for all types of land uses and is divided into 7 FIAs, each with an average size of 273 ha. Only 65% of the area is under rice crops. The main source of water is the many laterals, i.e., D, E, E-X, F, & G of the SD main canal and 2 creeks (Pajo & Labong). All farmers in SDA-C depend on pumping for additional water supplies during the dry season and can obtain

water only when no water is required in the upstream area. That is why the cropping pattern of SDA-C is 2-3 weeks later than other areas of District 1. Santa Rita is the only check dam in SDA-C that captures re-used water through small creeks and serves as a major source of water for SDA-C and the lower part of the SDA-D area.

2.3 Water delivery schedule

An efficient water distribution plan can only be implemented with effective water control and measurement structures. NIA has divided the area of District 1 into 3 zones with sub-zones, and 88 FIAs for better management of the irrigation system. Every farmer is a member of one Rotation Unit Group (RUG) with about 10 ha. Five RUGs are affiliated with one Farmer Irrigators Group (FIG) covering 50 ha. These 8 to 10 FIGs are federated into one FIA covering 500 to 750 ha and a bigger organization called the Federation of FIA (FFIA) at the division level (3,000 ha each) is formulated. The FIAs are core organizations that contract with NIA on water management and irrigation service-fee collection. The on-farm level water distribution system in District 1 was constructed based on design criteria, which provided one turnout structure with every 50 ha, and one farm ditch with every 10 ha. On average, canals or laterals within each distribution system have an irrigation density of 75 ha/km; canal structures of 27.30 ha/unit; turnouts of 40.63 ha/unit; main farm ditches of 15.12 m/ha; supplementary farm ditches of 37.86 m/ha; drainage ditches of 12.28 m/ha, and improved existing drainage channels of 9.94 m/ha (NIA 1977).

The development of the seasonal water distribution plan begins with the submission by the Assistant Water Management Technicians (AWMTs) of their target irrigation area with crop-type information based on the estimated available flow. It also includes the weekly discharges necessary to support the programmed areas. These plans are submitted to the Zone Engineers (ZE) who consolidates them into the seasonal plan for the zone within District 1. The zone plans are consolidated into the District plan by the Operations Engineer (OE) who then submits the plan to the Water Control Coordinating Council (WCCC) of UPRIIS. Based on OE district plans, the WCCC develops the plan for the entire UPRIIS depending on the available water from all sources. The WCCC revises the plan if there is not enough available water to support the program areas.

This plan is disseminated to farmers through farmers meetings, pre-seasonal trainings and advertisements (Maglinao 1992). The advertisement specifies the locations by the Water Master's Divisions, sometimes by laterals and barangays. Sometimes farmers do not understand the reasons behind the plan. As only a part of such laterals or barangays is programmed, the locations of the programmed area are not specified. It is not uncommon to find farmers who do not know which Divisions they belong to. Our field investigation showed that most of farmers also do not know beforehand whether they are included in the program or not.

2.4 Present conditions of irrigation system

The physical condition of the irrigation system (such as the condition of the canals, laterals, ditches and turnout structures) affects the amount of water available as it determines conveyance losses and consequently the efficiency of water delivery. Efficient control structures in an irrigation system are necessary for all crops. The irrigation system of District 1 was rehabilitated in 1975 and all turnouts (double-gated/combined single-gated) were equipped with flow-measurement devices (NIA 1977). Originally, flow-measurement devices like weirs and flumes were installed at all lateral off-takes and at various turnouts in District 1. NIA maintained these records, but these flow-measurement activities were stopped many years ago due to lack of funds.

It was found that the tail-end portions showed serious water deficiencies, while the head or upper portion had excess water. The Santo Domingo canal was overflowing at some locations, while at the same time the farmers downstream of SDA-C were facing water shortages . There is water inadequacy during the dry season, while some areas are flooded during the wet season. Every year during the wet season, 405 ha of the SDA system are submerged under excessive backwater flood from the Talavera River. In the dry season 2001, scarcity of irrigation water at the tail end of the irrigation systems was observed, which affected the cropping pattern. One of the constraints in the water control is the time lag of irrigation water delivery on the long conveyance distance. If the travel time of water in the system is long, water already released for irrigation becomes excess water if it suddenly starts to rain.

Major problems observed within District 1 are inoperable control structures, inaccurate or non-workable measuring structures and siltation and erosion of canals.

Many hydraulic gates, stems and lifting mechanisms are damaged, indicating unsuitable design and fabrication to meet the hydraulic pressure, as well as lack of maintenance, especially lubrication. The steel gates of turnouts and some check structures are already missing in District 1. The siltation problems are often observed at smaller laterals and tail portion of canals, where flow velocities becomes low and the canal receives suspended loads from upstream. Canals have critical flow limitations, that when a certain flow is diverted to such canals, no flow arrives at the turnouts unless excessive checking is done. The farmers create their own checkpoints to divert water to their fields at such low flows.

Strong growth of aquatic vegetation also reduces the creek flow capacity and chokes up the check. Presently, most of these re-use structures do not function properly due to deteriorated control gates. Unauthorized turnouts are often to be found, e.g., there were more than 100 illegal turnouts in the 3-km area of the SDA main canal. The conditions of service roads along main canals (49 km in length) and major laterals (217 km) are well maintained in District 1, except for the road alongside the downstream SDA main canal, although in the TRIS-Lower area many check dams cannot be accessed through service roads. Large investments are again required to rehabilitate the system and turnover to farmer organization for better water distribution and management. Flows in irrigation channels need to be measured, including the discharge rate and volume of water delivered to a farm, or in some cases, to each field belonging to the farm. There is an urgent need to improve NIA's performance particularly in the maintenance of the irrigation facilities in District 1.

2.5 Climate

The climatic data observations on rainfall, temperature, humidity, wind speed, sunshine hours, solar radiation and evaporation were available from the Philippines Atmospheric Geophysical and Astronomical Services Administration (PAGASA) and PhilRice agro-meteorological stations in District 1. The climate in District 1 of UPRIIS is characterized by two pronounced seasons, i.e., wet and dry. The dry season lasts from November to April, the rainy season from May to October. Long-term rainfall data (1974-2001) from the PAGASA station indicated that more than 70% of the annual rainfall occurred from June through September, and more than 90% between May and

October. The remaining 10% are generally distributed between the months September to April, which means that there is a pronounced need for irrigation during the dry season. April and May are the hottest months and the average maximum temperature is 33°C, while December and January are the coldest months when the minimum temperature rarely falls below 19°C. The average relative humidity is about 83% and varies from 65-90% in the dry season. The average wind velocity is 1.9 m/sec in the plain area of District 1, where altitude varies from 30-80m.

2.6 Soils

The texture of the soils in District 1 ranges from moderately coarse to very fine (loamy sand to massive clay). The structure of the surface soils ranges from granular to weak fine and medium sub-angular blocky to massive. The soils are grouped into five categories based on terrace position such as most recent alluvial terrace, recent alluvial terrace, natural levees, old alluvial terrace, and residual terrace. Six soil series were identified: namely Maligaya, Qunigua, Prensa, Bantog, Zaragosa and unclassified (NIA 1971). Several studies were undertaken during the 1970s to investigate the soil structure, texture and drainage characteristics of the project area. Soils are Vertisols, Entisols and Inceptisols (US Department of Agriculture classification) and have typically silty clay, silty clay loam, clay loam and clay, with seepage and percolation (SP) rates varying between 0.2 and 20 mm d^{-1} (Wickham and Singh 1978; Tabbal et al. 1992).

2.7 Cropping calendar

The cropping calendar is the schedule of the different farming activities within the system such as land soaking (LS), land preparation (LP), transplanting (TP) and harvesting (H). It is important because it serves as the basis for estimating the water requirement for the entire season. The estimated water requirement is matched with the estimated water supply and if the farmers exceed the latter, the cropping calendar is revised to make the necessary adjustments. The cropping calendar of District 1 is generally adjusted to fit the rainfall pattern in the command area of the irrigation system. In general, farmers take advantage of the rain for land soaking and harvest, when rainfall is minimum.

The cropping calendar of NIA for different areas of District 1 dates from 19 November 2000 to 12 May 2001, and is based on the release of irrigation water in the canals. In reality, the land soaking activities took place from 1-15 December (upstream) to 1-7 February (downstream), land preparation varied from 23-31 December to 16-22 February, and harvesting from 1-7 April until 13-20 May. It was observed that in the SDA-C area the last rice crop was harvested on 29 May 2001. The actual cropping calendar of District 1 differed considerably from the cropping calendar of the NIA, which is highly related to the availability of water. The cropping calendar variations for different farming activities in District 1 were obtained from the NIA office (Figure 2.2). The major reason for the large variability is a head-tail difference in water availability.

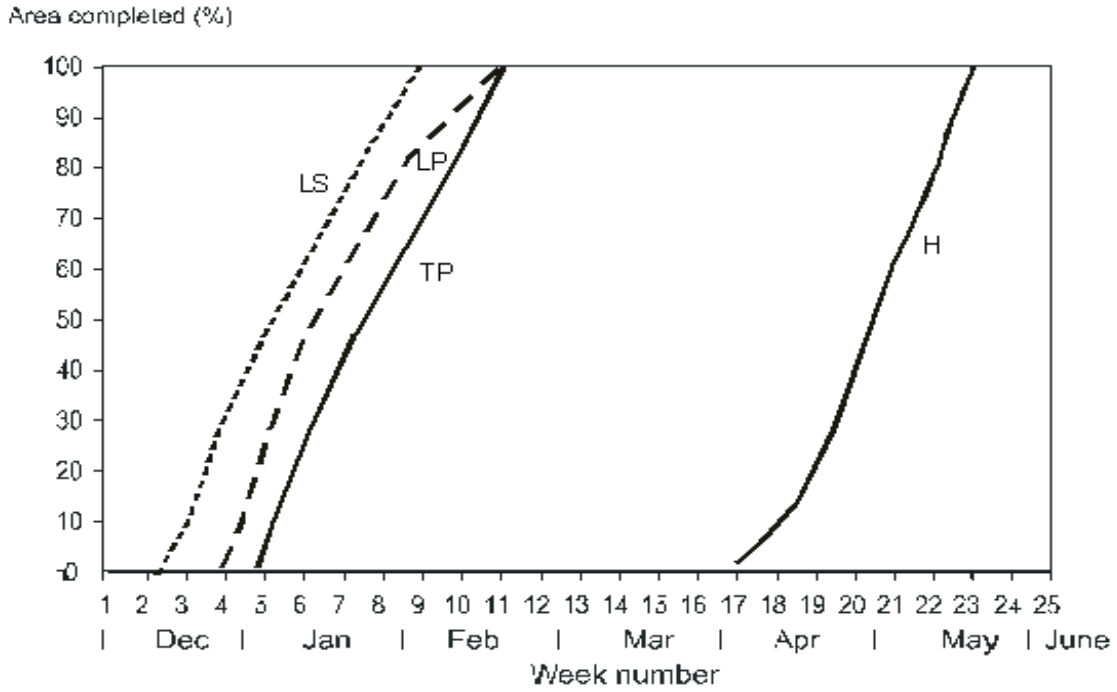

Figure 2.2: Graphical illustration of cropping calendar for District 1

2.8 Land use

Rice is the major crop during the wet season, followed by rice-upland crops during the dry season. The most common method of rice cultivation is transplanting, though direct wet seeding is becoming increasingly popular. The field investigation showed that about 10 % of the farmers at the tail-end area of TRIS-Lower, and the SDA-C area are growing short-duration upland crops (corn, water melon, vegetables like tomatoes, garlic, onions, egg plant, chili and white squash) in the dry season due to shortage of

water. Due to the high climatic yield potential in the dry season, increasing the area under irrigation is an attractive strategy to increase rice production (NIA 1996).

3. WATER FLUX MEASUREMENT

3.1 Water flux measurement

Irrigated agriculture is by far the greatest user of water on earth and a great deal of emphasis is placed on improving water management practices in irrigated agriculture systems. Improvement in the water management of irrigation systems has become most important during the past few decades, where water has become expensive and often scarce. Sound water management in irrigation systems requires a balance of physical facilities utilization, field operations, personnel management, participation, farmer's reaction to system management, the procedures of water delivery planning and allocation at various levels within the system. The last requirement cannot be achieved without knowing the exact quantity of water available at each location within the system. As Shafique et al. (1998) stated, "how can you improve the management of a resource when the quantity is not known, let alone the resource quality". The water balance for an irrigation project is a complex set of inflows, outflows, consumptive use, and recycling of water. Understanding of water balance and water performance in an irrigation system permits improvements in water management.

3.1.1 Water balance

The water balance approach is based on the law of conservation of mass: The sum of inflows must equal the sum of outflows plus any change in storage within an irrigation system. The optimization of irrigation systems requires knowledge of the water balance: the amount of inputs (rainfall, irrigation, run-on, lateral inflow) and outputs (evapotranspiration, percolation, seepage, run-off, drainage). A clear understanding of all the components of the water balance is, therefore, necessary to determine all the possible water saving measures. Many components of the water balance approach like groundwater inflows and outflows at different spatial scales are difficult to estimate. Although the actual crop evapotranspiration can be estimated at a large-scale irrigation system due to recent advancements in remote sensing, the model is still not widely applicable due its complexity. Normally, special importance is placed on the measurement of irrigation system inflows, and drainage outflows are often ignored. However, this study considers the measurement of irrigation, drainage and evapotranspiration (by remote sensing) at different spatial scales in District 1.

This study deals with the methodology for measuring different parameters of the water balance during the dry season of 2001 in District 1 of UPRIIS. District 1 has a gross area of 34,000 ha and comprises the San Augustin Extension (SAE), Talavera River Irrigation System (TRIS; Upper and Lower) and Santo Domingo Area (SDA). However, the area of SAE, TRIS-Upper and the lower part of SDA (SDA-D) were excluded from this study because it was impossible to measure the numerous inflow/outflow points of those areas. The rest of the study area was divided into four sub-areas, i.e., TRIS-Lower, SDA-A, SDA-B, and SDA-C.

3.1.1.1 Precipitation

Rainfall in the District 1 of UPRIIS is mainly the combination of tropical typhoon and monsoon rain. A good network of spatially distributed rain gauges is required to monitor the areal variation of rainfall within sub-zones of an irrigation system. The daily rainfall data was collected from two meteorological stations, i.e., the Philippines Atmospheric Geophysical and Astronomical Services Administration (PAGASA), Munoz, and PhilRice, Maligaya, located within District 1. In addition, 6 rain gauges were installed in District 1 to determine the spatial distribution of rainfall at different spatial scales. Overall, rain gauges at 8 locations (Radial gate 3, Tondod, PAGASA, PhilRice, Baloc, Edwin house, Governor creeks and Santa Rita dam) were installed to represent the rainfall pattern for the different areas of District 1. The rainfall data for all 8 locations were manually observed and recorded by hired local observers twice a day (at 08:00 and 17:00) during the whole dry season of 2001.

It is likely that the intensity of rainfall in the vicinity of a measurement point will be approximately the same intensity, but further away from the point this will not be true. Point rainfall can be considerably higher than areal rainfall, depending on the duration of the rainfall and size of the area. The shorter the rainfall duration and the larger the area, the lower is the areal rainfall with respect to point rainfall. There are many techniques to obtain areal rainfall from point rainfall, but each technique has its own merits and drawbacks. The Thiessen Polygon method is the most appropriate method when the stations are not evenly distributed over flat areas (Ritzema 1994). Since the locations of the 8 rain gauges were not evenly distributed in District 1, which is relatively flat area with altitudes ranging from 30-70 m, the Thiessen method was

used for interpolating the point values of rainfall data to obtain the representative rainfall area. The rainfall volume was calculated by multiplying the area with the quantity of rainfall. The variations of average monthly rainfall data for the 8 rain gauge stations within District 1 are shown in Figure 3.1.

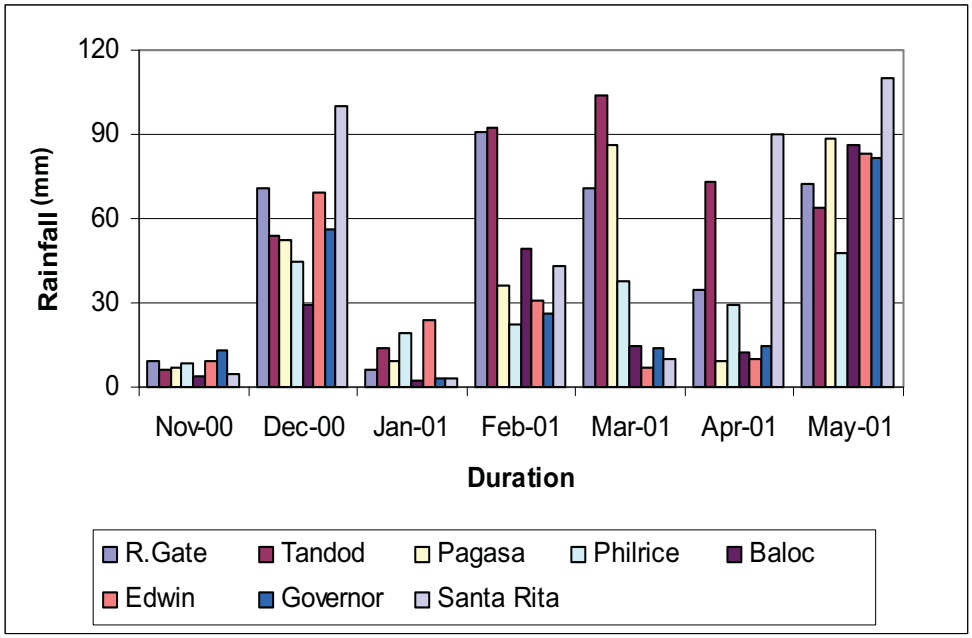

Figure 3.1: Monthly average rainfall variations at the 8 rain gauge locations within District 1

3.1.1.2 Surface inflow

There are two major sources of water for the TRIS-Lower and Santo Domingo areas: the diversion Canal No. 1 (getting its water from the Pantabangan dam) and the TRIS main canal (getting its water from the Talavera diversion "TRIS" dam). The irrigation system is designed in such a way that the water from the main diversion canal is diverted through a big creek "Sapang Kawayan", and the check dam "De Babuyan", built on the Sapang Kawayan creek, is the origin of the Santo Domingo main canal. The Santo Domingo area (SDA) was further subdivided into 3 sub-areas through detailed field survey, and the boundaries of each area were established based on existing roads as criteria.

A total of 67 inflow points were selected along the boundary of the 4 spatial scales. The surface water inflows were measured at 67 inflow points by installing 57 staff gauges, 2 parshall flumes and 8 culverts at the boundaries of the spatial scales

(TRIS-L, SDA-A, SDA-B, and SDA-C) to determine the exact quantity of water available for that particular area as shown in Figure 3.2 (red points show the location of flow-measuring devices (inflow/outflow)). The stream flows can be estimated by measuring the water level either manually from the graduated wooden staff gauges installed in the canal or electronically using automatic D-Divers (D1212 with automatic data loggers). Eleven automatic divers for recording the water head at 5-minute intervals were installed along the major creeks and canals during later part of the dry season 2001.

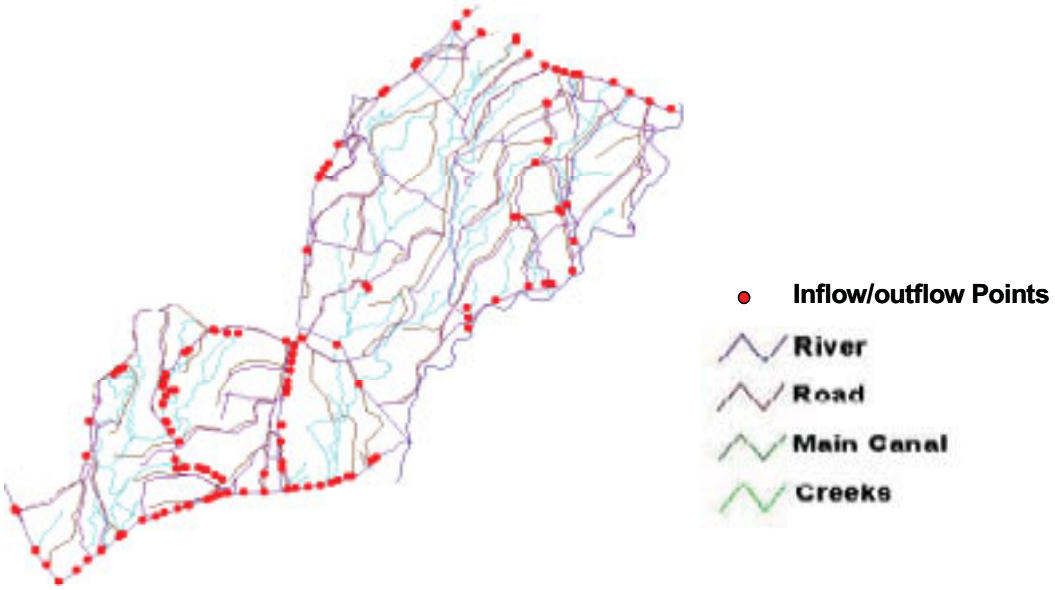

Figure 3.2: Location of flow-measuring instruments in spatial scales of District 1

The discharge-regulating structures in the main diversion Canal No. 1 and all secondary canals were calibrated using a current meter in the irrigation system as shown in Figure 1 (Appendix A). The wooden staff gauges (Figure 2 in Appendix A) were installed in such a way that a reading of zero was considered the lowest anticipated stage to avoid negative readings. The gauge datum was checked on a quarterly basis and the same gauge datum maintained throughout the recording period. The readings of the staff gauges were recorded twice a day throughout the dry season 2001. All staff gauges installed on the big canals/drains/creeks were calibrated 7-9 times at different water levels using the current meter (Model D622 Digital Price Meter with a Model 1100 Flow Indicator). A pygmy current meter/v-notch weir was used along small

canals/creeks and farm drainage ditches. The meter-stick technique was used as a flow-measuring device for small farm ditches with circular culverts.

Finally, the rating curve of every staff gauge location was developed for measuring the total discharge as shown in Appendix B. The discharge was converted equivalent to the volume of water by multiplying the discharge with time. The total volume of water for all 4 areas was then estimated by summing up the discharge of all inflow points within each area over the dry season 2001 (19 November, 2000 to 18 May, 2001) as shown in Table 3.1. The daily variation of discharge in these 4 spatial scales is shown in Figure 3.3. The daily variation of discharge depends upon farmer's water requirement downstream and rainfall water availability at a particular time during the dry season.

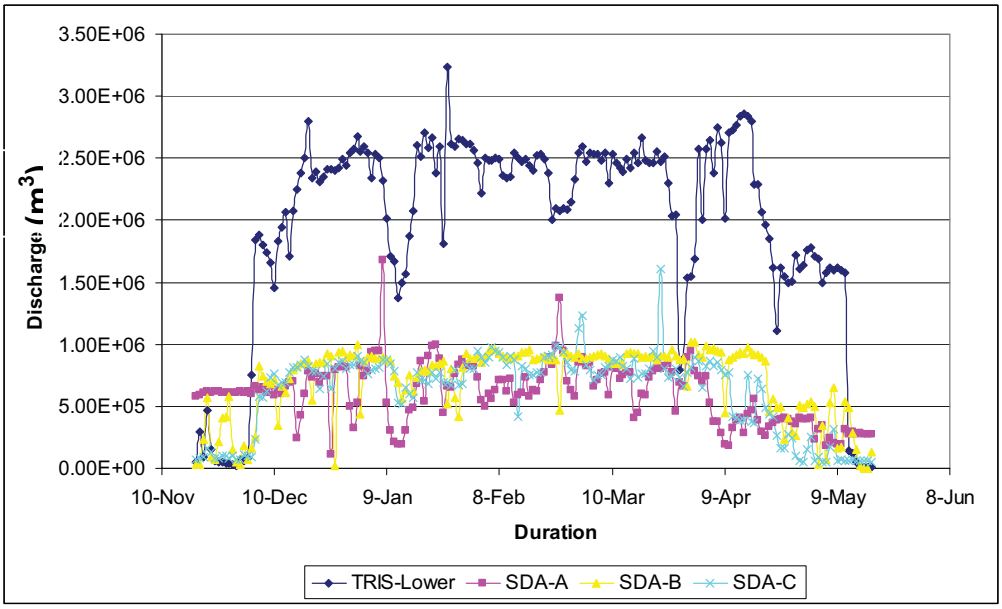

Figure 3.3: Major surface inflows for different areas of District 1 over dry season 2001 (19 November 2000 to 18 May 2001)

3.1.1.3 Surface outflow

The irrigation system was designed in such a way that all re-used water in the upper part of District 1 (TRIS-Lower) is captured through interceptor drains, which divert the water into creeks that serve as a major source of water for the southern (Santo Domingo Area) irrigation area. A total of 91 points were selected as outflows from the boundary of the 4 sub-areas (TRIS-Lower, SDA-A, SDA-B, and SDA-C) and the quantity of surface water was measured by installing 62 graduated wooden staff gauges, 2 parshall

flumes and 27 culverts. This was done to determine the exact quantity of water flowing out for that particular area as shown in Figure 3.2. The discharge of every outflow point was estimated manually by measuring the water level from the graduated staff gauges.

The wooden staff gauges were calibrated 7-9 times at different water levels using a current meter (Model D622 Digital Price Meter with a Model 1100 Flow Indicator) as shown in Figure 3 (Appendix A). The staff gauge was set in such a way that a reading of zero was considered the lowest anticipated stage to avoid negative readings. The gauge datum was checked on a quarterly basis and the same gauge datum maintained throughout the recording period. The readings of the staff gauges were recorded twice a day throughout the dry season 2001. A pygmy current meter/v-notch weir was used along the small canals/creeks and farm drain ditches. The meter-stick technique was used as a flow-measuring device for small farm ditches with circular culverts. Finally, the rating curve of every staff gauge was developed for measuring the total discharge as shown in Appendix A. The discharge was converted to an equivalent of the volume of water by multiplying the discharge with time. The total water volume was estimated by summing up the discharge of all outflow points within each area over the dry season 2001 as shown in Table 3.1.

Table 3.1: Total volume of surface water available for different areas of District 1 during the dry season (19 November 2000 to 18 May 2001)

Item	TRIS-Lower	SDA-A	SDA-B	SDA-C
Gross area (ha)	11,239	1513	2240	3011
Rice area (ha)	8,713	1177	1709	1972
Inflow (m^3)	3.55E+08	1.10E+08	1.29E+08	1.12E+08
Outflow (m^3)	2.80E+08	9.54E+08	1.09E+08	9.84E+07

The daily variation of outflow at 4 spatial scales of District 1 for the entire dry season 2001 is shown in Figure 3.4. The water carried through laterals and canals is treated as committed water for downstream areas, while the quantity of water directly discharging into Talavera River is treated as uncommitted outflow from District 1 of UPRIIS. The amount of water required for environmental purposes in the downstream areas of UPRIIS is considered zero due to lack of information about these areas.

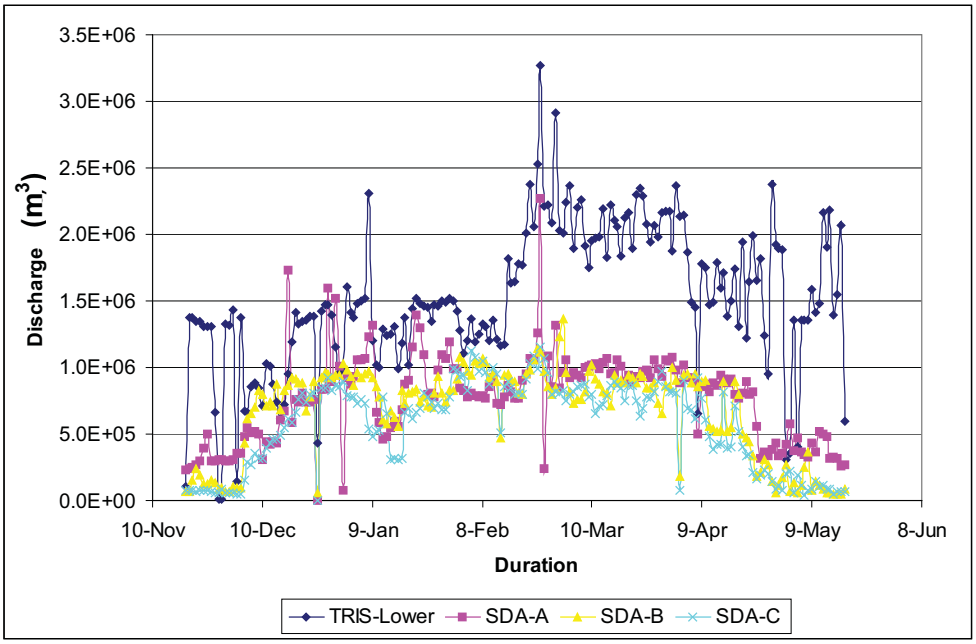

Figure 3.4: Major surface outflows from SD main canal over dry season 2001.

3.1.1.4 Seepage and percolation

Seepage is the lateral movement of water through and under paddy bunds, which may reappear on the surface at a lower elevation. Percolation is the portion of soil water that passes vertically downward and eventually reaches the water table. Seepage and percolation (SP) constitutes water movement into the soil and it is difficult to measure these components separately. The flow rate of SP is governed by the water head (depth of pounded water) on the field and the resistance to water movement in the soil. Many techniques exist for measuring SP like sloping gauges, rapid response percolation meter, and small drums, etc., in the rice fields. In this study, a simple low-cost method involving, a small metal drum (baby-milk powder with an internal diameter of 15-20 cm) connected with a plastic bag through a plastic tube, was used to determine the percolation rate without disturbing the measurement site in the rice fields. The method ensures that the water pressure in- and outside the drum remains exactly the same. The experimental set-up is shown in Figure 3.5. The upper half or third of a drum was carefully inserted into the soil to a depth of 9 to 12 cm and a clear plastic tube was tightly connected to the hole at the top of the drum. A urine bag without air and filled with a known quantity of water was connected to the other side of the plastic tube through a T-valve. The T-valve must remain closed while connecting the drum to the urine bag and opened only in the surrounding water in the rice fields. The water

pressure in the drum will equilibrate (for about 10 minute) to the water pressure in the urine bag. The urine bag was disconnected after 24 hours and the volume of water inside the bag determined. The difference in the volume of water in the bag, the time and the surface area of the drum were used to estimate the infiltration rate.

In this study, 50 sets of percolation instruments were installed to measure the percolation rate in 10 different rice fields during the whole month of April in the dry season 2001 in various parts of District 1. In each rice field, 5 percolation instruments were installed.

Figure 3.5: Layout of small percolation drums installed in rice fields

Overall, 1512 readings from the percolation drums were taken to determine the average percolation rate in a rice field. One major limitation was the leakage of urine bags due to damage by rats. The damaged bags were immediately replaced by the new bags. The mean values and range (in brackets) of the percolation rate variation within different rice fields are summarized in Table 3.2.

The percolation rate is governed by several factors including soil texture, structure, longer irrigation interval and the height of water standing over the soil. The major soil types in the study area are Vertisols, Entisols and Inceptisols (USDA classification), and have typically silty to clay textures. The field investigation showed

that the drums placed near soil cracks measured higher percolation rates, which were as high as 10.6 mm/day in a rice field. The reasons could be soil cracks near the percolation drum and leakage of the urine bag. DeDatta et al. (1973) also reported that percolation losses are higher due to longer intervals of irrigation because of deeper and bigger cracks forming on the soils. The magnitude of cracks depends upon type of clay.

Table 3.2: Mean and range of percolation rate within different rice fields (mm/day)

Rice fields	Locations in rice fields				
	A	B	C	D	E
1	1.5 (0.3-3.8)	1.3 (0.2-9.3)	2.7 (0.3-7.4)	7.5 (0.2-10.0)	1.7 (0.5-5.7)
2	0.5 (0.2-1.4)	2.4 (0.2-9.7)	0.7 (0.3-2.3)	2.3 (0.2-9.7)	0.8 (0.4-1.9)
3	7.2 (0.7-9.9)	2.5 (0.2-9.9)	2.8 (0.2-9.9)	2.7 (0.2-9.9)	-
4	5.4 (0.2-10.1)	1.7 (0.3-10.1)	4.7 (0.2-9.9)	2.1 (0.2-9.2)	1.5 (0.2-3.9)
5	1.9 (0.4-10.2)	2.0 (0.3-10.6)	2.3 (0.2-9.9)	2.8 (0.2-9.1)	3.1 (0.6-9.1)
6	1.3 (0.5-3.2)	2.2 (0.2-5.5)	0.5 (0.2-1.5)	2.0 (0.4-9.4)	1.1 (0.4-9.4)
7	0.8 (0.2-2.4)	1.4 (0.4-9.4)	2.0 (0.3-7.8)	0.7 (0.2-3.4)	2.7 (0.3-9.1)
8	4.0 (0.4-9.9)	2.8 (0.2-7.4)	0.9 (0.2-2.5)	1.1 (0.3-2.7)	3.8 (0.5-9.7)
9	2.4 (0.2-4.3)	0.6 (0.2-2.0)	0.8 (0.3-2.1)	0.9 (0.4-2.3)	1.7 (0.2-5.8)
10	1.7 (0.2-7.2)	1.3 (0.3-7.3)	1.8 (0.5-6.9)	0.8 (0.6-6.0)	-

The percolation rate of 10.6 mm/day was observed when the standing water was left throughout the rice field and the lowest (0.2 mm/day) when the soil was maintained near saturation. Clay colloids swell upon irrigation and hold a large amount of water in the profile and do not form any deep cracks deeper down. The other possible explanation is air trapped or locked in soil crevices during irrigation, which act as a barrier, thus minimizing percolation.

Typically, SP rates for paddy fields during the crop growth period vary from 1-5 mm/day in heavy clay soils to 25-30 mm/day in sandy and sandy loam soils (Bouman and Toung 2001; Wickham and Singh 1978; Jha et al. 1981). Sattar (1992) reported that the average SP rate varied from 1-4 mm/day (mean 2 mm/day) during the dry season in District 1. According to Lucero (1984), the SP rate varied from 1.7-2.5 mm/day with a mean of 2.0mm/day (TRIS-L and SDA). Overall, the monthly average values of percolation measured for each experimental site varied from 0.6-10.6 mm/day with a mean of 2.1 mm/day, which is in agreement with the other percolation studies carried out in District 1.

3.1.1.5 Storage change

The change in water storage can be related to surface water, groundwater, and soil water. No information was available about the changes in surface and soil water, so it was assumed to be zero at different spatial scales within the system. Fluctuations in groundwater levels below surface reflect changes in groundwater storage within the aquifers. As the groundwater levels generally respond very slowly to external changes, continuous measurement is not necessary. Therefore, systematic observations at fixed time intervals are adequate for the purpose of monitoring seasonal change in groundwater storage. The field investigation showed that the average groundwater table depth is 0.5 m in the wet season and 1.5 m at the end of the dry season, which is within the local range of 0.1 m to deeper than 6 m.

In a parallel study, Hossain (2001) reported that the groundwater level varies from 2.85-6.55 m in February; 2.95-6.94 m in March; 3.01-5.18 m in April; and 2.93-5.80 m in May for 4 selected shallow wells in District 1 during the dry season of 2001. The 50 spatially distributed existing wells (tube wells) were monitored at 14-day intervals to observe the groundwater fluctuation. The electrical measuring device works by lowering of two electrodes to water level; contact with the water closes the circuit and a warning light with buzzer indicates the groundwater level. The individual electrode must be of sufficient weight to keep the cable extended in the well but not stretched. The cable is calibrated with markers at fixed intervals, say, every 1 or 2 m, and the exact depth to water level is measured by a steel rule to the nearest marker on the cable. The experimental set-up is shown in Figure 3.6.

The representative area of each groundwater observation well was created with the help of Theisen polygons. The storage coefficient (soil water content at saturation – soil water content at field capacity) data were available from the comprehensive soil properties study of District 1 by Ramos (1986). A fair estimate of the change in the groundwater storage was obtained by multiplying the storage coefficient with the changed groundwater table at the beginning and end of the dry season 2001. The total change in groundwater storage for each area is shown in Table 3.3.

Figure 3.6: Experimental set-up for measuring groundwater level

Table 3.3: Seasonal groundwater storage in different areas of District 1

Scales	Net groundwater storage (m^3)
Talavera River Irrigation System-Lower (TRIS-L)	2.58E+06
Santo Domingo Area-A (SDA-A)	4.46E+05
Santo Domingo Area-B (SDA-B)	2.25E+06
Santo Domingo Area-C (SDA-C)	1.28E+06

The results show that some individual polygons show groundwater outflow for some months but in all, the areas TRIS-L and SDA had net groundwater inflow during the dry season of 2001. The monitoring of groundwater table data was started late in the dry season for the Santo Domingo areas. In addition, some existing tube wells were used for monitoring the groundwater table. This might have led to less accurate groundwater storage data. The observation well data at the time of land preparation was lost for SDA-B and SDA-C, which might leads to less accurate groundwater storage of these areas. As the total volume of groundwater storage change is less than 1.5 % of gross inflow for different scales, it would, therefore, not significantly affect the water accounting results. Overall, the results show that there was net groundwater outflow from the system over the dry season 2001 in different sub-areas of District 1.

3.1.1.6 Evapotranspiration

The actual evapotranspiration is the most important component in water balance studies and is very difficult to measure at larger scales. The actual evapotranspiration was estimated with the Surface Energy Balance Algorithm for Land (SEBAL) developed by Bastiaanssen et al. (1998). The practical procedure for estimating seasonal evapotranspiration through remote sensing is described extensively in Chapter 4. The actual seasonal evapotranspiration of District 1 was estimated using 11 satellite images (3 Landsat 7 ETM+, 1 TERRA/ASTER and 7 TERRA/MODIS) over the dry season 2001. The results were compared with the potential crop evapotranspiration calculated from the two meteorological stations, PAGASA and PhilRice, using the modified Penman Monteith equation (Allen et al. 1998) and discussed in Chapter 4. The information about different land use types i.e. rice area, upland crops, natural vegetation, settlements and water bodies in sub-areas were obtained from classified image of District 1. The seasonal actual evapotranspiration of rice crops is treated as process depletion for the different sub-areas of District 1. The evapotranspiration from all other land-use types (upland crops, water bodies, and fallow lands) were treated as non-process depletion in this study.

3.2 Re-use of water

Irrigation systems usually consist of a complex network of irrigation and drainage canals with a considerable amount of water re-use (Zulu et al. 1996). The total volume of water re-use can be divided into two parts: official and unofficial. The official part is the volume of water re-used using facilities installed by the system management (through gravity or pumping); the unofficial part is generally the unknown volume of water re-used by the farmers. Water outflows from one particular section of an irrigation system may be re-used in another section by damming drains or pumping water from creeks or both. Water lost from an individual field is not necessarily lost for the whole irrigation system or for the water basin at large. Water that flows out of a field will enter drains, creeks or groundwater, and flow downstream. Often, this water is again available for re-use, through blocking creeks and diverting the water into new irrigation canals, by pumping directly from creeks and drains, or by pumping from the (shallow) groundwater. Re-use can be practiced at the farm level, irrigation system level, and

regional level provided the water is of good quality. Farmers can pump irrigation water directly from the open drains or use shallow wells to pump groundwater. Re-use at irrigation system level is practiced when the water in downstream areas is pumped back into the irrigation system.

Irrigation water that percolates deeply and recharges an aquifer adds to the water supply available to the users of groundwater. Aquifers are sometimes used to store excess surface water or to meet the water requirements in the dry seasons. Some farms and small irrigation systems depend entirely on supplies of recoverable groundwater. Irrecoverable groundwater is water that cannot be pumped economically or that needs to flow out of the area to prevent the groundwater from becoming saline. It may be collected on-farm and pumped back into the distribution system for re-use, or it may be intercepted by users as a supplemental or even primary water source downstream.

Reuse of water offers an effective way to increase the water-use efficiency and productivity of an irrigation system. Seckler et al. (1998) stated that recycling of water occurs for both agricultural and non-agricultural uses in irrigation systems and its importance is often ignored. Guerra et al., (1998) reported that recycling is being practiced in rice irrigation systems of many countries. Zulu et al. (1996) reported that average drainage water reuse was about 14-15 % of the original irrigation water inflow in a rice irrigation system in Niigata Perfecture, Japan. In this study, an attempt was made to estimate the total amount of water re-used from pumps, creeks, and check dams within different spatial scales of District 1.

3.2.1 Pumps

There are at least 15-20 million pumps located in Asia for lifting water from groundwater, rivers, canals or reservoirs. More than five million small pumps are used to lift water out of canals and rivers for use on rice crops in Thailand alone (Yudelman 1993). In many irrigation systems like District 1, water shortage in the dry season is a major constraint for growing high water consuming crops like rice. This is common not only in the Philippines but also in Indonesia, where groundwater is pumped to supplement the water supply during the dry season (Bhuiyan et al. 1990, Undan et al. 1992).

Groundwater utilization to fully irrigate or supplement canal system deliveries can significantly alleviate the farmers' water scarcity problem. The first step to quantify the contribution is to measure the discharges being pumped so as to manage the exact quantity of water at the irrigation system level, which is rarely done at present. In this study, NIA carried out a comprehensive survey at the FIA level to determine the exact numbers of pumps, their sizes, types, type of installation (permanent or mobile), source of water (groundwater, creek or canals), irrigated service area (rice/upland crops), number of farmers sharing that pump, etc., in District 1. In all, 1154 pumps are used by the farmers, pump size varying from 3-5 inches in diameter, with the 4-inch tubes being the most common in all four areas of District 1. Pumping depths ranged from 6-15 m and only a few farmers in the Santo Domingo area had extended uncased boring of up to 15 m to achieve better water yield. The prime movers of the pumps were all diesel engines of various brands and power ratings ranged from 4-10 horsepower. The majority of pumps just discharged water directly to the nearby farm ditch.

Later, 50 farmers were selected in different areas of District 1 depending upon the location, pump size and source of water, and the total pump usage by these farmers for all farming activities starting from land preparation to harvesting were monitored in the dry season 2001. The farmers were provided with survey forms in Philippine language (Filipino) for recording the total pumping time for each farming activity, fuel used and total irrigated area by each pumping day. The farmers' pumping records were continuously checked through frequent visit to the farms, and the recorded forms were collected at the end of each month. The pumping data of 6 farmers were omitted from that study due to great uncertainties in total pumpage timing and farmers' behaviour. Finally, 44 pumps of different sizes were calibrated 5-7 times either with a V-notch weir or Pitot tube for measuring the actual discharge for different sizes of pumps.

The total pumping time per hectare was obtained by dividing the total pumping time over the irrigated area for the dry season 2001. The total amount of water being pumped by each monitored farmers was determined by multiplying the actual discharge with the total pumping times/hectare. In this way, the total amounts of water pumped by these selected 44 farmers were estimated. It was assumed that the remaining farmers had almost the same pumping trends for the different farming activities in the dry season 2001. The average value of water pumped for different pump sizes was

obtained from the average water pumped by the 44 selected farmers. The total water pumped can be estimated by multiplying the average water being pumped for each pump size with total number of pumps. The total amount of water being pumped for 4 spatial scales (TRIS-L, SDA-A, SDA-B, and SDA-C) during the dry season 2001 is presented in Table 3.4.

Table 3.4: Volume of re-used water from groundwater, creeks and check dams for different areas of District 1

Item	**TRIS-L**	**SDA-A**	**SDA-B**	**SDA-C**
Gross area (ha)	11,239	1513	2240	3011
Rice area (ha)	8,713	1177	1709	1972
Number of FIA's	48	5	6	7
Number of pumps	519	109	107	419
Number of pump users	655	91	146	694
Rice irrigated area by pumps (ha)	1,674	204	227	954
Groundwater pumping (m^3)	1.40E+07	1.62E+06	1.78E+06	8.53E+06
Pumping from canal/creek (m^3)	7.13E+05	2.21E+05	1.79E+05	4.08E+04
Total pumping (m^3)	1.47E+07	1.84E+06	1.96E+06	8.57E+06
Water re-use from check dams (m^3)	5.39E+07	-	6.99E+06	2.88E+07

The re-used water includes pumping from groundwater and creeks in the different areas of District 1. The next step was to determine the pump density through an analysis with the help of a geographic information system (GIS), which provides information on the number of pumps installed per hectare in each FIA level in the study area. The pump density analysis provides information at 5 levels as shown in Figure 3.7. The yellowish color shows the pump density ranges from 0-0.39 pumps/ha, implying that these farmers do not fully depend upon pumps, while the dark reddish color shows that the pump density range is very high from 4.53-6.93, which means that the majority of the farmers depend on groundwater through pumping. It is clearly visible that pump density increases across the downstream areas of SDA-B and SDA-C.

The total amount of water pumped at each FIA level in District 1 was estimated on the basis of the discharges and location of the pumps in the study area. In addition, the total volume of water per ha was estimated using the GIS analysis as shown in Figure 3.8. The total volume pumped per ha at each FIA level during the dry season was categorized in 5 classes.

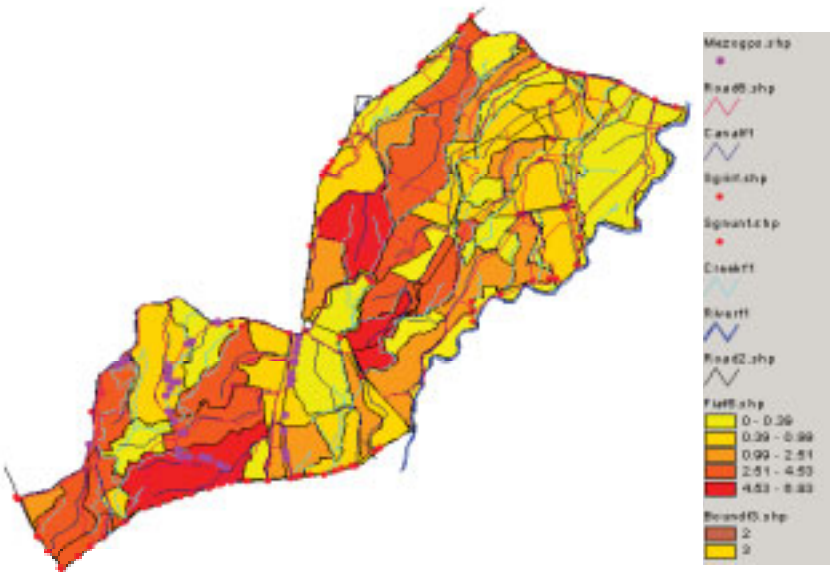

Figure 3.7: Pump density (pump/ha) at each farmers irrigator association (FIA) in District 1

This analysis shows that the total pump volume per ha in the tail end areas, i.e., SDA-B and SDA-C is very high (reddish color). The total amount of re-used water by pumping is equivalent to 30 % of the water lost through rice evapotranspiration during the dry season 2001. It can be concluded that small pumps owned by farmers play an important role in capturing the re-used water from groundwater (percolation losses of upstream) and creeks (re-used water from farmer fields) and increase the water productivity in the irrigation system.

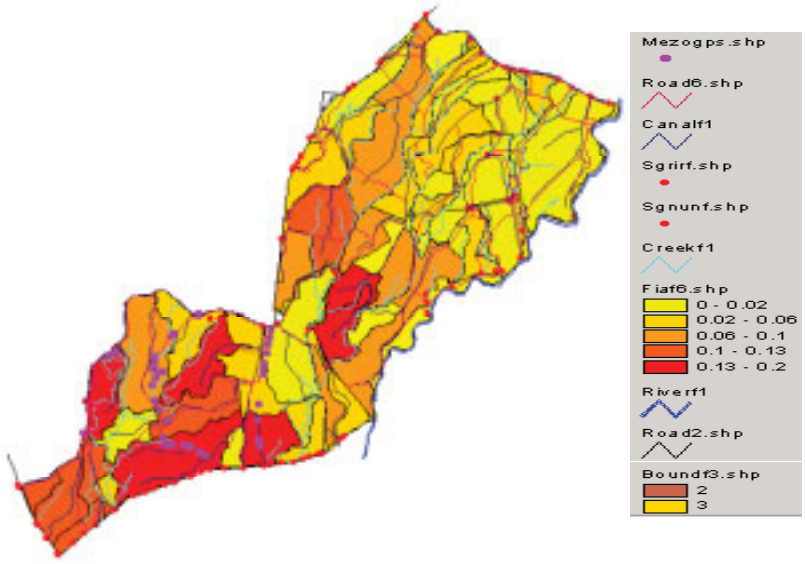

Figure 3.8: Pumps volume (m^3/ha) at each FIA in District 1

3.2.2 Creeks

Farm drainage networks, such as main and secondary drainage canals, do not exist in the area. Drainage water flows from paddy field to paddy field and finally reaches the natural drainage creeks. There are many small- to medium-scale check gate structures on the drainage creeks to collect the local flow, including the irrigation return flow from the paddy field. Farmers build small earth dams in the creeks, especially in the downstream area far from the turnouts. The networks of creeks found in District 1 that carry excess water from the paddy fields are shown in Figure 3.9.

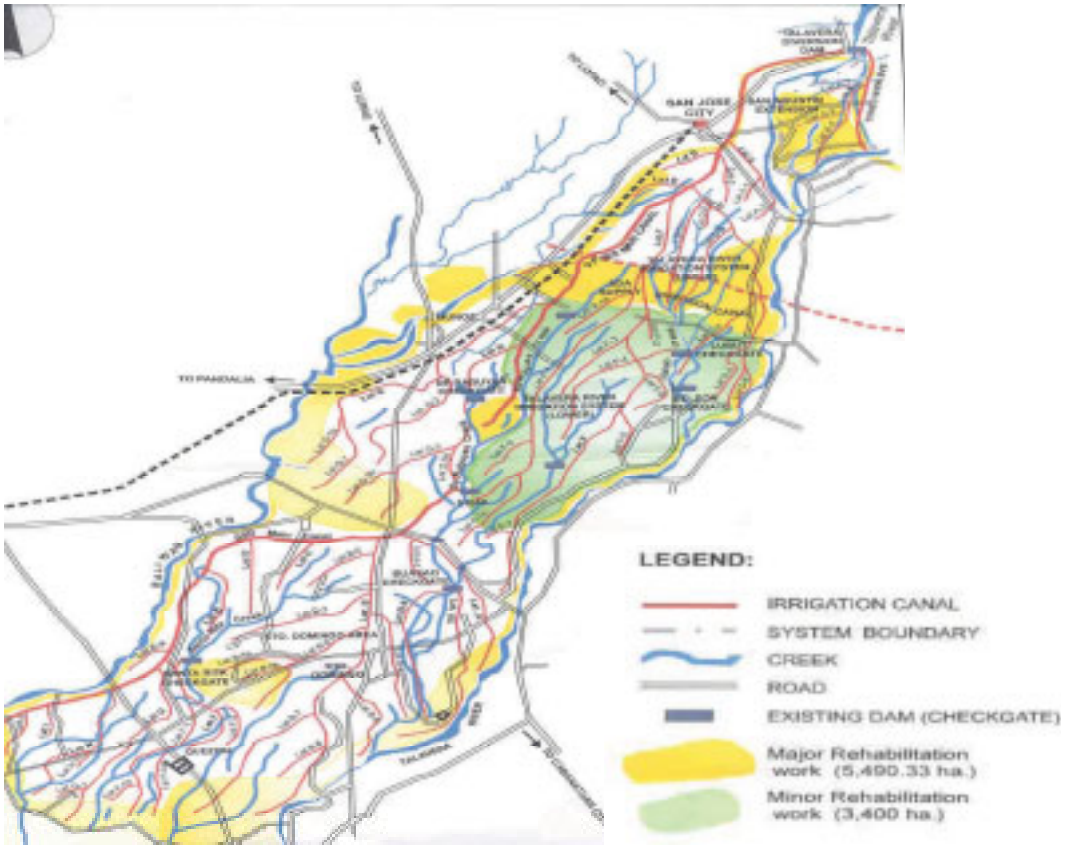

Figure 3.9: Layout of creeks and check dams in the study area

In the dry season, many farmers at the downstream areas use mobile pumps for getting additional water from creeks. The information about the total number of these pumps was collected through the comprehensive survey by the NIA staff. The total duration of pumping for all farming activities was obtained by monitoring the respective pumps. In that way, the total amount of water re-used from creeks through pumping was

obtained for each area of District 1 for the dry season 2001. The amount of water being pumped from creeks is shown in Table 3.4.

3.2.3 Check dams

Check-dams are small barriers built across shallow rivers and streams for the purpose of water harvesting. The small dams retain the excess water flow during the monsoon rains in a small catchments area behind the structure. The major environmental benefit is the replenishment of nearby groundwater reserves and wells. Surface and subsurface water entrapped by the dam is primarily intended for use in irrigation during the dry season, but can also be used for livestock and domestic needs.

The irrigation system works in such a way that all unused water in the upstream area will be recaptured downstream in the small creeks and drain ditches. NIA and influential farmers (Senator; in case of SWA dam) built the small earth fill dams for storing all the used upstream water and for overcoming the water shortage problems in District 1. There are total 15 check dams in District 1 (shown in Figure 3.9), which are operated and maintained either by NIA or the group of influential farmers. Realizing the need to harvest the excess rainfall or run-off water, hundreds of small farm ponds were constructed by groups of farmers and these ponds can supply irrigation water to 50-100 ha of rice land. It is not practically possible to measure the re-used water through these small ponds at the irrigation system level, but they play a vital role in capturing rainwater. Normally, the small creeks/drain ditches getting water from the rice fields are the main source of water for these small check dams. These check dams have regular structures for releasing the water from small creeks that will supply additional water to the laterals downstream for irrigation purposes.

Wooden staff gauges for measuring the water head were installed on 6 dams and observed twice a day by field staff. These staff gauges were calibrated 5-7 times at different water heads with the current meter for estimating the exact quantity of water re-used from these check dams. It was not possible to install staff gauges on 9 check dams in the TRIS-Lower area because the service roads could not be accessed. Automatic divers were also installed to record the water head at 5-minute intervals on the Bausao dam (SDA-A), Pajo dam (SDA-B) and Santa Rita dam (SDA-C) for later part of the dry season 2001. However, the automatic diver at the Bausao dam was stolen

a week after installation. On Pajo dam (SDA-B), the water always remained stagnant in the creek just after the dam spillway, but this creek gets re-used water from both sides through many small drain ditches and becomes a big creek with a high water-carrying capacity just 2 miles downstream from the dam. There is hardly any data available on the catchments area of each dam, the total irrigated area and the amount of water available from these checks dams in District 1. The estimated total amounts of water from these 4 dams (De Leon and Veriens (TRIS-L), SWA (SDA-B) and Santa Rita (SDA-C)) for the dry season 2001 are summarized in Table 3.4. The daily variation of discharge at the Santa Rita dam (SDA-C) over the entire dry season 2001 is shown in Figure 3.10.

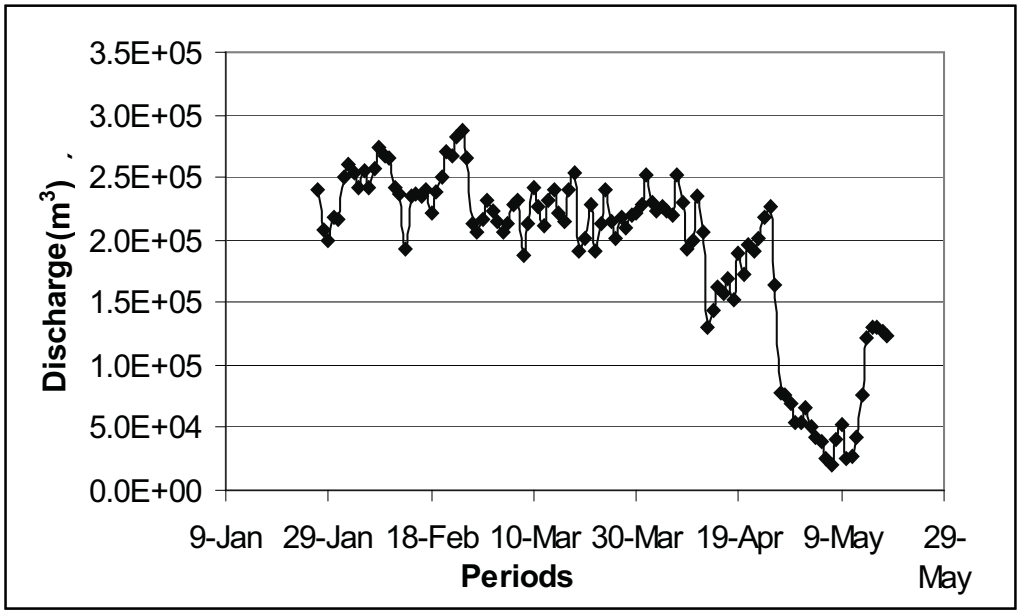

Figure 3.10: Daily variation of discharge at Santa Rita Dam during dry season 2001

3.3 On-farm water management

In most of Southeast Asia, irrigation systems were built and designed specifically for irrigating rice during the wet and dry seasons. The scarcity of water during the dry season has however consistently caused low cropping intensities in most national irrigation systems (Rosegrant et al. 1986). The Philippines is one of the countries in the region where large investments in irrigation systems have contributed to an increase in rice production. These investments were made in response to the increasing price of rice, population growth, and also with the ultimate aim of self-sufficiency and food

security. However, during the dry season, available water from irrigations canal is inadequate for rice growing in the whole service area. Although farmers in the upper reaches of the irrigation system may have sufficient water for rice production, water scarcity in tail ends is a common phenomenon in the dry season. Diversified cropping in irrigated lands is gaining ground as an alternative to rice production in the dry season.

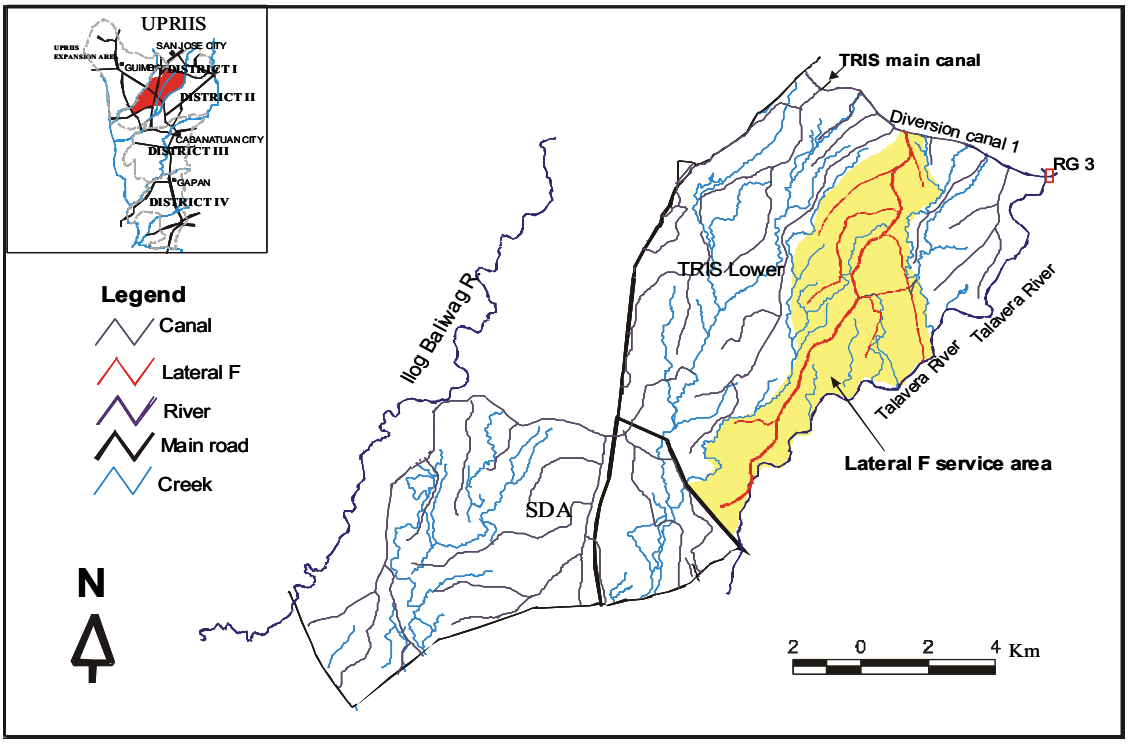

Figure 3.11: Map of District 1 (UPRIIS) showing Lateral F service area (adapted from Moya et al. 2002)

In the dry season of 2000, the Social Science Division of the International Rice Research Institute (IRRI) conducted a survey in District 1 to compare the on-farm water management practices of 60 farmers, some of whom irrigate their fields through a surface gravity system and others using the pumping system within the service area of lateral F (Figure 3.11). Use of small pumps is common among the upper and lower reaches of the lateral canal (Moya et al. 2002). The selection of 60 farmers was giving equal representation in the upper, middle and lower reaches of the Lateral F. Overall, only 20 farmers from midstream solely depend on canal water, and the rest, i.e., 40 farmers (upper and tail end) use small pumps to irrigate the rice fields. The sample farmers have more or less similar characteristics in terms of age, schooling and family size. Only some farmers at the tail end of Lateral F planted short-duration high-value

non-rice crops such as corn, onions, eggplant, string beans, and mung bean, etc. These crops require less water than lowland rice crops.

Results show that 55 % of the farmers used surface water (irrigation/drainage canals or creeks), 22 % used only groundwater, and 23 % used both surface and groundwater (in case of non-availability of surface water). In terms of water delivery system, 32 farmers get water through a gravity system and 28 farmers used both sources of water (gravity and underground) to deliver water to rice fields.

The farmers irrigating by means of a gravity system used only 11 % more water (1058 mm) than pump users (949 mm), this excludes the water used for land preparation. However, both categories of farmers achieved the same yield: 6.7 and 6.8 tons/ha for pump and gravity system, respectively (Moya et al. 2002). All other inputs costs (labor, seeds, and fertilizers) are the same for both types of farmers, except the additional pumping cost (diesel, engine oil and pump rentals) for the pump users. In case of pump system, the water costs consist of the pumping cost, the delivery of water to rice fields, and the fee paid to NIA (farmers who pump water from the irrigation canal pay an equivalent of 50% of the irrigation fee paid by those using the gravity system). In respect of net benefits, the return over paid-out costs for pump users is almost US$ 220/ha lower than for the gravity system (Moya et al., 2002). Despite the high pumping costs, pump users are still achieving a substantial profits from rice production, even though the profits are lower in comparison to those achieved at farms irrigated by the surface gravity system.

4. REMOTE SENSING RESULTS

4.1 Land-use classification

4.1.1 Introduction

An accurate estimation of the rice grown in the area is important for the design of food supplies, revenue collection and cultivation programs for any large irrigation system like District 1 of UPRIIS. Such an estimation is possible using data obtained through remote sensing. However, there are several techniques for using satellite data to develop land-use databases at regional scales, and each method has its own merits and drawbacks. For instance, automatic unsupervised classification and visual image interpretation are procedures that are used to analyze and classify satellite data. However, most image classification algorithms are based on spectral information. Since many land-use classes exhibit similar spectral properties, these procedures can lead to classification errors. On the other hand, image interpretation procedures can be used to analyze both spatial and spectral information to map land-use classes. However, this requires detailed knowledge of the area, which is usually not possible for large irrigation systems. Thus, the alternative approach is to integrate image classification and image interpretation procedures so that the strong points of each method can be utilized to classify an image.

NIA conducts weekly surveys of rice growing areas in District 1 for revenue collection and irrigation scheduling. Since it is prohibitively expensive to physically cover all the area for every cropping season, data estimation is resorted to, and data collected through this survey cannot be fully reliable as it involves human judgment errors. However, an accurate estimation of rice-grown area is important for NIA's irrigation scheduling and revenue collection activities. In this regard, remote sensing could provide a potential solution to the dilemma.

In this study, the reliability of the weekly agriculture statistics prepared by NIA was examined through the use of Landsat 7 ETM+ images. Different land-use classes using the false color composite of Landsat 7 ETM+ images were produced through integration of the unsupervised classification procedure with the image interpretation procedure. Two well geo-referenced Landsat 7 ETM+ images, i.e., 16

April and 18 May 2001, with a spatial resolution of 30 m for visible bands, were utilized.

4.1.2 Methods

A subset of District 1 using false color composite (FCC) was created after geo-referencing the image using several ground control points (GCP) with root mean square error (RMSE) of less than 1 pixel size. Then an unsupervised classification algorithm was used to generate 40 spectral classes of land use for the entire District 1. This large number of spectral classes was used to minimize the number of classes that relate to more than one land-use classification. The spectral classes were later used to create nine land use classes utilizing ground truth data, knowledge of the study area, and visual interpretation of the images. These nine land-use classes were validated against ground truth data collected on the satellite overpass day.

Most of the comprehensive ground truth campaigns for measurement of crop parameters at 50 randomly-distributed fields were taken the same day as the image acquisition while some were taken one to two days before or after image acquisition. The ground truth campaign about the land use was carried out at 15-day intervals during the whole dry season of 2001, and this information was utilized in evapotranspiration (ET) estimation through remote sensing throughout the cropping season. The campaign includes information like crop type, crop height, field size, planting methods, and comments about the surrounding area of the field using handheld Global Positioning System (GPS). Information about all water bodies, natural vegetation, and urban areas were also collected during that ground truth campaign.

It should be noted that this study has a limitation. Only two (2) high-resolution satellite images covering the entire District 1 were available during the last part of the dry season 2001. Land-use classification through remote sensing can control the NIA's weekly monitoring activity over space and time. It would have been ideal to estimate different land-use classes if high-resolution images like Landsat 7 or ASTER representing different periods of dry season 2001 had been available. Since it was not possible due to cloud coverage in the early part of the dry season, this study instead provides a comparison of the rice area based on the NIA records with that determined by the remote sensing method.

4.1.3 Results and discussion

The major land-use classes found in District 1 (shown in Figure 4.1) are: rice, upland crops (different kind of vegetables), bare fields (harvested rice), natural vegetation (forest and trees), settlements, water bodies (small check dams, river, and fish ponds), clouds and others (roads, small canals, and uncultivated land).

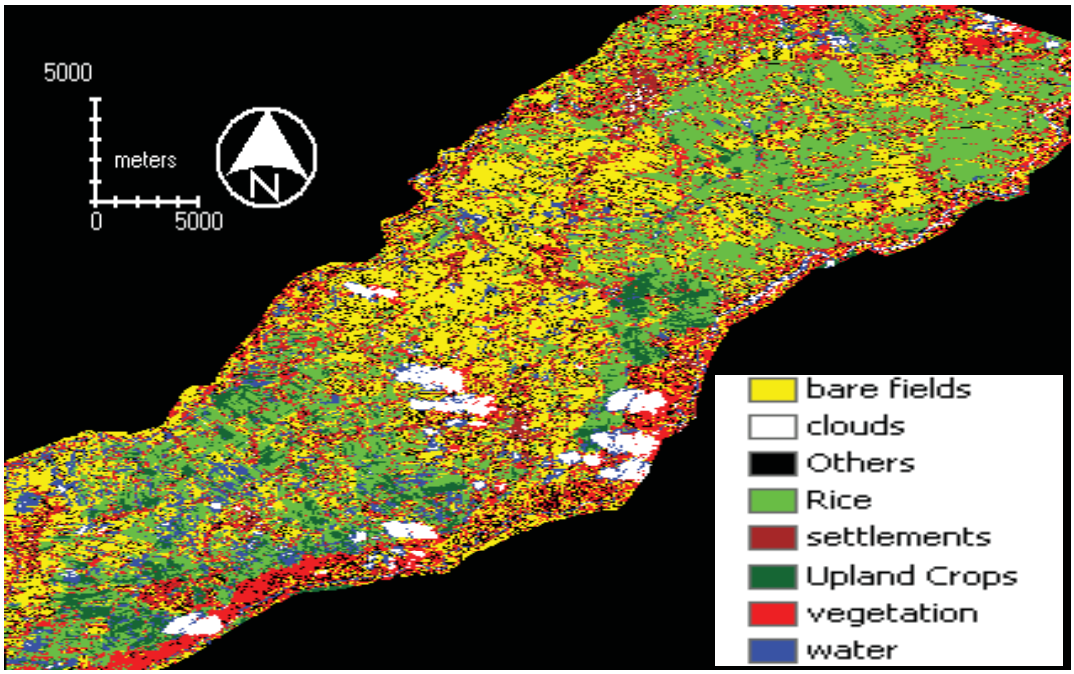

Figure 4.1: Land-use classification maps of District 1, 16 April 2001

For the purpose of this study, District 1 was divided into five (5) spatial parts, i.e., TRIS-Lower, SDA-A, SDA-B, SDA-C, and SDA-D (a brief description is given in the next section). This division was derived from NIA's initial subdivision of District 1 into 3 zones and several sub-zones that cover 88 farmer-irrigators associations (FIA) for better management of the irrigation system.

NIA's weekly data on the rice-growing area was compared with those derived from satellite images using remote sensing on 16 April and 18 May 2001 (Table 4.1). Based on this comparison, the rice-growing area that was measured through remote sensing is significantly different from the NIA-recorded area for all 5 spatial scales and time references. It should be noted that the total program area of rice crops is the same for both the NIA-reported rice area was 87% (14766 ha) of the total program area on 16 April 2001 while the remote sensing results showed that only 50% (8357 ha) was under

rice cultivation. The ground truth survey, which revealed that most of the rice farms are found in SDA-A and SDA-B, verified the findings from remote sensing. It also showed that many farmlands in the tail end of TRIS-Lower (Lateral F), in SDA-C and SDA-D were growing short-duration upland crops (water melon, vegetables like tomatoes, onions, egg plant, chili and white squash) during the dry season due to water shortage.

Table 4.1: Land-use classes in District 1 (in hectares)

Section	Program rice area[1]	NIA-monitored rice[2]	Remote sensing[3]							
			Rice area	Bare rice fields	Upland crops	Vegetation	Clouds	Settlement	Water body	Others
16 April 2001										
TRIS-L	8599	6729	4430	3258	430	779	124	983	334	826
SDA–A	877	830	290	587	69	83	79	123	61	154
SDA–B	1311	1230	189	1026	9	233	253	216	129	241
SDA–C	1911	1794	1027	715	218	338	31	257	230	199
SDA–D	4346	4113	2421	2300	898	1460	134	760	1176	724
District 1	17044	14766	8357	7886	1624	2893	621	2339	1930	2144
18 May 2001										
TRIS-L	8599	222	575	7255	395	750	-	963	495	783
SDA–A	877	15	83	840	47	93	-	125	68	190
SDA–B	1311	2	95	1323	57	233	-	230	82	275
SDA–C	1911	2	153	1521	82	309	-	253	214	481
SDA–D	4346	10	859	4567	264	1510	-	758	1183	732
District 1	17044	251	1765	15506	845	2895	-	2329	2042	2461

[1]Refers to the total area planted with rice crops.
[2]Refers to the rice crop standing in the field at the end of week (16 April and 18 May).
[3]Refers to the different land uses measured through RS.

The reliability of the NIA-recorded data is questioned because most of the time, the data for harvested rice area at a particular FIA level was more than the programmed rice area of that particular FIA. In another instance, NIA records showed that on 18 May 2001, all but two 2% of the rice crop was harvested, while remote sensing results showed that 10% of the program area still had standing rice crops. Field investigation showed that in the SDA-C area, the last rice harvest took place on 29 May. It was also noted that the NIA records have limited information. For example, while it had no record of the total land area under upland crops, remote-sensing results provided information that 10% of the area was under upland crops on 16 April 2001.

Overall, it can be said that the unsupervised classification method to estimate the different land-use area through remote sensing is practical and yields more accurate results than the method involving human monitoring but no temporal coverage.

4.2 Evapotranspiration

Evaporation is the loss of water in the form of vapor from the earth surface to the atmosphere and transpiration is the vaporization of water through the stomata of the living plants. It is very difficult to separate transpiration from vegetation and direct evaporation from the soil and small water surfaces. Thus, evapotranspiration (ET) is commonly used to describe water loss from the two processes. ET accounts for an average of 60% of the precipitation from all continents (Brustaert 1982). In tropical regions, up to 90% of the water flowing through a river basin may be used in the evaporation process (Jensen 1990).

Research has been undertaken in the past to estimate reference evapotranspiration (ET_o) from meteorological data (see Allen et al. 1998, for review) and convert it to actual evapotranspiration (ET_a). However, most methods used in estimating ET_a based on meteorological data generate only point values that are not representative of larger areas. ET_a is the most difficult component to measure in the field and its estimation through remote sensing has attracted many scientists for the last 20 years (Jackson et al. 1977; Seguin and Itier 1983; Moran et al. 1994; Kustas and Norman 1996 and Bastiaanssen et al. 1998).

Satellite remote sensing is a powerful means to provide ET measurement at a wide range of spatial scales ranging from individual pixels to an entire raster images that may cover a whole river basin. Remote sensing methods use surface reflectance and radiometric surface temperature from satellite spectral data in combination with ground based meteorological data to solve the energy balance equation and estimate evaporation from local to regional scales. These satellite radiances are related to ET in two steps. First, the surface parameters such as surface albedo, surface emissivity, surface temperature and normalized difference vegetation index (NDVI), are derived. Second, these surface parameters together with measured field data are used to solve the energy balance and ET_a is taken as a residual term. Since satellite data are obtained at the top of the atmosphere, corrections for atmospheric interference have to be made. The corrections are based on information on the atmospheric properties (e.g., temperature, relative humidity and wind speed) at the satellite overpass time and the use of radiative transfer models. However, simple correction procedures can be used in the

absence of atmospheric information. For instance, surface parameters could be measured at a few locations to calibrate the satellite-derived surface parameters.

Remote sensing methods for estimation of ET can be grouped into three major classes according to their complexity (Kustas and Norman 1996): (i) Statistical/semi-empirical methods (Jackson et al. 1977; Seguin and Iteir 1983). These methods directly relate the difference between satellite-observed surface and air temperatures to ET. They are relatively simple and require few input data. Apart from surface temperature, all the other input variables are assumed spatially constant. The application of the statistical methods is limited to homogeneous fields or regions only. (ii) Physically-based analytical approaches (Carlson and Buffman 1989; Diak and Whipple 1993). With these methods, net radiation, soil heat flux and sensible heat flux are evaluated separately, and latent heat flux is determined as a residual in solving an energy balance equation. (iii) Numerical models (Sellers et al. 1992; Carlson et al. 1995). These methods continuously simulate the surface energy flux exchanges by solving numerical equations of the energy and mass flow processes in the soil vegetation-atmosphere system. Many input parameters describing soil-vegetation-atmosphere system properties are required, but are seldom available in tropical watersheds. In view of the above-mentioned merits and drawbacks of different ET measurements through remote sensing, a physically based method, i.e., SEBAL (Surface Energy Balance Algorithm for Land) developed by Bastiaanssen et al. (1998), was applied on a near real time basis to estimate seasonal actual evapotranspiration (ET_s) in the study area.

A brief description of SEBAL and its application is given in ASTER article (Section 4.2.1), while sections 4.2.2 and 4.2.3 discuss the application of SEBAL for Landsat 7 ETM+ and MODIS. Section 4.2.4 discusses crop-water deficit using MODIS and Landsat sensors on the same overpass day and Section 4.2.5 the comparison of all three (MODIS, Landsat 7 and ASTER) sensors for the same study area. The final Section 4.2.6 discusses the estimation of seasonal actual evapotranspiration (ET_s) using remote sensing.

4.2.1 Evapotranspiration estimation using TERRA/ASTER Sensor: A case study in District 1 of UPRIIS, Central Luzon, Philippines1

Abstract: Evapotranspiration is the most important component in water balance studies. Remote sensing techniques for the estimation of ET have tremendously increased since 1990. Recently, the ASTER sensor (on board of the TERRA satellite), which provides a high spatial resolution image, free of charge, has been launched for monitoring land-surface properties. This study aimed to test the feasibility of using ASTER L1B data for ET_a assessment.

The Surface Energy Balance Algorithm for Land (SEBAL) was applied to ASTER sensor for the estimation of evapotranspiration in District 1 of UPRIIS. All pre-processing and processing steps of L1B data were discussed in detail for SEBAL. The ET_a was computed during satellite overpass and integrated for 24 hours on a pixel-by-pixel basis. Due to the cloud cover in the whole dry season 2001, only one image (02 February 2001) could be processed.

Comparison of ET derived from weather data collected at 2 meteorological stations in District 1 using the modified Penman-Monteith method found close relationship with ET estimation by SEBAL. From the findings presented, it can be concluded that ASTER L1B data can be used for the computation of ET_a studies in the tropical climate but with necessary caution.

4.2.1.1 Introduction

The world's thirst for water is likely to become one of the most pressing resource issues of the 21st century. A clear understanding of all the terms of the water balance is necessary to determine all the possible water saving measures. One of the dominant aspects of the water balance is ET_a, which is one of the most difficult components to measure in the field. A number of studies have been undertaken in the past to estimate ET_o from meteorological data and convert it to ET_a. The major disadvantage in ET_a estimation based on meteorological data is that most methods generate only point values, which are not representative of larger areas. Remote sensing can provide ET_a estimation on a pixel-by-pixel basis

[1] Hafeez MM and Chemin Y (2003). "Evapotranspiration Estimation Using TERRA/ASTER Sensor: A Case Study in District 1 of UPRIIS, Central Luzon, Philippines." Canadian Journal of Remote Sensing (CJRS), Canada. 11 pages (in press).

The use of remote sensing techniques towards the estimation of the water evaporation component of the water balance by solving the energy balance of thermodynamics fluxes at the surface of the earth has tremendously increased since 1990. Various methods for ET_a estimation have been developed by combining satellite images and ground meteorological data for large areas (Vidal and Perrier 1989; Choudhury 1994; Granger 1997). Another method for estimating ET_a is Surface Energy Balance Algorithm for Land (SEBAL) by Bastiaanssen et al. 1998. It is a thermodynamically based model, using the partitioning of sensible heat flux and latent heat flux.

Amongst all literature on SEBAL, the following different sensors were studied. Originally, Bastiaanssen developed SEBAL in Spain and Egypt with Landsat TM 5 in 1995. Further applications to irrigation performance were later found for the same sensor in Argentina (Roerink et al. 1997). Water consumption of large irrigation systems has also been addressed with NOAA AVHRR in Pakistan (Bastiaanssen et al. 1999; validation in Bastiaanssen et al. 2002). Farah (2001) studied modeling of evaporation under various weather conditions in the Navaisha Basin, Kenya. His results extended SEBAL calculations of NOAA AVHRR under clouds with a Penman-Monteith approach supported by a Jarvis-Stewart type model. Combinations of Landsat and NOAA are found in Timmermans and Meijerink (1999), where Landsat TM 5 was used, and in Chemin and Alexandridis (2001), where Landsat 7ETM+ was used.

The TERRA satellite was launched in December 1999, and was activated for science operations in February 2000. The TERRA mission carries two potentially useable instruments for estimation of ET: ASTER and MODIS. ASTER stands for Advanced Spaceborne Thermal Emission and Reflection Radiometer, which started monitoring global environment changes in March 2000. ASTER is the only high spatial resolution instrument on the TERRA platform with theoretical repeating cycle of 16 days around the earth and covering an area of 60 x 60 km^2. ASTER images are freely available and easily downloadable from the web (http://asterweb.jpl.nasa.gov). Only one cloud-free image (02 February 2001) covering District 1 in the entire dry season of 2001 was available. There is a lot of potential to use ASTER images for detailed water consumption studies due to high spatial resolution and free availability of images.

4.2.1.2 Study area

The Philippines is an agricultural country with a total land area under crop cultivation of 13 million hectares. Irrigated rice is about 61 % of the 3.4 million hectares utilized for rice production (IRRI 1997). UPRIIS covers a total area of 102,591 hectares and is important rice producing area in Nueva Ecija, the latter being considered the "Rice Bowl" of Central Luzon. UPRIIS is divided into 4 districts, and gets its water from the Pantabangan Reservoir, which is operated by the National Irrigation Authority (NIA).

The study area, "District 1" is about 34,000 ha and is divided into a northern (with San Jose city) and a southern part (with the main cities Santo Domingo, Quezon and Licab). The diversion Canal 1 originating from the Pantabangan Dam is the major source of water for the whole District 1. The Talavera and Ilog Baliwag Rivers form the boundaries of District 1. The most common land use is double cropping of rice by the transplanting method though direct wet seeding is becoming increasingly popular. The soil texture ranges from moderately coarse to very fine (loamy sand to massive clay). The climate is characterized by two pronounced seasons, a dry season from November to April with an average rainfall of 170 mm and a wet season from May to October with an average rainfall of 1730 mm. This study concentrated on the dry season of 2001 (November to May).

The main objective of this study is to determine the feasibility of using SEBAL with L1B ASTER data. This sensor is still in the science mode, and disclaimers on its use mention the non-reliability of the calibration functions. It is proposed that results be validated with meteorological data collected in District 1.

4.2.1.3 Methodology

The ASTER sensor on board the TERRA has 14 spectral bands ranging from 15-90 m spatial resolution (Table 4.2). A fifteenth band is a backward view of the NIR (15 x 15 m in the 0.76 to 0.86 μm) for stereoscopic imaging. A False Color Composite (FCC) of the ASTER image of the study area is shown in Figure 4.2.

The designed characteristic of the sensor provides 5 bands in the thermal Infrared (TIR) window, enabling enhanced accuracy in temperature radiances on top of atmosphere calculations. The ASTER Science Team uses the TIR bands to enable the generation of brightness temperature at the sensor, or product AST04 (Alley 1999).

With a spatial resolution of 90 x 90 m, the thermal bands of ASTER are larger than its equivalent Landsat 7ETM+, which has a 60 x 60 m pixel size.

Table 4.2: Overview of the TERRA/ASTER sensor

Sub-systems	Number of bands	Spectral range (μm)	Spatial resolution (m)
VNIR	3 (+ 1 in double)	0.52 up to 0.86	15x15
SWIR	6	1.60 up to 2.43	30x30
TIR	5	8.125 up to 11.65	90x90

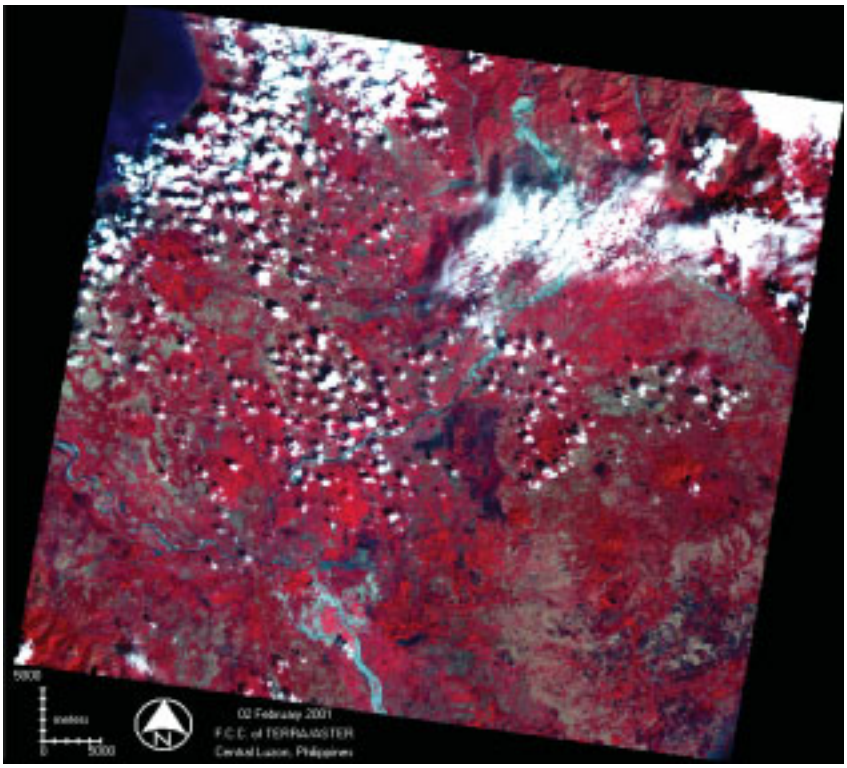

Figure 4.2: False Color Composite of Central Luzon from TERRA/ASTER

Alexandridis and Chemin (2001) stated that water consumption applications in irrigation systems of China are still under the threshold of the 125 x 125 m pixel size. This ceiling corresponds to the highest mean local variance of ET observed in the rice field areas. Thus, the application of ASTER thermal bands to calculate the ET is very well applicable in irrigated areas with field sizes larger than the Chinese fields, as in the case of Central Luzon.

The L1A image was acquired by ftppull (file transfer protocol) from the Eros Data Center Redhook Internet website (http://redhook.gsfc.nasa.gov/~imswww/pub/imswelcome/plain.html). The data were then sent to the Earth Remote Sensing Data

Analysis Center (ERSDAC, Japan) to be preprocessed into the L1B level product. L1B was found to be radiometrically calibrated and geometrically co-registered. Extraction of the binary file was performed for 3 visible near infrared ('vnir') bands (1, 2, & 3N), all 6 shortwave infrared ('swir') bands (4, 5, 6, 7, 8, & 9) and all 5 thermal infrared (TIR) bands (10, 11, 12, 13 & 14), respectively.

Rotation, pixel coordinate and size were provided to the image after the HDF-file information was gathered, finishing the geo-referencing by specifying a coordinate system in UTM/wgs84/zone51. The gains and offsets (found in the metadata of the HDF file) for respective bands were applied for the conversion of digital numbers to radiance of bands.

Calculation of pre-processing parameters for SEBAL included the Normalized Difference Vegetation Index "NDVI" (band 2 and band 3N), emissivity, broadband surface albedo and surface temperature. The similar range and description level of the NDVI was found as in Landsat 7ETM+, making it reasonable to consider it a surface value. The broadband albedo was calculated using weighing factors of all visible, near-infrared and short-wave infrared bands of ASTER. The Temperature Emissivity Separation (TES) algorithm is used to extract the surface temperature and 5 emissivities from the 5 thermal infrared bands of the ASTER data. The TES provides an accurate estimate of surface temperature within about ± 1.5° K and emissivities within about ± 0.015 (Gillepsie et al. 1998). It makes use of an empirical relation between the range of observed emissivities and their minimum value.

Energy balance

The energy balance was summarized at an instant time *t* (at the time of satellite overpass) by the following equation (Bastiaanssen 1995):

$$Rn = G_0 + H + \lambda E \qquad (W/m^2) \qquad \textit{Equation 4.1}$$

where Rn =net radiation of the earth surface (W/m^2);
G_0 =soil heat flux (W/m^2);
H =sensible heat flux (W/m^2); and
λE =latent heat flux, or the energy necessary to vaporize water (W/m^2).

Net radiation

Even though net radiation monitoring technology has become well-affordable, it is still difficult to find appropriate instruments for uniformly distributed good quality data in some developing countries of Asia, especially in near-real time of data collection. To improve the non-dependency on ground data, a general equation was, therefore, used. Net radiation is the electromagnetic balance of all incoming and outgoing fluxes reaching and leaving a flat surface (considered Lambertian in SEBAL). It can be described physically as:

$$Rn = (1-\rho_0)\times\left(K^{\downarrow}\right)+L^{\downarrow}-\left(\varepsilon_0\sigma T_0^4\right)-(1-\varepsilon_0)\times L^{\downarrow} \qquad (W/m^2) \qquad \textit{Equation 4.2}$$

where $K^{\downarrow}$ = incoming short-wave solar radiation *(W/m²);*
$L^{\downarrow}$ = incoming broadband long-wave radiation *(W/m²);*
ρ_0 =surface albedo;
ε_0 = surface emissivity*;*
σ = Stefan-Boltzman constant *(W/m²/K⁴);* and
T_0 =surface temperature *(K).*

Soil heat flux

The semi-empirical equation for soil heat flux (Bastiaanssen, 1995) is given below:

$$G_o = R_n \times \left[\frac{(T_0 - 273.15)}{\rho_0}\right] \times \left(0.0032 r_0 + 0.0062 r_0^2\right) \times \left(1 - 0.978 \times NDVI^4\right) \qquad (W/m^2) \qquad \textit{Equation 4.3}$$

where T_0 = surface temperature (K);
ρ_0 = surface albedo *(-);*
r_0 = average daytime surface reflectance *(-);*and
NDVI = Normal Difference Vegetation Index.

The empirical relationship between r_0 and ρ_0 at 10.00 a.m. (local time of satellite overpass) is $\rho_0 = 0.9\ r_0$ (Bastiaanssen, 1995).

Sensible heat flux

Sensible heat flux is part of the energy balance of a substance and is proportional to the substance's temperature. Physical formulation of H is based on the theory of mass transport of heat and momentum between the surface and the near surface environment.

$$H = \frac{\rho_{air} \times C_p \times dT_{air}}{R_{ah}} \qquad (W/m^2) \qquad \textit{Equation 4.4}$$

where ρ_{air} = atmospheric air density *(Kg/m^3);*
C_p = air specific heat at constant pressure *(J/Kg/K);*
dT_{air} = near surface air temperature difference (K)*; and*
R_{ah} = aerodynamic resistance to heat transport *(s/m).*

Because one component of R_{ah}, namely the Monin-Obukov Length (L, as shown in Figure 4.3), requires the Sensible Heat Flux (H) as input, an iterative procedure is run to approximate parameters of the sensible heat flux equation. The whole interest of iteration is to refine the value of a parameter. Here, the most uncertain variable (but not the only one to be recalculated) is dT_{air}, which is the near-surface air temperature difference. The iterations focus on refining the image processing of the sensible heat flux (H) by repeating the determination of the surface air temperature difference (dT_{air}) as a linear function of the digital elevation model (DEM) adjusted soil surface temperature *(T_0_dem)* Other variables like the atmospheric air density and the aerodynamic resistance to heat transport are also recalculated in the same process with adjusted input parameters (Figure 4.3). To calculate the first surface air temperature difference for the "hot" pixel (i.e., where the latent heat flux is assumed null, after Bastiaanssen and Sakthivadivel 1999), a first estimation of the air density was performed. This information was produced by generalizing meteorological data of relative humidity and maximum air temperature from two meteorological stations in District 1. A difference of 8 % was found between the air density estimation from the ground and the first estimation of the Tasumi et al. (2000) method, based on atmospheric pressure relationship to elevation. The set of iterations for sensible heat flux calculations is also summarized in Figure 4.3 (note the initial calculations of dT_{air} and R_{ah} being set up from specific calculations after Bastiaanssen 1995).

The variations arising in the dT_{air} calculations from the first iteration compared to the other ones are due to the adjustment of R_{ah}, having psychometric buoyancy parameters for heat and momentum transport (ψ_h and ψ_m) that are recalculated accordingly during each new cycle. Those iterations, approximating the sensible heat flux values, were conducted three times. Hafeez et al. (2002) observed that the Tasumi et al. (2000) method stabilized the air-soil temperature difference slower than the method used by Bastiaanssen (1995). Thus, it was still preferred over the earlier method, having the comparative advantage of a simpler Monin-Obukov Length to surface roughness parameterization that enhances the automation level while keeping the output quality high over the drawback of a larger iteration number. These results were also found while comparing experiences from other sensors (NOAA-12 in Bastiaanssen et al. 1999; NOAA-14 in Ahmad and Chemin 2000; NOAA-15 in Chandrapala and Wimalasuriya 2001; Landsat 7ETM+ in Alexandridis and Chemin 2001). It is a practical constraint to make SEBAL operational, since it requires manual sampling of pixel values of the previous iteration output image files before the next iteration can be launched. Automation in pixel data collection (once the "hot" pixel is identified) of the results would lead to resolution of this constraint.

Evaporative fraction

The ET was calculated in SEBAL from the instantaneous evaporative fraction, Λ, and the daily averaged net radiation, R_{n24}. The evaporative fraction, Λ, was computed from the instantaneous surface energy balance at the moment of satellite overpass for each pixel:

$$\Lambda = \frac{\lambda E}{R_n - G_0} = \frac{\lambda E}{\lambda E + H_0} \qquad (W/m^2) \qquad \textit{Equation 4.5}$$

where λE = latent heat flux (or the energy allocated for water evaporation); &
Λ = ratio of actual to potential ET (as interpreted in irrigated areas); it is dependent on the atmospheric and soil moisture conditions equilibrium.

The original assumption in SEBAL tends to show that Λ is rather preserved during daytime hours, while the H and λE fluxes vary to a large extent. The difference between instantaneous evaporative fraction at the moment of satellite overpass and the

evaporative fraction derived from the 24-hour integrated energy balance is considered marginal, and can be neglected (Brutsaert et al. 1992). A recent study mitigates such assumptions, finding diurnal variations to be large (Farah 2001). Farah concluded, "*a good relationship between Λ_{mid} values (12.00 to 13.00 hrs) and the average day Λ was obtained with R^2 of 0.74 at the two experimental sites"*, keeping SEBAL unchanged on this matter. However, it is added that the actual timing of mid-morning or mid-afternoon satellites are actually providing an accuracy that can deviate by as much as 10 % of the real values. In the opinion of the author, it is a well-known weak point of SEBAL, which needs some fundamental researches and modeling to enhance the daily integration of instantaneous ET_a estimates.

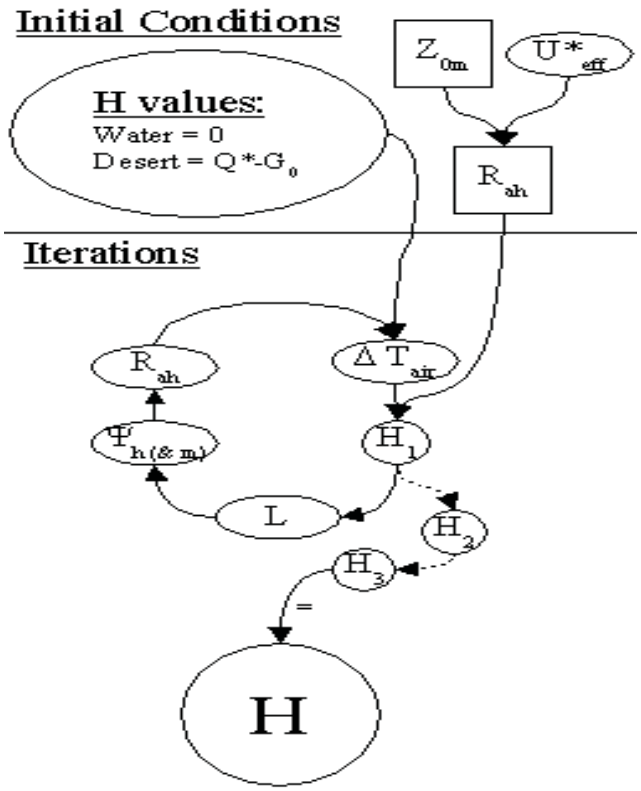

Figure 4.3: Overview of the sensible heat flux calculation method

Evapotranspiration

Calculation of ET included the transformation of daily net radiation (R_{n24}) from W/m^2 to mm/day by the T_0 dependent latent heat of the vaporization equation.

$$ET_{24} = \Lambda \times \left[R_{n24} \times \left((2.501 - 0.002361 \times T_0) \times 10^6\right)\right] \quad (mm/day) \quad \textit{Equation 4.6}$$

where ET_{24} = daily ET_a (mm/day);
R_{n24} = average daily net radiation (W/m^2); and
T_0 = surface temperature (°C).

4.2.1.4 Results and discussion

The main output of SEBAL is the partitioning of the energy balance, referred to as the evaporative fraction (Figure 4.4, left-side image). The Λ values range from 0.05-0.95. A directly derived product is the daily ET_a, as shown in Figure 4.4 (right-side image). The ET values range from 0.35-5.35 mm/day (Figure 4.5).

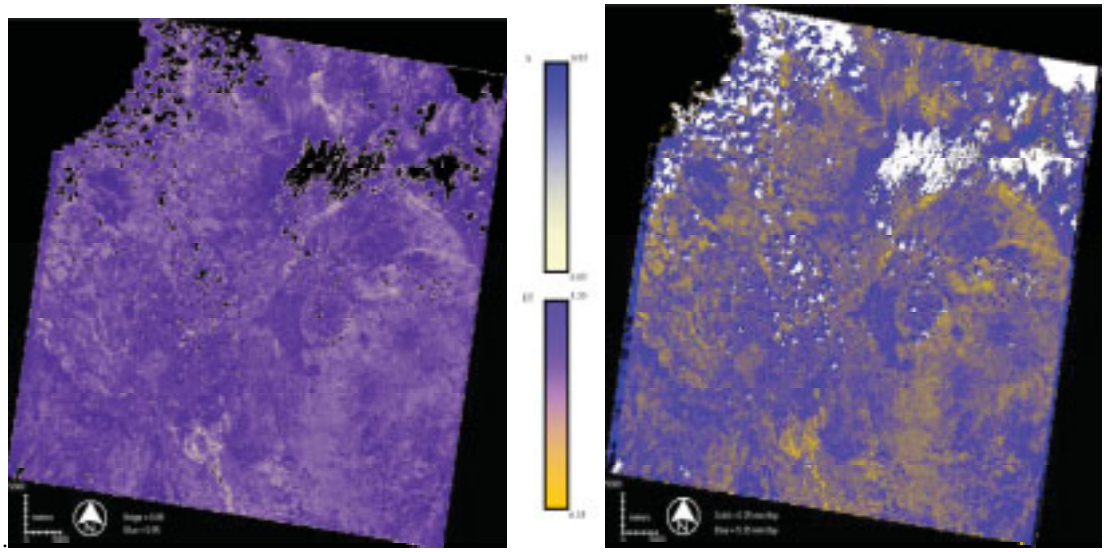

Figure 4.4: Evaporative fraction (-), and actual evapotranspiration (mm/day)

The histogram of the ET_a shows a mode around 3.2 mm/day, with extremes of 0.35 and 5.35 mm/day. The area covered is mono-modal with some peak features in 2.34 mm/day @ 50 km^2, 3.2 mm/day @ 75 km^2, and 3.71 mm/day @ 60 km^2. On a cumulative area curve of the same histogram, these three points would be translated into inflection points.

A sample of rice field pixels was averaged from selected irrigation systems located on the southern part of the image corresponding to District 1. Meteorological stations are within a distance of 1-10 km from the daily ET_a pixels sampled for comparison. The average value of the daily ET for these fields, and E_{pan} estimates from the two meteorological stations located nearby are shown in Table 4.3.

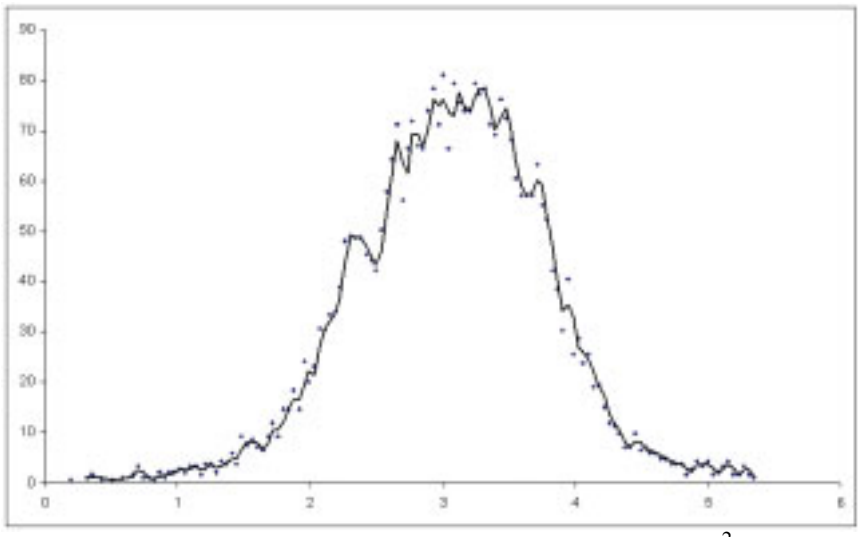

Figure 4.5: Histogram of daily ET_a (mm/day) per area covered (km^2)

Table 4.3: Comparison of ET_o, ET_c, E_{pan} and daily ET_a in ASTER

Location of meteorological stations	E_{pan} met. stations (mm/day)	ET_o Penman Monteith (mm/day)	ET_c (Kc=1.05) (mm/day)	Daily ET_a rice fields in ASTER (mm/day)
PAGASA, Munoz (15° 43' N, 120° 54' E)	5.3	4.25	4.46	4.20
PhilRice, Maligaya (15° 39'N, 120° 53' E)	4.7	3.57	3.75	

The distance between two meteorological stations is only about 10 km, but E_{pan} readings at these stations differ considerably, while all other climatic parameters are close to each other. The Class A Pan (circular, 120.7 cm diameter, and 25 cm deep) mounted on a wooden open frame platform was used at both meteorological stations within District 1. The possible reasons for this variation in E_{pan} readings (11%) are lack of accurate measurement and poor maintenance of the pans, as observed during visits to these meteorological stations. The ET_a values determined from ASTER image are 20.7% and 10.5% less than the meteorological data of water evaporation. These results match very well the expectations on the difference of ET values between open water bodies and rice crops.

With reference to the daily ET-values histogram (Figure 4.5), the E_{pan} readings correspond to the last upper part of the ET_a axis. This part has a nearly flat slope, and can be bounded between 4.8 and 5.35 mm/day. It can be assumed that it corresponds to

the highest ET rates practically found on the image of 02 February 2001 and correlates almost perfectly to the E_{pan} measurements.

Application of the modified Penman-Monteith method (Allen et al. 1998) for calculation of the reference ET (ET_o) from the meteorological stations data showed a difference to the remote sensing data of +1% and -15%. Adjustment for the crop coefficient (K_c) of rice at the end of the tillering stage with a corresponding K_c factor of 1.05 for general rice crops from the same author give also significant results. The differences observed are of +6 % and –11 %, with mean rice plant height of 27 cm on 50 ground-sampled fields and maximum height reaching 36 cm. These results confirmed the ET_o and ET_c calculations from ground data.

4.2.1.5 Conclusion

The ASTER instrument, on board the TERRA platform, is a newly launched Landsat-type sensor with a high spectral resolution. While still being in the science mode, Level 1B images are widely available for scientific audit out of the development team. Pre-processing of the Level 1B (L1B) ASTER data was made possible by using a HDF file viewer, displaying the metadata contents of the HDF-type format. Most of the information necessary to calibrate the geometry and the radiometry of the file was searched manually.

Calculation of the evaporation through the SEBAL algorithm was done according to its original framework, but the sensible heat flux determination incorporated recent developments from the studies of the University of Idaho carried out by Tasumi et al. in 2000. Validation from meteorological data found accurate matching with remotely sensed daily ET. Results are encouraging and further use of ASTER, even in L1B format, should be considered for such applications. This new sensor will hopefully improve the temporal availability of Landsat family sensors, resulting in high spatial and temporal ET integration over irrigation seasons.

4.2.2 Estimation of spatially-distributed evapotranspiration through remote sensing: a case study for irrigated rice in the Philippines[2]

Abstract: This study looks at the use of remote sensing to estimate spatially distributed ET_a from irrigated rice in UPRIIS in Central Luzon. SEBAL was used to compute ET_a from three Landsat 7 ETM+ images acquired during the second part of the crop growth period in the dry season 2001. Ground-truth data for the calibration of SEBAL was obtained during satellite overpass. The outputs of the SEBAL computations were geo-referenced maps and frequency distributions of daily ET_a on the days of satellite overpass. The calculated ET_a values were some 6% lower than potential rice ET values calculated with the modified Penman-Monteith method using weather data from two meteorological stations in the area. It was concluded that SEBAL provides realistic ET_a estimates for irrigated rice over spatially extended areas in the tropics.

4.2.2.1 Introduction

Water resources for agriculture are becoming increasingly scarce and ways must be sought to optimize the use and efficiency of irrigation systems (Postel 1997). This is especially true for irrigated rice systems that account for more than 50 % of the total irrigation water volume in Asia (Barker et al. 1999). Rice is the most important staple food in Asia where it provides 35-80 % of the total calorie uptake (IRRI 1997). More than 75 % of the rice supply comes from 79 million ha of irrigated land. Thus, the present and future food security of Asia depends largely on the irrigated rice production system. The optimization of irrigation systems requires knowledge on the water balance: the amounts of inputs (rainfall, irrigation, run-on, lateral inflow) and outputs (evapotranspiration, percolation, seepage, run-off, drainage). Moreover, this knowledge should be available at different spatial scale levels.

Irrigation systems usually consist of a complex network of irrigation and drainage canals with a considerable amount of water re-use (e.g. Zulu et al. 1996). Water outflows from one particular section of an irrigation system may be re-used in another section by damming drains or pumping water from creeks (or both). Therefore,

[2] Hafeez MM, Chemin Y, Bouman BAM and N van De Giesen (2002) "Estimation of Spatially-Distributed Evapotranspiration through Remote Sensing: A case Study for Irrigated Rice in the Philippines." A paper presented during the Conference on Water Wise in Rice Production, International Rice Research Institute (IRRI), Los Banos, Philippines, 8-12 April 2002 (Page 347-356).

a number of studies focus attention on the quantification of the water balance of irrigation systems at different scale levels (e.g., Dong et al. 2001; Keller et al. 1996; Seckler 1996). The measurement of surface in- and outflows is relatively straightforward (Dong et al. 2001). However, the measurement of ET poses more problems. Many methods exist for estimating ET using meteorological data (see Allen et al. 1998, for overview), but these are based on point data, which do not provide good estimates of ET for larger areas. Moreover, most of these methods estimate ET_c or ET_o and not ET_a. The problem of ET_a estimation over large areas can be solved by using imagery obtained with satellite remote sensing. Bastiaanssen (1995) and Bastiaanssen et al. (1998) developed the thermodynamically based SEBAL to estimate ET_a from agricultural areas using optical satellite imagery. However, SEBAL has not yet been tested for rice-based cropping areas in the tropics. In this paper, we present results of the application of SEBAL to estimate ET in a multi-scale water-balance study of an irrigated rice production system in the Philippines. The specific objectives of the study reported here are to evaluate the performance of SEBAL in tropical irrigated rice areas, and to compute the spatial variation in ET within a large-scale surface irrigation system.

4.2.2.2 Study area

UPRIIS in Central Luzon (Figure 4.6) covers an area of 102,000 ha and is divided into four Districts. It gets its water from a combination of various run-of-the-river flows and the Pantabangan reservoir. There is a dry season from November to April and a wet season from May to October. The average annual rainfall is about 1900 mm, of which 90% falls in the wet season (Tabbal et al., 2002). Soils are Vertisols, Entisols and Inceptisols (USDA classification), and have typically silty clay, silty clay loam, clay loam, and clay textures. The average groundwater table depth is 0.5 m in the wet season and 1.5 m at the end of the dry season, although locally it can come up to 0.1 m and go down to deeper than 5 m. Double cropping of rice is the most common land use and UPRIIS produces an average of 63 million tons of rice every year. However, where water is scarce, upland crops such as onion, tomato, watermelon and maize are grown in the dry season.

The water-balance study focuses on District 1 that covers a total area of 28,205 ha including rice fields, upland crops, vegetables, roads, settlements and water bodies.

District 1 is bounded by the Talavera river on the east and the Ilog Baliwag river in the west, and consists of an upper part, called the Talavera River Irrigation System-Lower (TRIS-L), and a lower part, called the Santo Domingo Area (SDA). The TRIS-L receives its water directly from the main diversion Canal 1. Part of the water from the main diversion canal is diverted into the Sapang Kawayan creek, which also collects drainage water while it traverses TRIS-L. In the lower part of TRIS-L, the De Babuyan check dam raises the water level in the Sapang Kawayan creek and the water is diverted into the Santo Domingo main canal that irrigates the SDA. About 20 % of the farmers use pumps to draw water from shallow tube wells (or from drains and creeks) for supplementary irrigation. For the multi-scale analysis, the whole of District 1 was divided into five sections, based on the possibilities to monitor surface water in- and outflows (Table 4.4 and Figure 4.6):

Figure 4.6: District 1 and the five irrigation sections studied in UPRIIS

TRIS-L has 48 FIAs with an average size of 233 hectares. There are 12 small check dams, which capture internal drainage water. In 2001, farmers did not face water shortage, and planted rice according to the recommended cropping schedule. Only a few

farmers located at the tail end of Lateral F (near SDA) could not grow rice in the dry season because of water shortage.

Table 4.4: Sizes of the irrigation sections studied and their area under rice in the 2001 dry season

Section	Area (ha)	% Area of District 1	Rice area (ha)	% Rice area
District 1	28,205	100	17,045	60
TRIS-L	11,239	40	8,599	77
SDA–A	1,513	5	877	58
SDA–B	2,240	8	1,311	59
SDA–C	3,011	11	1,911	64
SDA–D	10,201	36	4,347	43

SDA-A is in the upper part of SDA. There are five FIAs with an average size of 175 ha. SDA-A receives water from laterals A and B and from two creeks coming out of TRIS-L. The De Buasao check dam is the origin of lateral A-Extra (A-x), which also supplies water to the lower part of SDA-A and to the upper part of SDA-D. The farmers far away from the main canal depend somewhat more on shallow tube wells for additional irrigation water than the farmers close to the beginning of the main canal.

SDA-B is the second smallest area. The major source of water is Lateral C, sublaterals of Lateral B and two creeks getting water from the Ilog Baliwag river. There are six FIAs with an average size of 373 ha. Water shortage forces farmers to get water either through pumping or by using illegal inlets along the Santo Domingo main canal. The Pajo check dam captures drainage water from farmers upstream and serves as a major source of water for SDA-C.

SDA-C is in the lower portion of the SDA. The laterals D, E, E-X, F, and G and two creeks (Pajo and Labong) are the main sources of water. There are seven FIAs with an average size of 273 ha. All farmers in SDA-C depend on pumping for additional supply of water. Normally, the farmers get surface water only when the upstream farmers do not need it. The cropping pattern depends totally on the availability of irrigation water and rice planting is about 2-3 weeks later than in TRIS-L. Santa Rita is the only check dam in SDA-C that captures drainage water in small creeks and serves as a major source of water for SDA-D.

SDA-D is in the lowest part of SDA. There are 22 FIAs with an average size of 198 ha. Because of water shortage in the canals, farmers do not grow rice in the dry season.

Also, the Irrigation Administration does not encourage farmers to grow rice because the dominant soil type is sandy loam, which has a high percolation rate. Only the farmers located near the canals and creeks plant rice using pumped groundwater as an additional source of water.

4.2.2.3 Materials and method

4.2.2.3.1 Satellite data

Three Landsat 7 ETM+ (Enhanced Thematic Mapper Plus) images were obtained from the second part of the dry season 2001: 16 April, 2 May, and 18 May. The ETM+ instrument of Landsat 7 is of the fixed "whisk-broom" type, having seven multi-spectral bands and one panchromatic band (Table 4.5). Orbiting at an altitude of 705 km, it registers spectrally filtered radiation from the sun-lit earth in a 183-km wide swath. Level 1G products are radiometrically and geometrically corrected to the user-specified parameters including output-map projection, image orientation, pixel (grid-cell) size, and resampling kernel. The gain and offset values for the images are provided in the header file. The geo-referencing of the images was done using the coordinates provided in the header file in UTM/WGS84/Zone 51.

Table 4.5: Characteristics of the Landsat 7 ETM+ sensor

Subsystem	Number of bands	Spectral range (μm)	Spatial resolution (m)
VNIR	4	0.45 up to 0.90	30x30
SWIR	2	1.55 UP TO 2.35	30x30
TIR	1	10.4 to 12.5	60x60
PAN	1	0.50 to 0.90	15x15

4.2.2.3.2 SEBAL-ET estimation

SEBAL is a thermodynamically based model, which partitions between sensible heat flux and latent heat of the vaporization flux (see Bastiaanssen 1995; Bastiaanssen et al. 1998; Tasumi et al. 2000 for the description of the model). Hafeez and Chemin (2003) give a detailed description of the calculation procedure followed in the application of SEBAL in this study. Pre-processing parameters required for SEBAL included the Normalized Difference Vegetation Index (NDVI), emissivity, broadband surface albedo and surface temperature. The NDVI was calculated from the spectral reflectance of the

red (band #3) and near-infrared (band #4) channels using equations developed by Bandara (1998). The surface emissivity was computed from the NDVI following the method of Van de Griend and Owe (1993). The broadband albedo was calculated using weighing factors of all visible, near-infrared and short-wave infrared bands.

The radiant temperature at the top of the atmosphere was computed from the inverse Planck function using the outgoing spectral radiance in band 6. Assuming that the internal calibration of the thermal bands of ETM+ is satisfactory, the calibration gain and offset provided with the L1G data can be used to generate the radiant temperature values. A thermal surface emissivity adjustment was used to adjust the surface temperature taking into account gray-body properties of the surface.

All essential meteorological data for solving SEBAL, like (hourly) temperature, humidity, wind speed and solar radiation at the time of satellite overpass were collected from two weather stations in District 1: PAGASA at Munoz (15° 43' N, 120° 54' E) and PhilRice at Maligaya (15° 39' N, 120° 53' E). Various vegetation parameters were also collected for SEBAL calibration across District 1.

Daily ET_a is calculated in SEBAL from the instantaneous evaporative fraction and the daily average net radiation. The latter has to be transformed from W m^{-2} to mm d^{-1} by inserting the temperature-dependent latent heat of the vaporization equation into the main equation:

$$ET_a = \Lambda \times \left[R_{n24} \times \left((2.501 - 0.002361 \times T_0) \times 10^6\right)\right] \quad (mm\ d^{-1}) \qquad \textit{Equation 4.7}$$

where ET_a = daily ET_a (mm d^{-1});
Λ = evaporative fraction (-);
R_{n24} = average daily net radiation (W m^{-2}); and
T_0 = surface temperature (°C).

The evaporative fraction is computed from the instantaneous surface energy balance at the moment of satellite overpass for each pixel:

$$\Lambda = \frac{\lambda E}{R_n - G_0} = \frac{\lambda E}{\lambda E + H_0} \qquad (-) \qquad \textit{Equation 4.8}$$

Where λE = latent heat flux (W m^{-2}); λ can be interpreted in irrigated areas as the ratio of actual over potential ET.
R_n = net radiation absorbed or emitted from the earth's surface (W/m^2);
G_0 = soil heat flux (W m^{-2}); and
H_0 = sensible heat flux (W m^{-2}).

4.2.2.3.3 Conventional ET estimation

Daily meteorological data were collected from the PAGASA and PhilRice weather stations, and used to calculate ET_0 using the modified Penman-Monteith equation (Allen et al. 1998). ET_0 was converted into potential rice evapotranspiration, ET_c, by multiplication with the crop coefficient K_c ($ET_c = K_c\ ET_0$). Based on the actual cropping calendar, the crop coefficients K_c for rice were 0.95 on 16 April, 0.85 on 2 May and 0.75 on 18 May 2001.

4.2.2.4 Results and discussion

Outputs of SEBAL are pixel-based, daily-average estimates of ET_a. Figure 4.7 gives a map of the ET_a for the whole of District 1 on 18 May 2001. Low ET_a values indicate areas where rice (or other crops) has been harvested and the soil is bare or covered with stubble. High ET_a values indicate areas where rice (or another crop) is still in the field and actively transpiring.

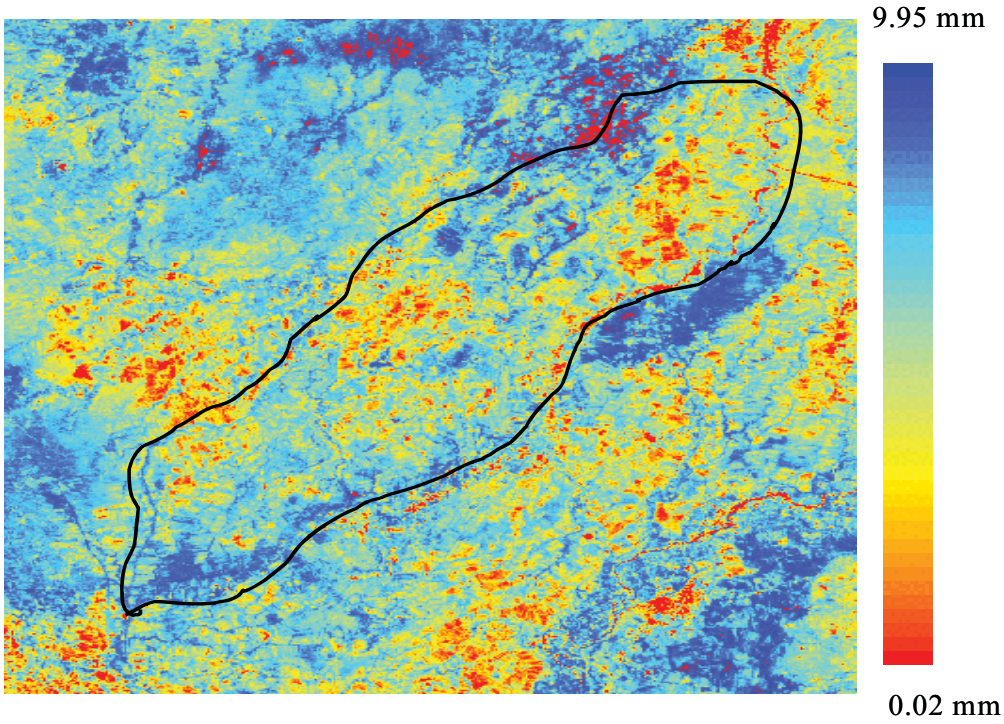

Figure 4. 7: Actual evapotranspiration ET_a for District 1 on 18 May 2001

Figure 4.8 gives the frequency distribution of the pixel-based ET_a values of District 1 for all three days of satellite overpass. ET_a ranges from 0.2-6.8 mm d^{-1} (16 April), 0.2-7.4 mm d^{-1} (2 May), and 0.2-7.3 mm d^{-1} (18 May). All three frequency distributions of ET_a are mono-model with peaks of 5.9 mm d^{-1} on a 589 ha area on 16 April, of 6.4 mm d^{-1} on 589 ha on 2 May, and of 6.6 mm d^{-1} on 589 ha on 18 May.-On 16 April, land use was relatively homogenous in the whole of District 1 because there was only one major crop (i.e. rice) planted at that time. On 2 May, there were two main land covers: bare fields after the harvesting of rice in the upper part of District 1 (TRIS-L), and ripening rice fields in the lower part of District 1 (SDA). On 18 May, the land cover was totally changed and only 20 % of the lower part of SDA was under rice cultivation, whereas the farmers in TRIS-L had sown short-duration upland crops like watermelon.

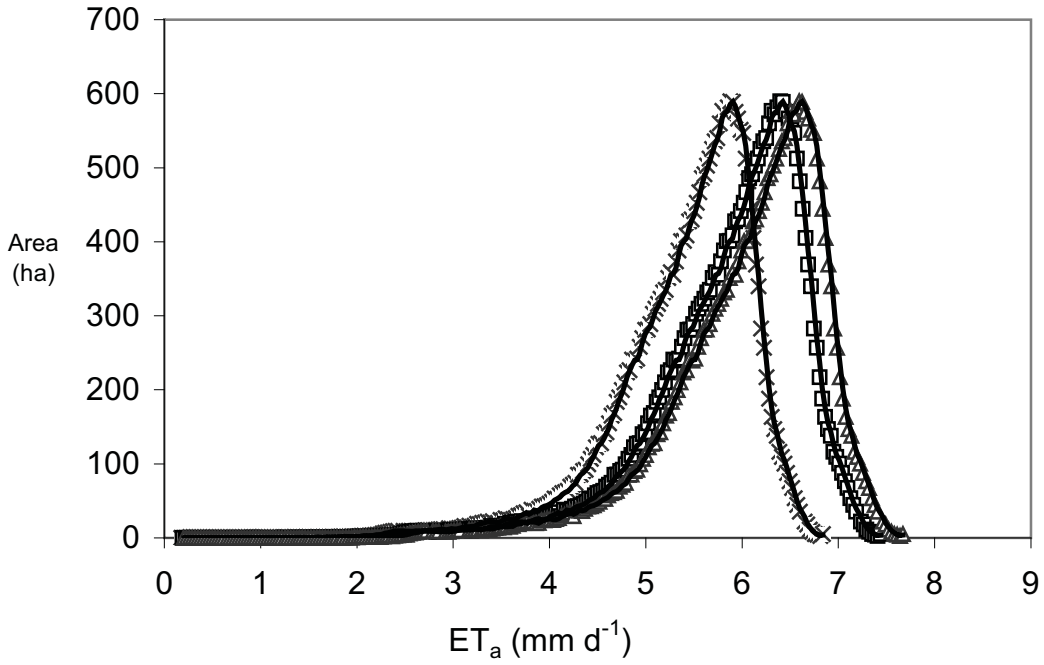

Figure 4.8: Frequency distribution of ETa in District 1 (in terms of area covered), 16 April (x), 2 May (□) and 18 May (Δ) 2001

The area-mean ET_a of District 1 and of the five irrigation sections are given in Table 4.6. Note that each value is calculated as the average from all pixel-based ET_a values in the area under consideration, and hence includes rice fields, other crops, forest, roads, settlements, and water bodies. On 16 April, when 90% of the area was

estimated to be under rice, the area-mean ET_a values were statistically not significantly different from each other (at the 5 % level) for all irrigation sections and District 1 as a whole. On 2 May, the differences among the areas were relatively large and can be explained by the fact that land use was most diverse on all three dates. Some rice fields were harvested and had either stubble or tilled soil, some fields still had standing rice, whereas other fields still had a cover of upland crops. On 18 May, there were statistically two groups of areas: SDA-A, SDA-B and SDA-C versus SDA-D and TRIS-L. The reason for the relatively high ET_a in SDA-D and TRIS-L was that farmers in these areas had started planting upland crops such as watermelon that actively transpired. The area-mean ET_a of the whole of District 1 was always statistically the same as those of its constituting sub-areas, except for SDA-A on 2 May 2001.

Table 4.6: Area-mean ET_a (mm d^{-1}) for each irrigation section and District 1 (16 April, 2 May, and 18 May 2001)

Section/Date	16 April 2001	2 May 2001	18 May 2001
District 1	3.5 a[1]	3.8 a b c	3.9 a b
TRIS-L	3.5 a	3.7 b c d	4.3 a
SDA–A	3.5 a	3.4 d	3.8 b
SDA–B	3.4 a	4.2 a	3.8 b
SDA–C	3.4 a	3.7 c d	3.6 b
SDA–D	3.7 a	4.1 a b	4.2 a

[1] Similar letter indicates that means are statistically the same at 95% confidence level.

Table 4.7 gives the E_{pan}, ET_o and ET_c at PAGASA and Phil Rice weather stations. For comparison, the SEBAL-calculated ET_a values of all rice pixels within a 10-km radius from the weather stations are also given. Except for 2 May, the E_{pan} values were about the same at both stations. On 16 April and 2 May, ET_o was considerably lower than E_{pan}, but only a little lower (0.1-0.2 mm d^{-1}) on 18 May. Because rice was in the ripening phase on all three-observation dates, their K_c values were smaller than 1, and ET_c was lower than ET_o. On all three dates, the SEBAL-calculated ET_a was lower than the potential ET (ET_c).

Table 4.7: Class-A Pan evaporation (E_{pan}), reference evapotranspiration (ET_o), and potential rice evapotranspiration (ET_c) at the PAGASA and PhilRice weather stations, and actual evapotranspiration (ET_a) of rice pixels surrounding the meteorological stations (all in mm d^{-1})

Meteorological station/Date		PAGASA	Phil Rice
16 April 2001	E_{pan}	6.8	6.8
	ET_o	5.8	5.8
	ET_c	5.5	5.5
	ET_a	5.2	
2 May 2001	E_{pan}	6.8	7.2
	ET_o	5.9	5.7
	ET_c	5.1	4.9
	ET_a	4.7	
18 May 2001	E_{pan}	7	6.9
	ET_o	6.8	6.8
	ET_c	5.1	5.1
	ET_a	4.9	

4.2.2.5 Conclusions and future directions

Optical satellite imagery and the SEBAL algorithm provided estimates of spatially distributed ET_a on the days of satellite overpass. The spatial patterns could generally be explained by the cropping patterns observed in the field. For pixels assumed to be under (ripening) rice, the estimated ET_a was on average 6% lower than the potential or crop evapotranspiration (ET_c) calculated using the modified Penman-Monteith equation at nearby weather stations. This can be explained by the fact that during ripening of rice, farmers drain the fields (to promote ripening) so that the crop experiences drought conditions and closes its stomata, thereby reducing its transpiration rate. Moreover, the evaporation from the underlying, drying soil surface is lower than that from a pounded water layer under potential evapotranspiration conditions. It is concluded that the SEBAL algorithm provided realistic ET_a estimates for irrigated rice in the tropics.

The difference in the ET_a values among sub-regions of the irrigation district was significant at the end of the growing season only when rice was harvested and new crops were planted. Differences were caused by differences in crop scheduling. It can be expected that differences will also occur in the beginning of the growing season when differences in availability of irrigation water among sub-regions will result in different planting times of rice. In the next steps of our study, ET_a estimates will be made for

each day of the season and used to calculate the water balance of District 1 at different spatial scales.

4.2.3 Evapotranspiration estimation through MODIS

4.2.3.1 Introduction

The problem of ET_a estimation at spatial scales can be overcome by the use of remote sensing techniques that provide ET_a on pixel-by-pixel basis. The most prominent method for estimation of ET_a is SEBAL (for detailed information refer to Bastiaanssen 1995). SEBAL is a thermodynamically based model that partitions sensible heat flux and latent heat of vaporization flux.

This study deals with 6 MODIS L1B images on different dates in the dry season 2001; 16 November 2000, 20 December 2000, 03 January 2001, 26 January 2001, 01 March 2001, and 24 March 2001. MODIS (Moderate Resolution Imaging Spectroradiometer) is the key instrument aboard the TERRA (EOS AM-1) satellite, which began operation in March 2000. MODIS is viewing the entire earth surface every 1-2 day, acquiring data in 36 spectral bands, or groups of wavelengths. The MODIS sensor has a spectral resolution featuring 36 bands ranging from 250 to 1000 meters spatial resolution.

4.2.3.2 Materials and methods

4.2.3.2.1 Pre-processing

Extraction of the binary file was performed for two visible bands (1 and 2) of 250 m resolution, five short wave infrared bands (3, 4, 5, 6, and 7) of 500 m resolution, and 2 thermal bands (31and 32) of 1000 m spatial resolution. The L1B image was created through the Red Hook Eros Data Center Internet web site using ftppull protocol (file transfer protocol). The L1B data was already calibrated for radiometric variations. Since geo-referencing parameterization was not feasible through the current software used, this was done manually in UTM/WGS/84/Zone 51 by selecting many well-distributed ground control points on the entire image, especially on the coastal features of the Central Luzon Island. A subset image for the Philippines was created from the whole image for better visualization and geo-referencing with RMSE less than 1 pixel.

The pre-processing parameters required for SEBAL include the Normalized Difference Vegetation Index (NDVI), emissivity, broadband surface albedo, and surface temperature for both sensors. The NDVI was calculated from two visible bands, 1 and 2 of MODIS data, and the broadband albedo was calculated using weighing factors of all visible, near infrared and short wave infrared bands of MODIS (Liang et al. 1999). Surface emissivity of the sensor was calculated from the NDVI of the sensors. Surface temperature of MODIS sensors was calculated from thermal bands 31 & 32 using the split-window technique found in Wan (1999).

4.2.3.2.2 Running SEBAL

Calculation of the net incoming radiation and the soil heat flux was done using the Bastiannssen (1995) method. To determine the sensible heat flux, the method developed by Tasumi et al. (2000) was adopted. However, to calculate the first temperature difference between air and soil for the "hot" pixel (i.e., where the latent heat flux is assumed null), first estimation of the air density was done generalizing meteorological data of relative humidity and maximum air temperature from two meteorological stations at the time of satellite overpass in District 1 for every sensor. Iterations of sensible heat flux were conducted five (5) times. In SEBAL, manual sampling of hot pixel values of the previous iterations output image files are required before the next iteration can be performed. This was a practical constraint in operationalization that was resolved by automation (after hot pixel identification) of data processing. Nonetheless, while five iterations improved sensible heat flux, the process proved to be time-and space consuming.

Evapotranspiration was calculated in SEBAL (Tasumi et al. 2000; Hafeez et al. 2002) from the instantaneous evaporative fraction, Λ, and the daily averaged net radiation, R_{n24}. The latter was transformed from W/m^2 to mm/day by the T_0 dependent latent heat of vaporization. The evaporative fraction, Λ, was computed from the instantaneous surface energy balance at the moment of satellite overpass for each pixel in the image.

4.2.3.3 Results and discussion

The main output of SEBAL was the daily ET_a image based on pixel as shown in Figure 4.9. The frequency distribution of ET_a for two images representing initial crop (16 November, 2000) and full vegetative crop stages (26 January, 2001) over the irrigation system of District 1 is shown in Figure 4.10. The frequency distribution of ET_a ranges from 0.02-4.6 mm d^{-1} on 16 November, 0.02-4.5 mm d^{-1} on 20 December, 0.1-5.0 mm d^{-1} on 03 January, 0.02-4.6 mm d^{-1} on 26 January, 0.02-6.3 mm d^{-1} on 1 March, and 0.02-6.6 mm d^{-1} on 24 March. The frequency distribution curves of ET_a show that the water consumption pattern in mono-modal with main peak features on covered area is 3.3 mm d^{-1} @ 1225 ha on 16 November, 2000, 2.0 mm d^{-1} @ 641 ha on 20 December, 2.7 mm d^{-1} @ 635 ha on 03 January, 4.0 mm d^{-1} @ 838 ha on 26 January, 5.3 mm d^{-1} @ 857 ha on 1 March, and 5.8 mm d^{-1} @ 1016 ha on 24 March.

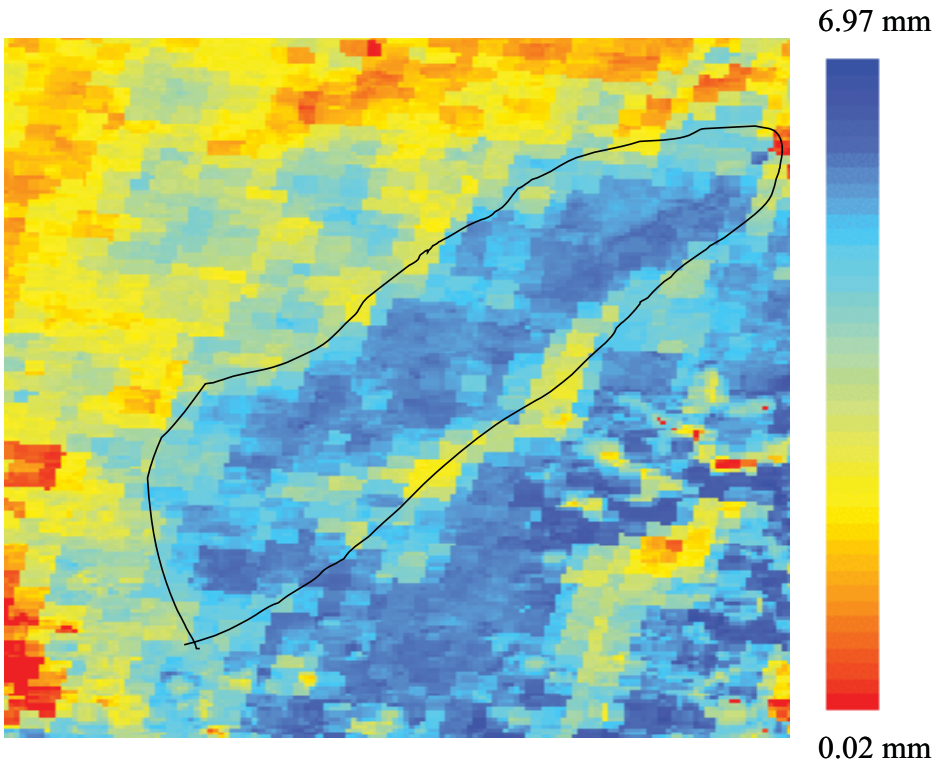

Figure 4.9: Actual evapotranspiration map of District 1 (250 m) on 24 March 2001

In the initial crop development stage (16 November, 20 December, and 3 January), the land cover was found in three (3) major types, i.e., rice fields, nursery plots and few upland crop fields, while in the full vegetative growth stage (26 January, 1

March, and 24 March), the land use was homogenous because rice formed the major crop in the dry season 2001. The shortage of water in the lower part of District 1 during the dry season forced farmers to change the cropping calendar and grow other crops besides rice in the downstream area. The E_{pan} readings correspond to the last upper part of the ET_a axis.

The ET_a estimated from MODIS images (250 m spatial resolution) was compared with (i) evaporation from Class A pan (E_{pan}), and (ii) ET_o and ET_c, using modified the Penman-Monteith method. ET_o and ET_c were derived from weather data of two meteorological stations (PAGASA and Phil Rice) located within a 10-km distance of District 1 of UPRIIS, as shown in Table 4.8.

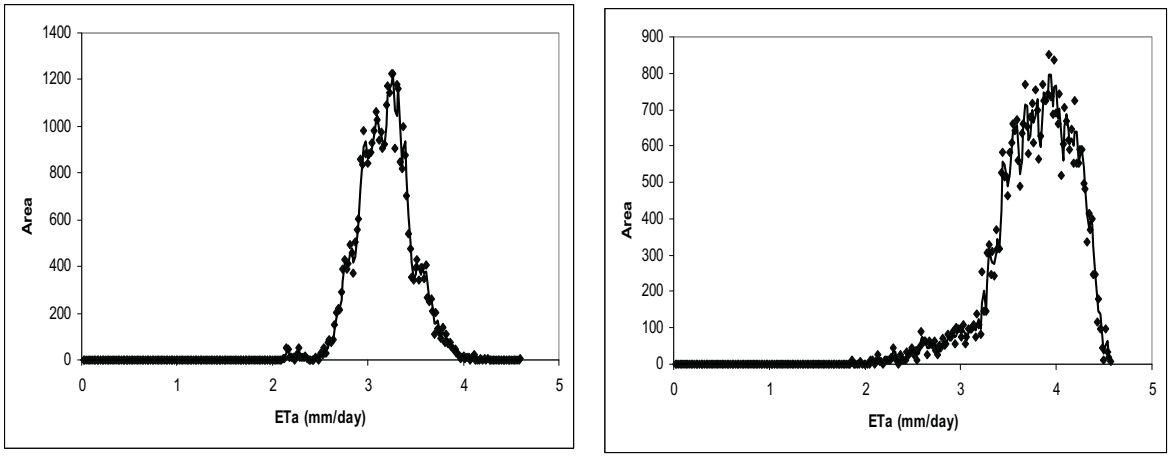

Figure 4.10: Frequency distribution of daily ETa (mm/day) per area covered (hectares) on 16 November 2000 and 26 January 2001

There is some discrepancy in the E_{pan} measured at the PAGASA meteorological station with the E_{pan} measured at the PhilRice station. It was observed that the E_{pan} measured by PAGASA was always less than the E_{pan} measured by PhilRice meteorological stations on all 6 image-acquisition dates during the dry season of 2001. This difference can be attributed to a number of reasons, but mainly to inaccurate (human) measurement and poor pan maintenance as observed during the comprehensive ground truth campaign at both meteorological stations on the satellite overpass dates in District 1 during the whole dry season 2001 (Hafeez and Chemin 2003).

The averaged daily ET_a values sampled over the rice pixels are found to be less than the PAGASA and PhilRice meteorological data of water evaporation. For instance, during the five observation periods, percentage difference of ET_a from PAGASA and PhilRice data was: -25 % & -27 % (16 November), -33 % & -39 % (20 December), -37 % & -42 % (03 January), -9 % & -14 % (26 January), -9 % & -19 % (1 March) and –3 % & -20 % (24 March), respectively. These results match very well the expectations concerning the difference of ET values between open water bodies and rice crops.

Table 4.8.Evaporation from Class A pan (E_{pan}), reference evapotranspiration (ET_o), and potential rice evapotranspiration (ET_c), at the PAGASA and PhilRice weather stations, and actual evapotranspiration (ET_a) of rice pixels surrounding the meteorological stations (in mm d^{-1}).

Meteorological stations/Date		PAGASA, Munoz	Phil Rice, Maligaya
16 November 2000	E_{pan}	4.5	4.6
	ET_o	4.0	4.2
	ET_c	4.2	4.4
	ET_a	3.6	
20 December 2000	E_{pan}	4.4	4.6
	ET_o	3.5	4.2
	ET_c	3.7	4.4
	ET_a	3.3	
03 January 2001	E_{pan}	4.8	5.0
	ET_o	4.0	4.3
	ET_c	4.2	4.5
	ET_a	3.5	
26 January 2001	E_{pan}	4.6	4.8
	ET_o	3.9	3.8
	ET_c	4.1	4.0
	ET_a	4.2	
01 March 2001	E_{pan}	5.7	6.2
	ET_o	4.4	4.2
	ET_c	5.2	5.0
	ET_a	5.2	
24 March 2001	E_{pan}	6.2	6.4
	ET_o	5.0	4.8
	ET_c	6.0	5.8
	ET_a	6.1	

Using the modified Penman-Monteith method, the ET_o on each day of MODIS sensor overpass was estimated at both meteorological stations in District 1. Fifty (50) farmer fields were selected randomly for monitoring different crop stages and growth activities on each day of satellite overpass during the dry season in 2001. This crop stages data was utilized to estimate the area under rice crop, vegetables, bare fields, settlements, roads and water bodies, and overlaid to estimate the ET_a of every land use in District 1.

The results of ET_o showed no significant difference from the calculated ET_a values at both meteorological stations in District 1. In the early part of the cropping season (16 November, 20 December, & 03 January), calculated ET_o values from both weather stations were higher than the ET_a of rice fields because the vegetation cover in the fields was not fully developed. During the crop maturity stage (26 January, 1 March & 24 March), calculated ET_o values were always lower than ET_a because the rice crop was actively transpiring at this stage.

The crop coefficient (K_c) adjustment of rice fields was applied to obtain potential ET_c (Allen et al. 1998) on different image acquisition days. The K_c values, 1.05 and 1.20, the at crop development stage (16 November 2000, 20 December and 03 January 2001) and crop maturity stage (26 January, 1 March, and 24 March 2001) respectively, were multiplied to obtain potential ET_c. The difference of average ET_c calculated from both meteorological stations to ET_a are –19 % (16 November 2000), -22 % (20 December 2000), -24 % (03 January 2001), 4 % (26 January 2001), 2 % (1 March 2001), and 3 % (24 March 2001). The results prove that calculated ET_a from MODIS data is within the acceptable range in comparison to ET_o and ET_c calculations from the weather data.

4.2.4 Crop water deficit through remote sensing in District 1 of UPRIIS, Central Luzon, Philippines[3]

Abstract: Estimation of crop water deficit continues to be a challenge especially when attempting to evaluate it for large areas. The limitation of cloud-free image availability

[3] Hafeez MM, N VD Giesen, Eggers H, and Chemin Y (2002) "Crop Water Deficit Through Remote Sensing in District 1 of UPRIIS, Central Luzon, Philippines" Second workshop of the EARSeL Special Interest Group on Remote Sensing for Developing Countries, University of Bonn, Bonn, Germany 18-20 September 2002, 7 pages (in press).

in a the tropical climate like that of the Philippines can be overcome with the combination of high spatial and temporal resolution images. In this study, Landsat 7 and MODIS satellite images on the same overpass date were selected on May 18, 2001 in the dry season 2001. Comparing positively-the results of MODIS and Landsat 7 ETM+ sensors for water consumption studies at different scales in irrigation system would enable better decision-making for crop-water requirement. SEBAL has been applied to Landsat 7 ETM+, and MODIS sensors for the estimation of crop water requirements in District 1 of UPRIIS in Central Luzon. The ET_a estimates were integrated for 24 hours on a pixel-by-pixel basis from instantaneous ET estimates.

This study shows a unique combination of ET_a derived from Landsat and MODIS images for water consumption studies in District 1. Volumes of water consumption and deficit were compared at different pixel sizes. The results were compared with ET calculations at two meteorological stations in District 1 of UPRIIS. The discussion provides the research orientation of the scale assessment of evaporation and further implications in applied research for water management supported by satellite images.

4.2.4.1 Introduction

Food security in Asia is challenged by increasing food demand and threatened by declining water availability. Irrigation is the largest user of fresh water - around 70 % of withdrawals are for irrigation. Rice is the major staple food in Asia, where about 92 % of the world's rice is produced and consumed (IRRI 1997). Irrigated agriculture accounts for 90 % of total diverted fresh water, and more than 50 % of this is used to irrigate rice in Asia (Barker et al. 1998). However, the water-use efficiency of rice is low, and to grow rice requires large amounts of water. To produce just one ton of rice requires between 2-3 Olympic-sized swimming pools full of freshwater (IRRI 2001). Measuring ET is of highest importance for understanding and eventually intervening in the water cycle of natural systems. However, the quantification of ET at different spatial scales of irrigation systems is not a simple task. The problem of ET_a estimation at spatial scales can be overcome by the use of remote sensing techniques that provides ET on pixel-by-pixel basis. Since the 1990s, many researchers (Vidal and Perrier 1999; Bastiaanssen 1995; Granger 1997) have developed various methodologies by

combination of satellite images and meteorological data for large areas. The most prominent method for estimation of ET_a is SEBAL (for detail information refer to Bastiaanssen 1995). SEBAL is a thermodynamically based model, which partitions between sensible heat flux and latent heat of the vaporization flux. Many researchers have applied SEBAL for irrigation systems in many countries like Argentine, China, India, Egypt, Kenya, Pakistan, the Philippines, Spain, and Sri Lanka. The combination of high spatial resolution of Landsat 7 ETM+/ASTER with the high-temporal resolution of NOAA AVHRR/MODIS provides higher accuracy for water balance type studies. Combinations of Landsat and NOAA are found in Timmerman and Meijrink (1999) where Landsat 5TM was used. Later, Hafeez et al. (2002) applied SEBAL on Landsat 7 ETM+ and TERRA/MODIS and ASTER sensors in UPRIIS. This study deals with two (2) images of different processing levels on the same overpass day (18 May 2001) in the dry season 2001: Landsat 7 ETM + L1G and MODIS L1B.

4.2.4.2 Study area

In the Philippines, some 61 % of the 3.4 million ha of rice land is under irrigation, with the majority of the rice production coming from the country's rice bowl, i.e., Central Luzon (IRRI 1997). Irrigation is provided by gravity systems and, increasingly, by shallow and deep tube wells. Water is always scarce in the dry season where the lack of rainfall makes cropping impossible without irrigation. Since the climatic yield potential is highest in the dry season, increasing the area under irrigation is an attractive strategy to increase rice production (NIA 1996). The study area, "District 1," is located in UPRIIS, which covers a total area of 102,591 hectares, taking its water from the Pantabangan Dam. District 1 covers about 34,000 ha and is divided into a northern and southern part. Talavera and Ilog Baliwag rivers bound both sides of District 1. The most common land use in District 1 is double cropping of rice through the transplanting method, although direct wet seeding is also becoming increasingly popular. The climate in UPRIIS is characterized by two pronounced seasons, dry from November to April with an average rainfall of 193 mm and wet from May to October with an average rainfall of 1654 mm. This study concentrates on the period from late November to mid May, when average rice yields range from 4.8-5.6.1 tons/ha.

This study addresses the assessment of the water deficit of an irrigation system in terms of spatial homogeneity. It makes use of two sensors, i.e., MODIS and LANDSAT 7, in assessing and cross checking the possibility of substituting one for the other on the same overpass day (18 May 2001).

4.2.4.3 Methods

4.2.4.3.1 Satellite images

The Landsat 7 ETM+ instrument has 8 multi spectral bands from 15 m (Panchromatic), 30 m (Visible and Short-wave infrared) and 60 m (Thermal). The gain and offset values for Landsat 7 ETM+ satellite images are extracted from the header file available with original CD-ROM provided by USGS. The MODIS sensor on the TERRA platform has a spectral resolution featuring 36 bands ranging from 250-1000 m spatial resolution. Acquisition of L1B image was done through the Redhook Eros Data Center Internet web site using the ftppull protocol.

The pre-processing parameters required for SEBAL include the Normalized Difference Vegetation Index (NDVI), emissivity, broadband surface albedo, and surface temperature for both sensors. The NDVI of Landsat 7 was calculated from bands 3 and 4, while the 16 days composite image of the NDVI (level 3) was available for MODIS. The surface emissivity of each sensor was calculated from the NDVI of the respective sensors and the broadband surface Albedo of each sensor was computed using the respective weighing factors of that sensor. Surface temperature of the MODIS sensor was calculated from bands 31 and 32 using the split-window technique, while surface temperature from Band 6L of Landsat 7 was computed using the inverse plank function.

4.2.4.3.2 Running SEBAL

Calculation of net incoming radiation and soil heat flux was done according to Bastiaanssen 1995, while the determination of the sensible heat flux incorporated the later development of Tasumi et al. 2000 for each sensor. However, to calculate the first temperature difference between air and soil for the “hot” pixel (i.e., where the latent heat flux is assumed null), a first estimation of the air density was done generalizing meteorological data of relative humidity and maximum air temperature from two meteorological stations at the time of satellite overpass in District 1 for every sensor. Iterations of sensible heat flux were conducted 5 times. In SEBAL, manual sampling of

hot pixel values of the previous iterations output image files are required before the next iteration can be done, which is a practical constraint in operationalization. This constraint can be resolved by automation (after hot pixel identification) in the data collection of the results. Although the iteration of 5 times improved the sensible heat flux, it is time and space consuming.

Evapotranspiration is calculated in SEBAL (Tasumi et al. 2000; Hafeez and Chemin 2003) from the instantaneous evaporative fraction, Λ, and the daily averaged net radiation, R_{n24}. The later has to be transformed from W/m^2 to mm/day by the T_0 dependent latent heat of vaporization. The evaporative fraction, Λ, is computed from the instantaneous surface energy balance at the moment of satellite overpass for each pixel in the image.

4.2.4.3.3 Assessing water deficit differences across platforms' sensors

The experiment assessed the water deficit ($ET_{potential}$ - ET_a) using both sensors. The water deficit represents the lack of water consumption to meet the crop's best evapotranspiration rate ($ET_{potential}$). Thomas et al. (1999) considered the optimum water consumption for an irrigation system performance in Pakistan as 75 % (100 %* ET_a / $ET_{potential}$) corresponding to the highest crop yield response. In terms of water evapotranspiration, $ET_{potential}$ is 100 %.

Assessing the spatial variations by simple statistics (mean and coefficient of variation) will give information on the equality of water consumed and its spatial homogeneity in the irrigation system. An Analysis of Variance (ANOVA) will give consistency of responses between sensors and pixel sizes.

4.2.4.4 Results

The pixel size of Landsat 7 ETM+ and MODIS images is 30 and 250 m, respectively. The ET image of Landsat 7 was degraded 9 times so that the pixel size of Landsat would equal that of MODIS for better comparison. In that way, the ET_{actual} was estimated from 3 images (Landsat 30 m, Landsat degraded 250 m and MODIS 250 m) with the meteorological data from the 2 stations in District 1.

Location of the water deficit from the optimum yield response water consumption is shown in Figure 4.11. The yellow and green areas show the best match to the water requirements for maximizing yields, while the red and blue areas

respectively show low and high water consumption tendencies that may have non-beneficial influences on crop production.

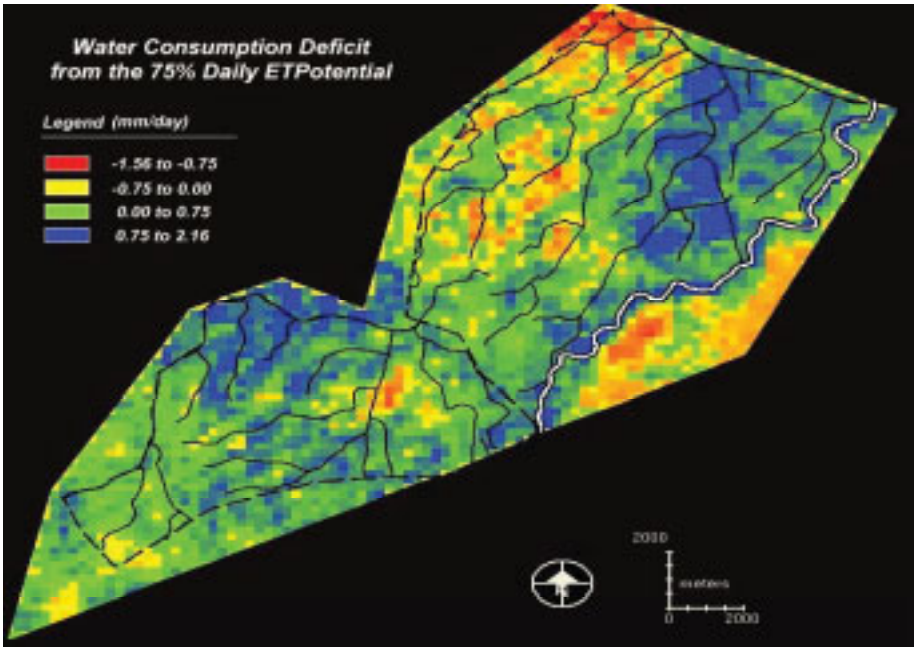

Figure 4.11: Water consumption deficit (Landsat degraded 250m)

Table 4.9: Comparison of ET from different sources (mm/day)

Evapotranspiration	PAGASA, Munoz	Phil Rice, Maligaya
E_{pan}	7	6.9
ET_o (Penman Monteith)	6.83	6.8
ET_c (Kc=0.8)	5.46	5.44
ET_a MODIS	4.94	4.22
ET_a Landsat	5.35	5.54
ET_a Landsat degraded	6.23	5.83

Considering the basic water productivity parameters (Thomas et al. 1999), the mean ET_a over the irrigation system is 5.4 mm (corresponding well with the ET_c of Table 4.9). The coefficient of variation of ET_a reaches 12.6 % for spatial inequality in water consumption. The same indicator (as comparison only) ranges from 9-24 % for season-wise ET_a in irrigation zones in Ferghana District (Uzbekistan) (Chemin et al. 2002). The E_{pan} results of both meteorological stations are almost equal on 18 May 2001 and the ET_a values, i.e., 21 % (Landsat), 13 % (Landsat degraded) and 33 % (MODIS) are less than the meteorological data of water evaporation. These results match very

well the expectations on the difference of ET values, except MODIS between open water bodies and rice crops. The differences of ET_c observed (modified Penman Monteith) from remote sensing are ±2 % (Landsat), +9.5 % (Landsat degraded), and –20 % (MODIS). These results are confirmed by the ET_o and ET_c calculations from ground data for all sensors. More researches on MODIS are, however, needed.

Comparison of histograms of ET actual for every sensor over an irrigation system of District 1 is shown in Figure 4.12. The ET_a histograms for Landsat (30 m), Landsat degraded (250 m) and MODIS images show mean values of 5.64, 5.63 and 4.08 mm/day with main peak features on covered area of 5.66 mm/day @ 374 ha, 5.45 mm/day @ 451 ha, and 3.63 mm/day @ 1637 ha, respectively. An ANOVA for a part of the irrigation system image from different sensors showed a positive and significant relationship with the p-value 0.004824 of the convergence between the three ET_a images.

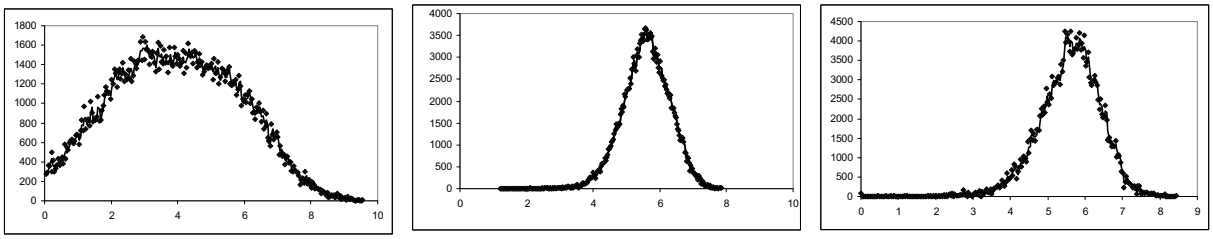

Figure 4.12: Sensor histograms of daily ET Actual (mm/day) per area covered (hectares) of MODIS, Landsat and Landsat-degraded on 18 May 2001.

4.2.4.5 Conclusion

Water deficit assessment based on 75% daily $ET_{potential}$ showed that 75 hectares suffer from severe water stress (-1.56 to -0.75 mm/day). Out of 20,000 ha command areas, 59.4% (11,800 ha) are in best conditions (water deficit of -0.75 to +0.75mm/day). The system uniformly performs quite well in most of the area. Many land-cover types are found in District 1, i.e., rice fields (within 3-4 days prior to harvest), which account for 10% of the area, and flooded fields without any crop, vegetable fields and fishponds that account for the remaining area. The shortage of water in the lower part of District 1 during the dry season forced farmers to grow other crops besides rice and this affects the cropping calendar.

Results do not prove complete consistency in both sensors ET_a assessment. Part of the variation can be attributed to the scale effects in terms of: (i) area variation;

(ii) pixel-area-dependent difference of the sensors calibration for the flux densities; and (iii) temperature and surface resistance. In this regard, more work is needed to further refine the application of energy balance model SEBAL to MODIS. Further research in using multi-sensors for studying irrigation system performance is encouraged.

4.2.5 Field evapotranspiration estimation in Central Luzon using different sensors: Landsat 7 ETM+, TERRA MODIS and ASTER[4]

Abstract: Satellite-derived estimates of ET_a over large areas have become popular in water balance studies since 1990. However, it is practically impossible to obtain well-distributed cloud-free images over the entire cropping season from one sensor in tropical countries like the Philippine. This limitation can be overcome through combination of high spatial resolution of Landsat and TERRA/ASTER images with high temporal resolution of TERRA/MODIS images. This section aimed to test the feasibility of using SEBAL with multi-sensors data at different processing levels: ASTER L1B, Landsat 7 ETM+ L1G, and MODIS L1B for the different periods of the dry season in 2001.

SEBAL was applied to ASTER (02 February 2001), Landsat 7 ETM+ (16 April 2001), and MODIS (18 May 2001) sensors for the estimation of ET in District 1 (All pre-processing and processing steps of all three sensors were discussed in details for SEBAL). ET_a was computed during satellite overpass and integrated for 24 hours on a pixel-by-pixel basis.

In this study, the unique combination and inter-relationship of ASTER and Landsat images with the MODIS images of water consumption in District 1 was examined. The results were compared with the calculations of ET at two meteorological stations in District 1 and data showed a non-significant variation. Comparison with other meteorological data showed close relationship with daily ET estimated by different sensors as predicted by SEBAL. Based on the presented findings, it can be

[4] Hafeez MM, Chemin Y, N Van De Giesen and Bouman BAM (2002) "Field Evapotranspiration Estimation in Central Luzon, Philippines, Using Different Sensors: Landsat 7 ETM+, Terra MODIS and Aster." Proceedings of joint conference on "Geospatial Theory, Processing, & Applications" organized by ISPRS/Canadian Institute of Geomatics Conference, Ottawa, Canada, 8-12 July 2002.

concluded that results from all three remote sensing platforms can be used for the computation of ET_a studies in tropical climates but with necessary caution.

4.2.5.1 Introduction

Water is becoming a scarce natural resource. The population increase puts a great demand on water resources for domestic, industrial and agricultural use. In Asia, more than 80 % of fresh water resources are used for irrigation, and 50 % of this is used to irrigate rice (Tabbal et al. 2002). Rice is the major staple food in Asia where 92 % of the world rice is produced and consumed (IRRI 1997). To keep up with the population growth and income-induced demand for food, rice production must continue to increase in the next decades. Since about 75 % of all rice produced is irrigated, rice production is threatened by the "looming water crisis" and ways must be sought to grow more rice using less water (Guerra et al. 1998). An understanding of the water balance of irrigation systems is crucial for developing alternative management strategies that are more efficient. ET is an important component of the water balance of any irrigation system. However, the quantification of ET at the spatial scale of irrigation systems is not a simply task. There are many methods to estimate ET (reference) using meteorological data: FAO-24 (Doorenbos et al. 1977), FAO-56 (Allen et al. 1998). Most of these methods are based on point data, which do not provide good estimation of ET for larger areas. Scintillometer instruments can be used to overcome the problem of ET computation for larger areas because it provides well-distributed ET_a over 1-5 km (De Bruin et al. 1996). Hydrological modeling like SWAP is another method for computation of ET_a that can be distributed (Droogers 2000).

The problem of ET_a estimation over a large area can be solved using remote sensing methods that provide ET on a pixel-by-pixel basis. Many researchers (Vidal and Perrier 1989; Bastiaanssen 1995; Granger 1997) have already developed various methodologies by combining of satellite images and meteorological data for large areas since the 1990s. This study focuses on ET_a estimation by using SEBAL by Bastiaanssen (1995). SEBAL is a thermodynamically based model, which partitions between sensible heat flux and latent heat of vaporization flux.

Bastiaanssen (1995) originally developed SEBAL in Spain and Egypt using Landsat 5TM. Furthermore, Roerink et al. (1997) also applied the same sensor for

monitoring irrigation performance in Argentina. Water consumption of large irrigation systems has also been addressed with NOAA AVHRR in Pakistan (Bastiaanssen et al. 1999; validation in Bastiaanssen et al. 2001). Farah (2001) has studied modeling of evaporation under various weather conditions in the Navaisha Basin, Kenya. His results extend SEBAL calculations of NOAA AVHRR under clouds with a Penman-Monteith approach supported by a Jarvis-Stewart type model. Combinations of Landsat and NOAA are found in Timmermans and Meijerink (1999), where Landsat 5TM was used, and in Chemin and Alexandridis (2001) who used Landsat 7ETM+. Later on, Hafeez and Chemin (2003) applied SEBAL using the TERRA/ASTER sensor in UPRIIS. The combination of the high spatial resolution of Landsat 7 ETM+/ASTER with the high temporal resolution of NOAA AVHRR/MODIS gives a higher accuracy for water balance type studies.

Cloud coverage is a prominent phenomenon in many parts of the world. The mean cloud cover per day may exceed 60 % in the humid tropics (Bussieres and Goita 1997). It is practically impossible to get well-distributed cloud-free images over the entire cropping season from one sensor in tropical countries like the Philippines. This limitation can be overcome with the combination of high-spatial resolution of Landsat and TERRA/ASTER images with the high temporal resolution of TERRA/MODIS images in the tropical climate. In this study, only 1 cloud-free image out of 92 for ASTER L1B, 3 cloud-free images out of 12 for Landsat 7 ETM+, and 7 cloud-free images out of 110 MODIS L1B were available over the entire dry season 2001. This paper deals with the 3 images of different sensors of different processing levels for different time periods in the dry season 2001: ASTER L1B (02 February 2001), Landsat 7 ETM+ (16 April 2001) and MODIS L1B (18 May 2001).

4.2.5.2 Study area

The Philippines is an agricultural country with a total land area of 13 million hectares under crop cultivation. The major part of rice production comes from the Central Luzon area. UPRIIS, with a total area of 102,591 hectares is an important rice-producing area in the Nueva Ecija province, Central Luzon. The study area, “District 1” is located in UPRIIS, taking its water from the Panatabangan Dam. District 1 covers about 34,000 ha and is divided into a northern (San Jose city) and southern part (main cities Santo

Domingo, Quezon and Licab). Talavera and Ilog Bliwag rivers bound both sides of District 1. The most common land use in District 1 is double cropping of rice using the transplanting method, while direct wet seeding is becoming increasingly popular. The climate in UPRIIS is characterized by two pronounced seasons, dry from November to April with an average rainfall of 193 mm and wet from May to October with an average rainfall of 1654 mm. This study concentrates on the dry season, from late November to mid May, where average rice yields amount to 4.8-5.6 tons/ha.

The main objective of this paper is to study the feasibility of using SEBAL with different sensors of different processing levels: L1B TERRA/ASTER, L1B TERRA/MODIS and L1G Landsat 7 ETM+ data, in order to compute spatially distributed ET_a by remote sensing. It is proposed to validate the results of ET_a with meteorological data collected in UPRIIS.

4.2.5.3 Methods

4.2.5.3.1 Sensors

Three sensors are used in this study, i.e., ASTER, Landsat and MODIS (see Table 4.10 for general overview). ASTER started monitoring global environment changes in March 2000 and provides images free of charge. The ASTER sensor on board the TERRA has 14 spectral bands ranging from 15 to 90 m spatial resolution. A fifteenth band is a backward view of the near infra red (NIR) (15 x 15 m in the 0.76-0.86 μm) for stereoscopic imaging. The L1B image was acquired by the ftppull protocol from the EROS Data Center Red hook Internet website. Extraction of the binary file was performed for 3 visible near infrared bands 'vnir' (1, 2, & 3N), all 6 short wave infrared bands 'swir' (4, 5, 6, 7, 8, & 9) and all 5 thermal infrared bands (10, 11, 12, 13 & 14) respectively. Rotation, pixel coordinate and size were provided to the image after HDF-file information was gathered for geo-referencing. Geo-referencing of the ASTER image was done in the UTM/WGS84/Zone 51.

LANDSAT 7 ETM+ was launched on 15 April 1999 to provide high-resolution image information of the earth surface. The Landsat ETM+ instrument has 8 multi- spectral bands from 15 m (Panchromatic), 30 m (Visible and Short-wave infrared), and 60 m (Thermal). Level 1G products are radiometrically and geometrically corrected to the user-specified parameters including output map projection, image

orientation, pixel grid-cell size, and resampling kernel. The gain and offset values for Landsat 7 ETM+ satellite images are extracted from the header file available with original CD-ROM provided by USGS. The geo-referencing of Landsat 7 ETM+ was done using the coordinates provided in the header file in UTM/WGS84/Zone 51.

MODIS is the key instrument aboard the TERRA (EOS AM-1) satellite, which also started operation in March 2000. TERRA/ MODIS is viewing the entire earth surface every 1-2 day, acquiring data in 36 spectral bands, or groups of wavelengths. The MODIS sensor on the TERRA platform has a spectral resolution featuring 36 bands ranging from 250 to 1000 m spatial resolution. Acquisition of the L1B image was through the Red hook Eros Data Center Internet web site using the ftppull protocol. Extraction of the binary file was performed for 2 visible bands (1 and 2), short-wave infrared bands (3, 4, 5, 6, and 7) and 2 thermal bands (31 and 32). A subset image for the Philippines was created from the whole image for better visualization and geo-referencing. The L1B data was already calibrated for radiometric variations, while geo-referencing parameterization was not feasible through the current software used. Therefore, geo-referencing was done manually by selecting many well-distributed ground control points on the entire image, especially on the coastal features of the Central Luzon Island. Geo-referencing was done in the UTM/WGS/84/Zone 51, because all the other images available for this study were provided in the same geo-reference.

Table 4.10: Overview of the different sensors

Sensor	Sub-systems	Number of bands	Spectral range (μm)	Spatial resolution (m)
TERRA/ASTER	VNIR	3 (+ 1 backward)	0.52 up to 0.86	15x15
	SWIR	6	1.60 up to 2.43	30x30
	TIR	5	8.125 up to 11.65	90x90
Landsat 7 ETM+	VNIR	4	0.45 up to 0.90	30x30
	SWIR	2	1.55 up to 2.35	30x30
	TIR	1	10.4 to 12.5	60x60
	PAN	1	0.50 to 0.90	15x15
TERRA/MODIS	VNIR	2	0.62 up to 0.876	250x250
	SWIR	5	0.459 up to 2.155	500x500
	SWIR	11	0.405 up to 0.965	1000x1000
	TIR	16	3.66 up to 14.385	1000x1000

4.2.5.3.2 Specificity of porting SEBAL to different sensors

The pre-processing parameters required for SEBAL include the Normalized Difference Vegetation Index (NDVI), emissivity, broadband surface albedo, and surface temperature for all above-mentioned sensors. The NDVI was calculated from the visible bands 2 and 3N for ASTER, 1 and 2 for MODIS, 3 and 4 for Landsat 7. The surface emissivity of MODIS and Landsat / ETM+ was computed from the NDVI following the method of Van de Griend and Owe (1993). The Temperature Emissivity Separation (TES) algorithm is used to extract the surface temperature and 5 emissivities from the 5 thermal infrared bands of ASTER data. The TES provides an accurate estimate of the surface temperature within about ± 1.5 K and emissivities within about ± 0.015 for the ASTER sensor (Gillepsie et al. 1998). The broadband albedo was calculated using weighing factors of all 7 bands including visible, near-infrared and short-wave infrared bands of MODIS (Liang et al. 1999). The broadband albedo of Landsat 7 ETM+ and ASTER was calculated using weighing factors of 6 and 9 bands including visible, near infrared and short wave infrared bands of both sensors. The surface temperature of the MODIS sensors was calculated from thermal bands 31 and 32 using the split-window technique found in Chandrapala and Wimalasuria (2001), while the surface temperature from Band 6L of Landsat 7 was computed using the inverse plank function.

4.2.5.3.3 Running SEBAL

Calculation of the net incoming radiation and the soil heat flux were done after Bastiaanssen (1995), while the determination of the sensible heat flux incorporated the later development of Tasumi et al. (2000) for each sensor. However, to calculate the first temperature difference between air and soil for the “hot” pixel (i.e., where the latent heat flux is assumed null), a first estimation of the air density was done generalizing meteorological data of relative humidity and maximum air temperature from two meteorological stations at the time of satellite overpass in District 1 for every sensor. Iterations of sensible heat flux were conducted 5 times, and it has been observed by the operator that this method does not stabilize the air-soil temperature difference as fast as the earlier method found in Bastiaanssen (1995). In SEBAL, manual sampling of hot pixel values of the previous iterations output image files are required before the next iteration can be done which is a practical constraint in operationalization. This

constraint can be resolved by automation (after hot pixel identification) in the data collection of the results. Although the iteration of 5 times improved the sensible heat flux, it is time and space consuming.

The ET is calculated in SEBAL (Tasumi et al. 2000; Hafeez and Chemin 2002) from the instantaneous evaporative fraction, Λ, and the daily averaged net radiation, R_{n24}. The later has to be transformed from W/m^2 to mm/day by the T_0-dependent latent heat of the vaporization equation inserted in the main equation (4.9).

$$ET_{24} = \Lambda \times \left[R_{n24} \times \left(\left(2.501 - 0.002361 \times T_0 \right) \times 10^6 \right) \right] \quad \textit{(mm/day)} \quad \textit{Equation 4.9}$$

where ET_{24} = Daily ET actual (mm/day);
R_{n24} = average daily net radiation (W/m^2); and
T_0 = surface temperature (°C).

The evaporative fraction, Λ, is computed from the instantaneous surface energy balance at the moment of satellite overpass for each pixel (Equation 4.10):

$$\Lambda = \frac{\lambda E}{R_n - G_0} = \frac{\lambda E}{\lambda E + H_0} \quad \textit{(-)} \quad \textit{Equation 4.10}$$

where λE = latent heat flux (the energy allocated for water evaporation). λ can be interpreted in irrigated areas as the ratio of actual to crop evaporative potential, it is dependent on the atmospheric and soil moisture conditions equilibrium.
R_n = net radiation absorbed or emitted from the earth's surface (radiative heat);
G_0 = soil heat flux (conduction); and
H_0 = sensible heat flux (convection).

4.2.5.4 Results and discussion

The main output of SEBAL is the partitioning of the energy balance, and can be visualized as the actual over the potential ET defined as the evaporative fraction. A straight derived product is the actual daily ET shown in Figure 4.13 for ASTER, Landsat and MODIS images. The range of ET values for the ASTER image of 2 February 2001 is (Figure 4.13, left) from 0.35-5.35 mm/day, while range of the ET for Landsat 7 on 16 April (Figure 4.13, center) and MODIS on 18 May 2001 (Figure 4.13, right) varies from 0.10-8.20 mm/day and 0.25-9.85 mm/day, respectively.

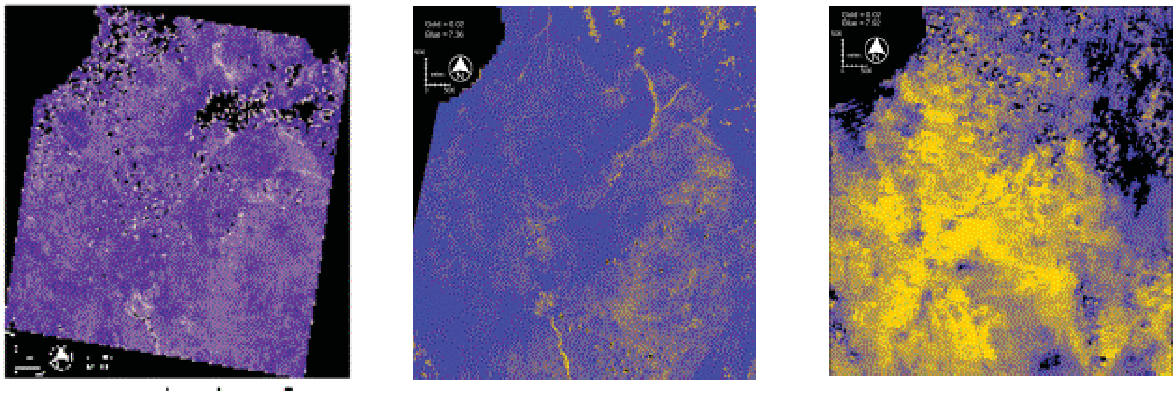

Figure 4.13: Daily actual evapotranspiration for subsets of ASTER, Landsat 7 and MODIS (mm/day)

The comparison of histograms of ET_a for every sensor over an irrigation system of District 1 is shown in Figure 4.14. The histogram of ET_a for the ASTER image shows a mode around 3.2 mm/day, with a main peak feature on a covered area of 3.27 mm/day @ 54 ha. The ASTER histogram shows the water consumption pattern mono-modal because 3 major types of land cover in the early part of the dry season (2 February 2001) in District 1 were found, i.e., flooded rice fields (nurseries), different vegetable fields (less water), and a few fishponds. For the Landsat histogram (16 April 2001), the water consumption pattern is bi-modal because again three different types of land cover were found, i.e., rice fields without irrigation (close to harvest), rice fields with standing water, and a few fishponds. In case of Landsat 7 ETM, the histogram of ET_a versus area covered shows peak features of 4.33 mm/day @ 66.60 ha, and 5.26 mm/day @ 64.70 ha, respectively.

The histogram of ET_a versus area covered for the MODIS image (18 May 2001) is multi-modal, which shows peak features in 2.43 mm/day @ 31.60 ha, 3.09 mm/day @ 32.75 ha, 4.22 mm/day @ 35 ha, 6.38 mm/day @ 26.4 ha and 7.65 mm/day @ 19.53 ha. The MODIS histogram shows the water consumption pattern in a multi-model form, because many types of land cover were found, i.e., 10% under rice fields (within 3-4 days of harvest); and the rest under flooded fields without any crop (rainy season starts in May), vegetable fields (some farmers had just planted water melons), and a few fish ponds. The shortage of water in the lower part of District 1 during the dry season forced farmers to grow other crops besides rice and also affected the cropping calendar. The major reason for the different types of land use in the lower part of

District 1 is shortage of water. Despite the fact that ET_a is computed from different sensors, it shows a good continuity of reliable information. This considers the spatial resolutions range from 15-90 m of ASTER, 30-60 m of Landsat 7 ETM+, and 250-1000 m of MODIS for different stages of the cropping season in the irrigation system of District 1.

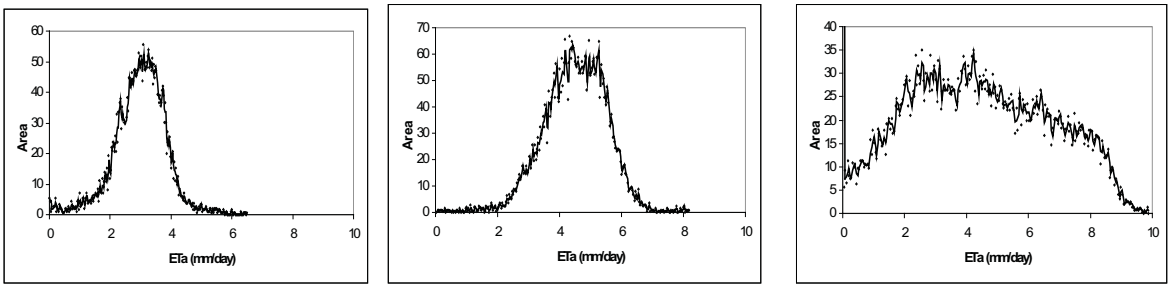

Figure 4.14: Sensors histograms of daily ET_{actual} (mm/day) per area covered (ha) of ASTER (left), Landsat (center), and MODIS (right)

An average from samples of rice pixels for every sensor was taken over the irrigation systems in the southern part of District 1. An average value of daily ET_a of these fields, and the ET_o, and ET_c and E_{pan} of 2 meteorological stations located within 10 km distance are shown in Table 4.11.

Hafeez and Chemin (2003) validated the results of daily ET_a by SEBAL with E_{pan}, ET_o, and ET_c and found the results of daily ET_a by SEBAL within a good accuracy for the ASTER sensor. The E_{pan} results of both meteorological stations are almost equal on the acquisition days of the Landsat and MODIS images, while, in the case of the ASTER sensor, the E_{pan} reading of one meteorological station differs by 11% from that of the other. The possible reasons of this variation in E_{pan} readings can be attributed to the lack of accurate measurement and the poor maintenance of the pan, which was observed by the author during the visits to these meteorological stations. The ET_a values found are 20.7 % & 10.5 % (ASTER), 25 % & 25 % (Landsat) and 11.5 % & 10% (MODIS), respectively, less than the meteorological data of water evaporation. These results match very well the expectations on the difference of ET values between open water bodies and rice crops.

Table 4.11: Comparison of E_{pan}, ET_o, ET_c and daily ET_a, (mm/day)

Date/Evapotranspiration		PAGASA, Munoz (15° 43' N, 120° 54' E)	PhilRice, Maligaya (15° 39'N, 120° 53' E)
2-Feb-01	Epan	5.3	4.7
	ET_o (Penman Monteith)	4.25	3.57
	ETc (Kc=1.05)	4.46	3.75
	ASTER	4.2	
16-Apr-01	Epan	6.8	6.8
	ET_o (Penman Monteith)	5.83	5.84
	ETc (Kc=0.9)	5.24	5.26
	Landsat 7 ETM+	5.11	
18-May-01	Epan	7	6.9
	ET_o (Penman Monteith)	6.83	6.8
	ETc (Kc=0.8)	5.46	5.44
	MODIS	6.19	

In the case of the Penman Monteith method (Allen et al. 1998), the results of the estimated ET_o from the meteorological stations data gave a difference from the remote sensing data of +1 % & -15 % (ASTER), +12 % & +12.5 % (Landsat), and +9.2 % & +8.9 % (MODIS), respectively. Adjustment for the crop coefficient (K_c) of rice in its different growth stages with a corresponding K_c factor of 1.05 (mid), 0.9 (end) and 0.80 (end) for general rice crops from the same author also provides significant results. The crop stages data were monitored continuously in 50 rice fields in District 1 during the entire dry season 2001. The differences of ET_c observed from remote sensing are +6 % & -11 % (ASTER), +2.5 % & +3 % (Landsat), and -13 % & -13.8 % (MODIS), respectively. It can be concluded that the results are confirmed by the ET_o and ET_c calculations from ground data within an acceptable range for all sensors.

4.2.5.5 Conclusion

It was proven possible to simultaneously use SEBAL for different sensors with the combination of high spatial and temporal resolution in tropical countries like the Philippines, where the cloud coverage is a big constraint in getting satellite images from one sensor. The interchangeability between Landsat 7 and ASTER images was explored, as well as the early study of the convergence of MODIS data to the high-resolution accuracy in terms of water consumption.

Field level spatially distributed ET_a can be estimated using ASTER, Landsat ETM+ and MODIS sensors with a deviation of 9 %, 3 % and 13.5 % from ET_c (Penman-Monteith). The possible reason for the large deviation of the ET_a estimates using the MODIS sensor is pixel size for such a small area (District 1), because the thermal bands of MODIS provide surface temperature information over 1 km pixel size.

The comparison shows that high spatial resolution sensors (ASTER vs. Landsat) can be used for ET studies even at smaller scale irrigation systems like District 1 in the tropical climate of the Philippines. The use of MODIS in combination with higher resolution satellites is found encouraging, supporting the earlier work of Chemin and Alexandridis (2001). More extensive work on MODIS operationalization at field/farm and tertiary/secondary canal command areas is required. It is of paramount importance for future end-user applications, since MODIS is freely available through Internet download and its processing levels are well standardized.

4.2.6 Seasonal evapotranspiration through satellite remote sensing

4.2.6.1 Introduction

Evaporation and transpiration are important components of the hydrological cycle for both the river-basin management researcher and the farmer. Reference and crop ET may be easily estimated at a point using climate station data but it becomes difficult when large areas such as irrigation systems or basin levels are concerned. Estimation of ET_a through airborne and satellite remote sensing has attracted many scientists for the last 20 years. (Jackson et al. 1977; Seguin and Itier 1983; Moran et al. 1994; Kustas and Norman 1996 and Bastiaanssen et al. 1998). The SEBAL model developed by Bastiaanssen in 1995 has been used to compute ET_a on a pixel-by-pixel basis through the energy balance method.

The main constraint in using remote sensing-based models is that ET_a is calculated only on the satellite overpass days. The non-availability of cloud-free images, intensive computing procedure, and cost also pose major constraints in processing visible/thermal-infrared satellite images for daily ET_a estimation. Temporal integration strategies have to be used in order to fill in the missing satellite data and get the integrated ET_a information for a season.

Cloud coverage is a prominent phenomenon in many tropical parts of the world. The mean cloud cover per day may exceed 60 % in the humid tropics (Bussieres

and Goita 1997). It is practically impossible to get well-distributed cloud-free images over the entire cropping season from one sensor in tropical countries like the Philippines. Farah (2001) provided evaporation estimates through remote sensing by coupling Penman Monteith and Jarvis-Stewards models to reconstitute evaporation under cloudy conditions in the Navaisha Basin of Kenya. Alternative solutions for cloud cover would encompass supplementing hydrological models with satellite ET_a images of high resolution for critical timings in the cropping patterns. Such study as the one performed by Droogers and Bastiaanssen (2000) could prove useful in such climates, with direct results of enhancing temporal and spatial variation of ET from a water balance model.

Table 4.12: Details of satellite image used in the study

Satellite	Sensor	Spatial resolution (m)	Temporal resolution (days)	Image acquisition dates
TERRA	MODIS	250 - 1000	1/2	16 November 2000 20 December 2000 03 January 2001 26 January 2001 01 March 2001 24 March 2001
TERRA	ASTER	15 - 90	16	02 February 2001
Landsat 7	ETM+	30 - 60	16	16 April 2001 02 May 2001 18 May 2001

The cloud-cover frequency limitation in a tropical climate can be overcome with the combination of high-spatial resolution of Landsat and TERRA/ASTER images with the high temporal resolution of TERRA/MODIS images. The main objective of this section was to develop a methodology for the estimation of seasonal ET_a, the most difficult component in water balance studies.

4.2.6.2 Satellite images

In this study, only one cloud-free image from TERRA/ASTER L1B, 3 from Landsat 7 ETM + and 6 from the MODIS L1B were available over the entire dry season of 2001 (compared to 92, 12 and 110 images, respectively, available in ideal situations). The ASTER image (2 February 2001) was not used for the integration of seasonal ET_a

because it covered only half the District 1 area. These nine satellite images covered the dry season 2001 (19 November 2000 to 18 May 2001) with an average representation of 20 days. The three Landsat images were degraded nine times to get the pixel size of MODIS for getting seasonal ET. Details of satellite images used, spatial resolution and revisiting period are shown in Table 4.12.

4.2.6.3 Material and methods

The ET_a calculation through remote sensing on specific dates provided a good indication of its spatial distribution in the irrigation system. However, this information could not be used directly, as ET_a directly depends upon weather conditions and water availability in the field, which varies from day to day. It was, therefore, necessary to simulate daily values to get an accurate estimation of seasonal ET_a. A larger sample of timely ET observations is necessary to obtain an accurate result and to adjust the daily fluctuation of ET_a for integration of seasonal ET_a. As proposed by Tasumi et al. (2000), missing values of ET_a could be obtained by daily calculation of ET_o using the modified Penman-Monteith method. Temporal integration was undertaken in four steps: (i) determination of the period represented by each satellite image, e.g., selecting the 16 November 2000 image to represent the month of November, etc.; (ii) computation of ET_o using the modified Penman-Monteith method for the whole period represented by each image (average monthly ET_o values collected from two meteorological stations, PAGASA and PhilRice, are summarized in Table 4.13); (iii) computation of K_m values for each period as shown in Table 4.14; and (iv) computation of cumulative seasonal ET_a using the following equation:

$$ET_S = \sum_{i=1}^{n} (ET_a)_i \times (K_m)_i \quad (mm) \qquad \textit{Equation 4.11}$$

where ET_a = actual daily ET value computed by SEBAL for each pixel of image "i";
K_m = multiplier for ET for the representative period;
n = number of satellite images processed; and
ET = seasonal ET (mm).

Table 4.13: Average ET_o and cumulative ET_o values representing both meteorological stations in District 1 of UPRIIS

ET	16 November	20 December	03 January	26 January	01 March	24 March	16 April	02 May	18 May
Cumulative ET_o (mm)	48.1	91.9	51.7	118.9	107.5	71.4	100.7	82.3	54.2
ET_o (mm)	4.1	3.8	4.2	3.8	4.3	4.9	5.7	5.4	6.0

4.2.6.4 Results and discussion

In this study, ET_a values calculated through SEBAL were compared with the measured evaporation through Class A Pan (E_{pan}), estimated ET_o and crop evapotranspiration (ET_c) using the modified Penman-Monteith method from PAGASA and PhilRice meteorological stations for the whole dry season 2000-2001 in District 1 as shown in Figure 4.15. There is a significant difference in ET values obtained from remote sensing and classical techniques, which utilize weather stations data. While the former provides spatial distribution results, the latter provides only point values.

Table 4.14: Values of K_m for dry season 2001 in District 1

	16-30 November	1-31 December	01-15 January	16 January –15 February	16 February -15 March	16- 31 March	1-20 April	21 April –05 May	06-18May
K_m	11.78	23.91	12.42	30.99	25.16	14.60	17.58	15.11	9.09

Although the comparison of ET_a with E_{pan}, ET_o and ET_c does not fully validate the remote sensing results as the Bowen ratio would, this method could still provide a good indication of ET_a values estimated from SEBAL. Since there were no available instruments for measuring the Bowen ratio or other potential indicators, point data at both meteorological stations were used for comparison because they show some trends in ET in the time domain of the dry season 2001.

E_{pan} indicates the evaporation from water bodies. As validated in Figure 4.15, E_{pan} values from both meteorological stations were always higher than ET_a values for all the ten (10) image acquisition dates during the dry season 2000-2001. The absolute values of ET_o and ET_c at both meteorological stations compared to ET_a provide an indication of the amount of confidence that can be given to the values of ET_a derived

from the remote sensing images. The ET_a is estimated from all the physical mediums within one pixel (250 m as in the case of MODIS), which might have mixed spectral signatures of road, settlement, water body, and rice field. Due to the large pixel size of MODIS (250 m), it is difficult to absolutely compare such information with the classical point data from meteorological data, even though Figure 4.15 shows a good trend regarding the accuracy of ET_a derived from the SEBAL model.

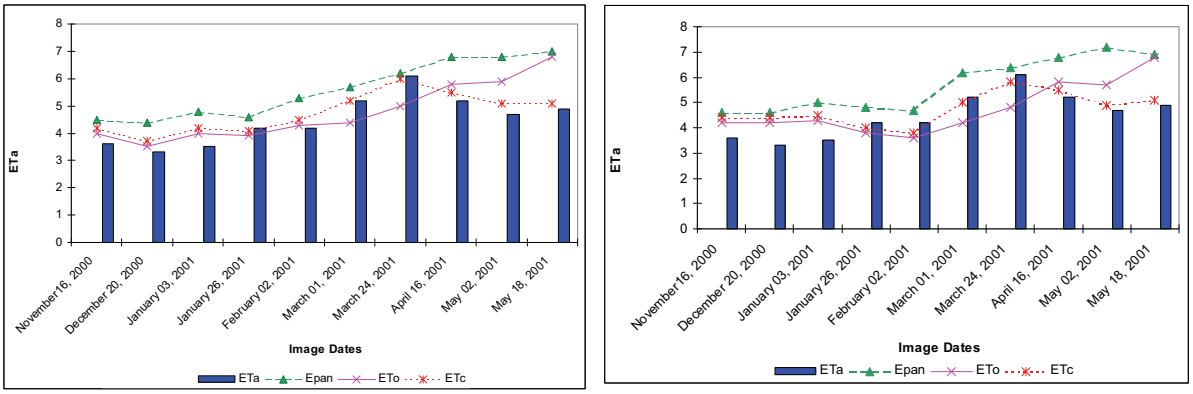

Figure 4.15: Comparison of ET_a of rice pixels with E_{pan}, ET_o, and ET_c, at PAGASA (right figure) and PhilRice (left figure) weather stations for dry season 2000-2001 in District 1 (all in mm d^{-1})

Table 4.15: Seasonal evapotranspiration (ET_s) at different scales in District 1

Scale	Area (ha)	Minimum ET_s (mm)	Maximum ET_s (mm)	Mean ET_s (mm)
TRIS-Lower	11239	393.5	743.3	568.4
SDA-A	1513	582.7	724.9	653.8
SDA-B	2240	543.7	707.4	625.6
SDA-C	3011	526.3	721.6	624.1
SDA-D	10201	510.46	748.1	629.3
District 1	28,205	382.6	756.3	569.1

The integration of daily ET_a raster maps was done using the straightforward method described in the temporal integration part of this section. The seasonal actual evapotranspiration (ET_s) map on a pixel-by-pixel basis was produced through integration of all daily ET_a images for the dry season 2001. The ET_s map illustrates the seasonal evapotranspiration per unit area during the dry season 2000-2001 (from 19

November 2000 to 18 May 2001), at different spatial scales in District 1 as shown in Table 4.15.

The irrigated rice fields (blue color) can be differentiated from the non- irrigated fields (red color) at a spatial resolution of 250 m as shown in Figure 4.16.

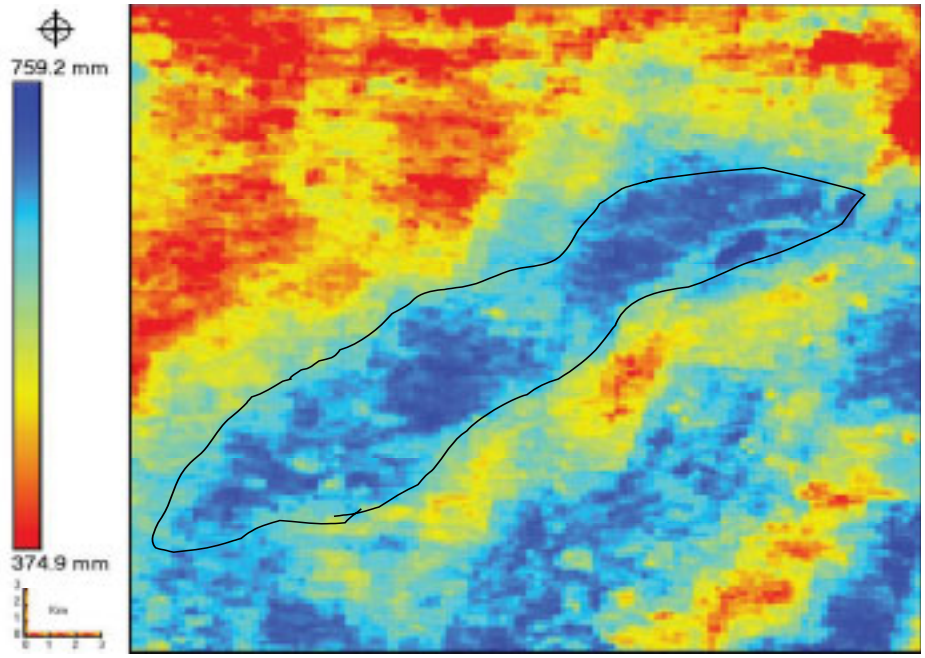

Figure 4.16: Seasonal actual evapotranspiration (ET_s) map (250 m) for dry season 2001

The comparison of ET_a estimated from SEBAL with potential crop evapotranspiration (ET_c) and pan evaporation (E_{pan}) measurements indicates relatively good accuracy and potential for use in the water balance and water productivity study District 1 for the dry season 2001.

5. WATER ACCOUNTING AND PRODUCTIVITY RESULTS

5.1 Water accounting and productivity at different scales

5.1.1 Spatial scales

A scale is a specific relative or proportional size or extent of phenomena as measured through space and or time. There are two different approaches when dealing with scale: scale as hierarchy or scale as magnitude (Brent et al. 2001). Each level in the scale has its own unique features that are not the simple summation of disaggregated parts. The major problem about the scale is that data may carry different information when presented at different scales and new properties emerge when data are aggregated spatially. For example in hydrology, scales to be considered are farmer's field, irrigation systems and river basins.

Dong et al. 2001 stated that water saving has different meanings for different people at various scales, i.e., farmer field to individual farm to sub-basin levels, and that the meaning is dependent on the scale of interest. In case of a farmer, the primary interest is to maximize his profit. If he faces any threat in profit reduction due to high input cost (service fee based on actual amount of water used or using pumps) then his priority will be to reduce the input cost. Tuong and Bhuiyan (1999) also reported that water savings at farm level refer to a reduction in irrigation water applied to crops. One farmer's drainage may be another farmer's water supply because of recycling and re-use of water (Seckler 1996). Then reducing drainage from rice fields is not real water saving for that irrigation system. In the same way, losses of an irrigation system may not constitute losses to the river basin.

It is often discussed whether the water saved locally in a farmer's field will result in water saving at the irrigation system or basin level. Actually, it depends on what happens to the amount of water (drainage) that is delivered to the field but not consumed through crop evapotranspiration. If the drainage water moves to oceans or deep saline aquifers, i.e., the water is lost permanently from the irrigation system, then that kind of reduction in drainage water can lead to real water saving. On the other hand, drainage water flows from one farmer's field to another farmer's field and this means that recycling occurs within the rice-irrigation system. One farmer's drainage may be another farmer's water supply because of recycling and re-use of water (Seckler 1996). An understanding of the water balance of the irrigation system is crucial in determining

current levels of efficiency and in developing alternative strategies that are more efficient. However, the effects of water saving at the field level on overall water saving and water productivity at the irrigation system level have hardly been assessed and are mostly unknown.

This study followed the concept of scale focusing on size or magnitude and tried to develop all possible combinations using top-down and bottom-up approaches to study water saving at different spatial scales of District 1, UPRIIS. District 1 is divided into four different sub-areas, i.e., Talavera River Irrigation System-Lower (TRIS-L), Santo Domingo Area-A (SDA-A), Santo Domingo Area-B (SDA-B), Santo Domingo Area-C (SDA-C), as shown in Figure 4.2. Later, six new scales were created by merging these sub-areas: SDA-(A+B) by merging SDA-A & SDA-B; SDA-(B+C) by adding SDA-B & SDA-C; SDA by adding (SDA-A, SDA-B & SDA-C); TRIS-L plus SDA-A; TRIS-L plus SDA-(A+B); and District 1 by adding (TRIS-Lower & SDA), respectively to measure the real water saving at different spatial scales.

5.1.1.1 Talavera River Irrigation System-Lower (TRIS-L)

The total area of TRIS-L is 11, 239 ha and 78 % was under rice crop (Figure 5.1). TRIS-L has 48 Farmer Irrigator Associations (FIA's) with an average size of 233 ha. There are 11 small check dams, which capture internal drainage water. In 2001, the

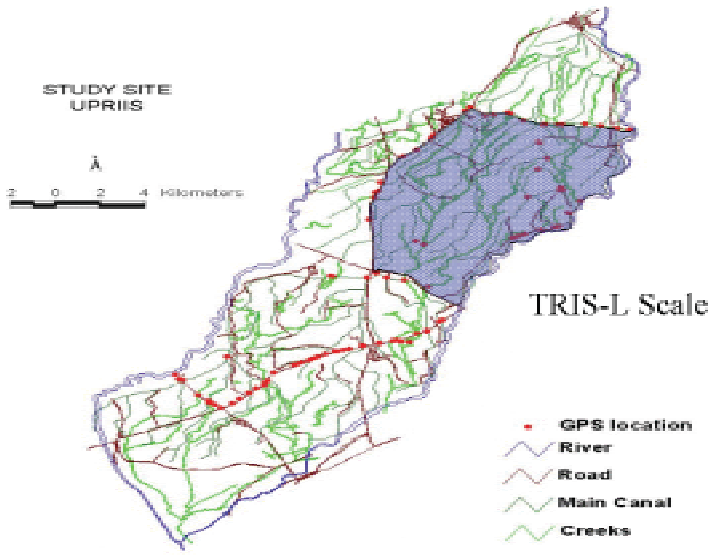

Figure 5.1: Location of TRIS-Lower scale in District 1.

farmers did not face a water shortage and planted rice according to the recommended cropping schedule. Only a few farmers located at the tail end of Lateral F (near SDA) could not grow rice in the dry season because of water shortage.

5.1.1.2 Santo Domingo Area-A (SDA-A)

SDA-A is in the upper part of SDA (Figure 5.2) and the total area is 1513 ha (78% under rice crop). There are five FIA's with an average size of 175 ha. SDA-A receives water from Lateral A of the SD main canal, sub-lateral B4 and two creeks coming out of TRIS-L. The De Buasao check dam is the origin of Lateral A-Extra (A-x), which also supplies water to the lower part of SDA-A and the upper part of SDA-D. The farmers far away from the main canal depend somewhat more on shallow tube wells for additional irrigation water than the farmers close to the beginning of the main canal.

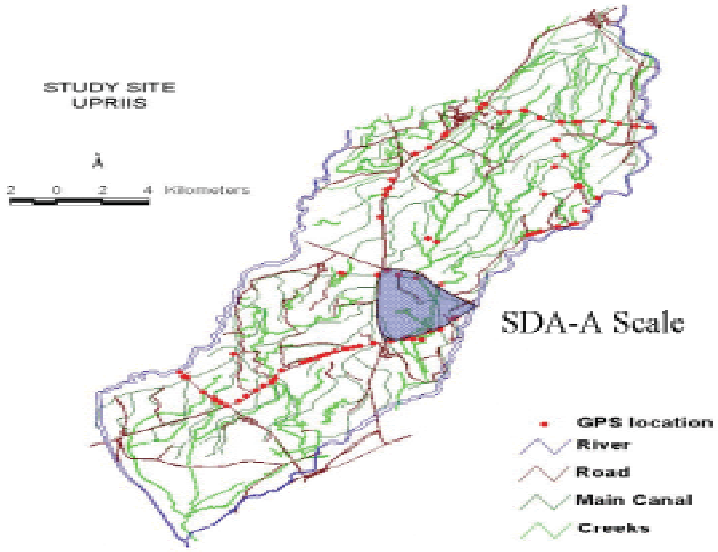

Figure 5.2: Location of SDA-A scale in District 1.

5.1.1.3 Santo Domingo Area-B (SDA-B)

The total area of SDA-B is 2240 ha (76% under rice crop) and is the second smallest area (Figure 5.3). The major sources of water are laterals B and C, and two creeks getting water from the Ilog Baliwag River. There are six FIA's with an average size of 373 ha. Water shortage forces farmers to get water either through groundwater pumping or by using illegal inlets along the Santo Domingo main canal. The Pajo check dam

captures drainage water from farmers upstream and serves as a major source of water for SDA-C.

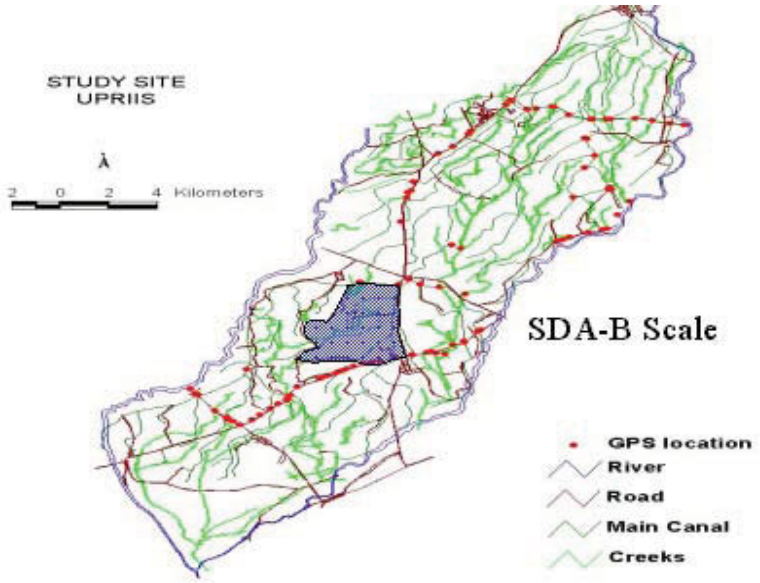

Figure 5.3: Location of SDA-B scale in District 1.

5.1.1.4 Santo Domingo Area-C (SDA-C)

SDA-C is in the lower portion of the SDA (Figure 5.4) and the total area is 3011 ha (65 % under rice crop). The laterals D, E, E-X, F, and G and two creeks (Pajo and Labong) are the main sources of water. There are seven FIA's with an average size of 273 ha. All farmers in SDA-C depend on pumping for additional supplies of water. Normally, the

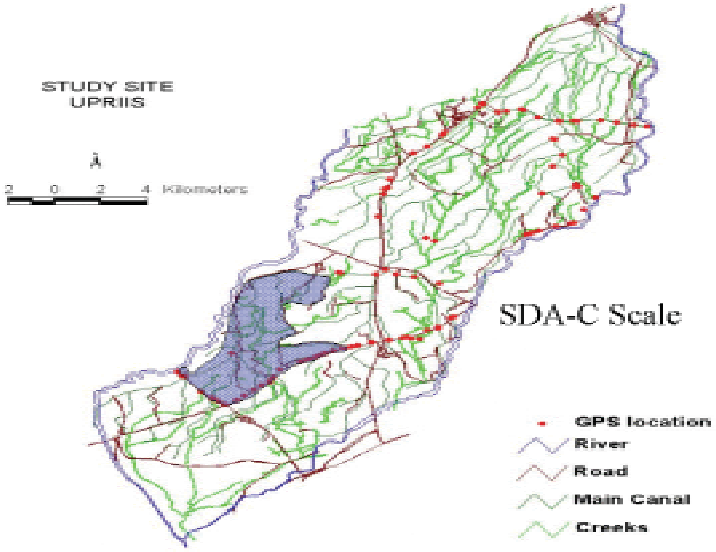

Figure 5.4: Location of SDA-C scale in District 1.

farmers get surface water only when the upstream farmers do not need it. The cropping pattern depends totally on the availability of irrigation water and rice planting is about 2-3 weeks later than in TRIS-L. Santa Rita is the only check dam in SDA-C that captures drainage water in small creeks and serves as a major source of water for SDA-D.

5.1.1.5 Santo Domingo Area -A+B

This scale is created by the merging of the areas SDA-A and SDA-B (Figure 5.5), the gross area is 3,753 ha (roads, settlements, woodlands, rice fields and water bodies), while 77 % of the area was under rice crop during the dry season 2001. The main source of water for SDA-A+B is Laterals A, B, & C (through SD Main canal) and 4 large creeks carrying re-used water from the TRIS-L and Ilog Baliwag River area. All the drainage at farm level is recaptured at 3 small check dams and this re-used water serves the downstream area of SDA-A, SDA-B and SDA-C. The majority of farmers depend on pumping for extra water supplies for activities in the dry season ranging from land preparation to harvesting.

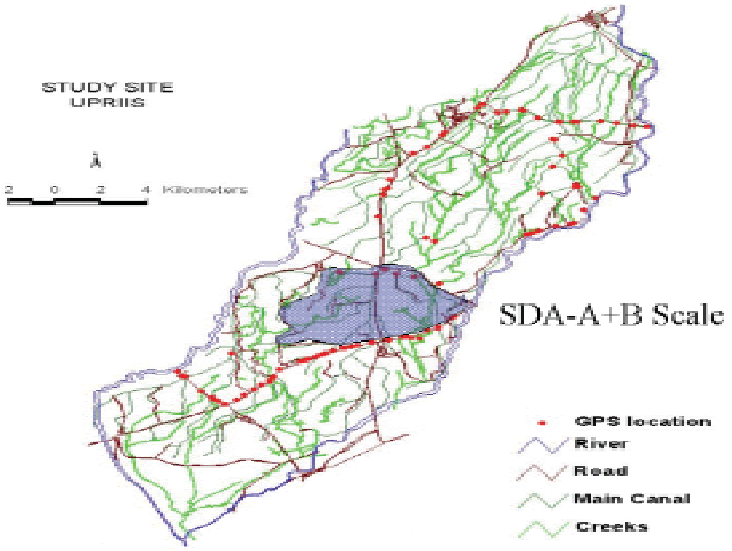

Figure 5.5: Location of SDA-A+B scale in District 1.

5.1.1.6 Santo Domingo Area -B+C

SDA-(A+B) is the tail end of District 1 (Figure 5.6), and was created by merging two areas of SDA-B and SDA-C. The gross area of 5,251 ha covers all types of land uses and 70 % of the area is under rice crop. The major source of water is the SD main canal (through laterals B, C, D, E, F, G & E-X), and 3 creeks getting water from Ilog Baliwag River. The 3 check dams play an important role in capturing all drainage water from the rice fields and this re-used water served within area and SDA-D. The majority of the farmers at the tail end depend on pumping for an additional supply of water during the dry season.

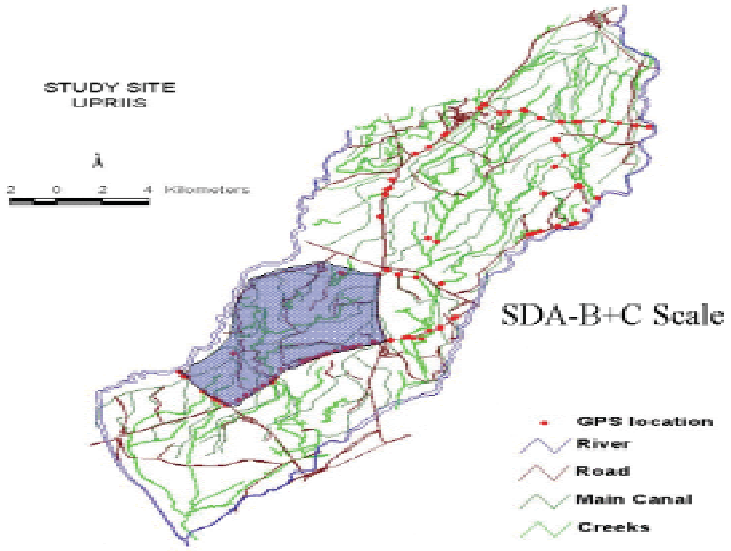

Figure 5.6: Location of SDA-B+C scale in District 1.

5.1.1.7 Santo Domingo Area -(A+B+C)

SDA is the southern part of District 1 and all sub-areas of the Santo Domingo (SDA-A, SDA-B, & SDA-C) area are merged to create this scale (Figure 5.7). The SD main canal is the major source of water for this scale and 4 big creeks carrying re-used water from the TRIS-L and Ilog Baliwag River area. The gross area is 6,764 ha (roads, settlements, woodlands, rice fields and water bodies), while 72 % of area was under rice crop during the dry season 2001. All the drainage water from the farmers' fields is recaptured through creeks at 4 small check dams which play an important role concerning the water supply in this and the downstream area of SDA-D The majority of farmers at the tail end depend on pumping for an additional supply of water during the dry season, and the

farmers can obtain water only when there is no need of it in the upstream area. That is the reason why the cropping pattern is 2-3 weeks later than in other areas of District 1.

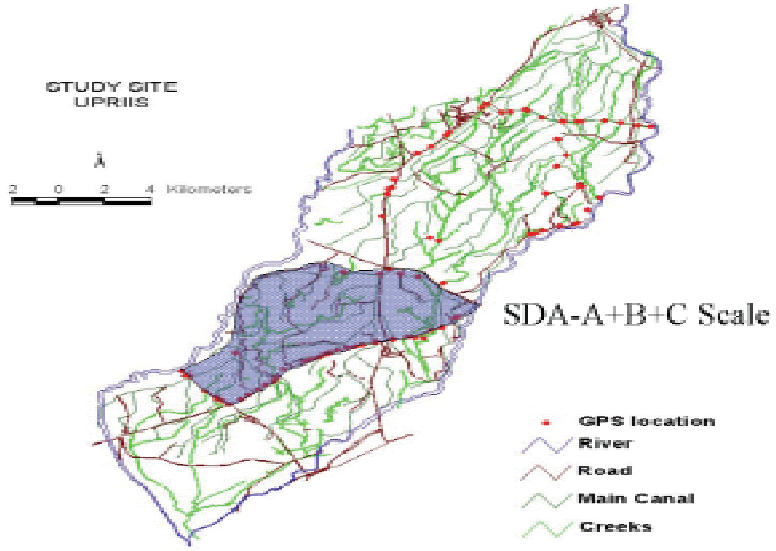

Figure 5.7: Location of SDA-A+B+C scale in District 1.

5.1.1.8 TRIS-L + SDA-A

Merging two areas, i.e., TRIS-Lower with SDA-A, creates this scale (Figure 5.8). The gross area is 12,752 ha (including fields, roads, woodlands, water bodies and settlements), while 78 % of the area was under rice crop in the dry season 2001. The diversion Canal 1 and several creeks (drainage water from TRIS-Upper) are the major

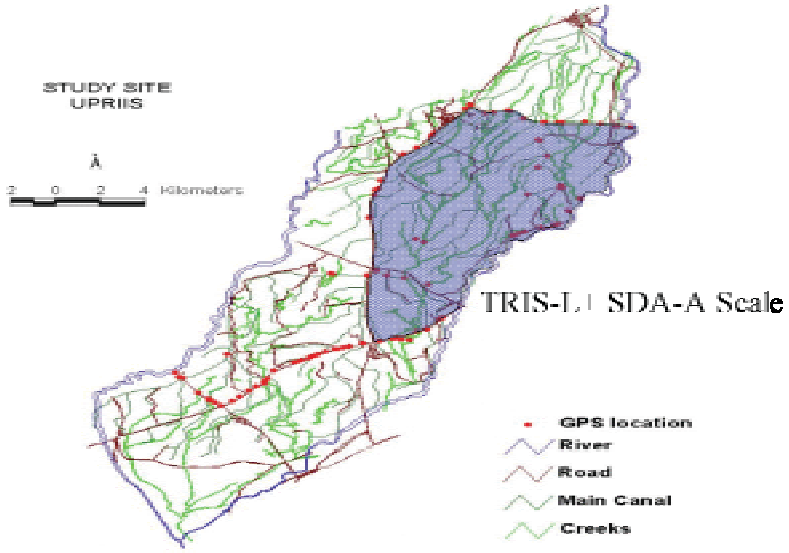

Figure 5.8: Location of TRIS-L + SDA-A scale in District 1.

source of water. There are 12 small check dams, which capture the re-used water from the rice fields through small creeks and then supplement irrigation water in the laterals and sub-laterals of the downstream areas. Most of the farmers have installed pumps, which are an alternative source of irrigation water in case of shortage.

5.1.1.9 TRIS-L + SDA-(A+B)

This scale is aggregated by merging the areas of TRIS-L, SDA-A, & SDA-B (Figure 5.9). The gross area is 14,992 ha (roads, settlements, woodlands, rice fields and water bodies), while 77 % of the area was under rice crop during the dry season 2001. All the re-used water of farmer fields is recaptured through creeks at 14 small check dams, which play an important role by supplying water within this area and the downstream area of SDA-D.

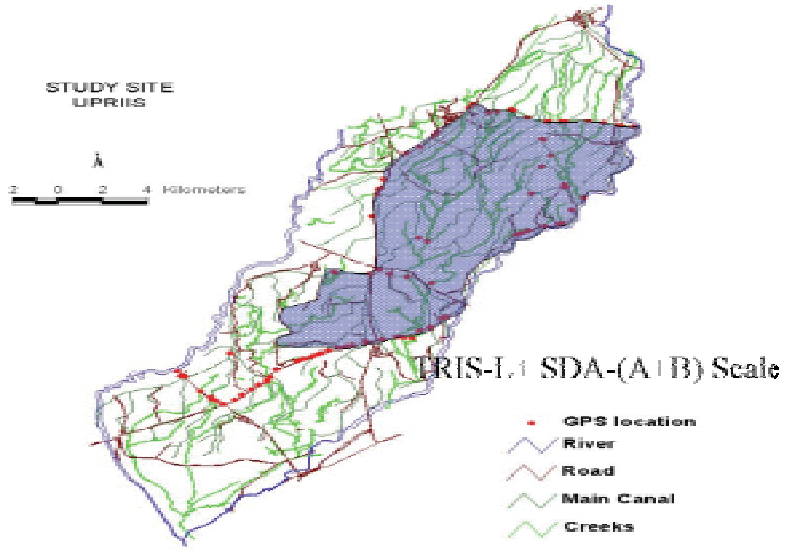

Figure 5.9: Location of TRIS-L + SDA-(A+B) scale in District 1.

5.1.1.10 District 1 (TRIS-L + SDA-(A+B+C))

This scale represents District 1 excluding the areas SAE, TRIS-Upper, and SDA-D (Figure 5.10). The gross area is 18,003 ha (roads, settlements, woodlands, rice fields, upland crops and water bodies), while 75 % of area was under rice crop during the dry season 2001. There are 15 small check dams that capture the re-used water from the rice fields through small creeks and then supplement irrigation water in the laterals and sub-laterals of downstream areas.

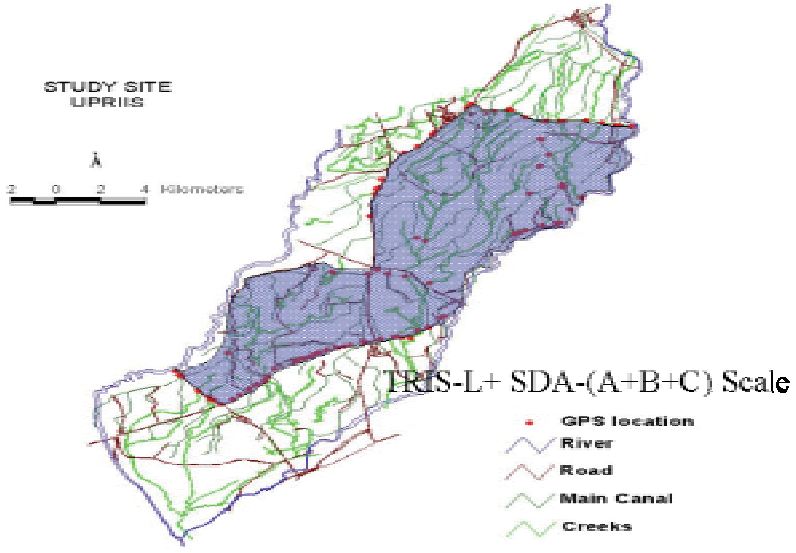

Figure 5.10: Location of TRIS-L + SDA-(A+B+C) scale in District 1.

5.1.2 Water accounting

Recently, the International Water Management Institute (IWMI) developed water accounting procedures (Molden 1997), based on water-balance approach to quantify the amount of water entering a system (through surface flows, groundwater flows by pumping, and rainfall) and the amount of water leaving a system (through evapotranspiration, surface outflow and groundwater flows). Water accounting classifies the amount of depleted water within an irrigation system based on uses, whether intended use or not, and whether beneficial use or not. It also classifies outflow water as committed water and non-committed water for downstream uses. Water accounting performance indicators were developed as an alternative to the classical irrigation efficiencies used in irrigation engineering. Water accounting definitions are summarized in Box 1.

The water accounting procedures were developed to study water saving at three different levels: micro (agricultural field), macro (irrigation system) and macro (basin or sub-basin). Many researchers have applied water accounting procedures in different countries to identify opportunities for water saving and improving productivity at different spatial scales from farmer's field to irrigation system, sub-basin and basin levels (Molden 1997; Molden and Skathivadivel 1999; Dong et al. 2001; Ronald et al.

Text Box 1.Water accounting definitions (Molden 1997)

Gross inflow is the total amount of water flowing into irrigation system from surface water resources, ground water pumping and rainfall.

Net inflow is the gross inflow plus any change in storage with in a domain of interest. Net inflow is greater than gross inflow when a large amount of water is removed (pumping) from the groundwater storage over the cropping season.

Committed water is that part of outflow from the system that is committed to downstream uses such as environment requirements or water rights.

Uncommitted Outflow is water which is neither depleted nor committed and is available for a use within a domain of interest, but flows out of system due to lack of storage or operational measures. Uncommitted outflow is further classified as utilizable or non-utilizable outflow. Outflow is utilizable if the water can be used through improved management of existing facilities. Non-utilizable outflow is the loss of water due to insufficient facilities for capturing outflow. For example, the creeks that discharge water into Talavera River from TRIS-Lower scale are utilizable uncommitted outflow for District 1 of UPRIIS.

Water depletion is a removal of water from a domain of interest that becomes unavailable for further use. Water can be depleted through four generic processes:

- Evaporation: water is vaporized from surfaces or transpired by plants.
- Flows to sinks: water flows into a sea, saline groundwater, or other location where it is not economically recoverable for re-use.
- Pollution: water quality becomes degraded and thus unfit for certain uses.
- Incorporation into a product: through an industrial or agricultural process such as bottling water, or incorporation of water into plant tissues.

Process depletion is that amount of water, which is depleted to produce a product intended for human use. For example, the amount of water lost through evapotranspiration by the rice crop.

Non-process depletion is that amount of depleted water that is not lost as the result of a production process. It can be classified as beneficial and non-beneficial depletion, e.g., evaporation from swampy areas will be called non-beneficial depletion, while evaporation from forest trees will be treated as beneficial depletion.

Available water is the net inflow less the committed water to downstream uses. It includes process and non-process depletion, and utilizable outflow.

2002). The clear understanding of all the components of water accounting at the spatial scales level will allow the measurement of the true water saving at that particular scale. Data for water accounting indicators are needed to evaluate water saving at different spatial scales for better understanding the performance of the irrigation system.

The measurement procedures for net inflow (surface inflow, rainfall, pumping from groundwater, and groundwater storage change), outflow (committed, non-committed, and percolation) at different spatial scales are discussed in detail in Chapter 3. The land-use classes, and the process and non-process depletion are discussed in Chapter 4. The system boundary of this study lies between root zone and canopy of the crop. All the water going out from these boundaries is treated either depleted or outflow from that particular scale. The water accounting for 10 different spatial scales in District 1 is presented in Table 5.1, which also shows that District 1 is an open basin.

Table 5.1. Water accounting components in different areas of District 1.

Description	Scales									
	TRIS-L	SDA-A	SDA-B	SDA-C	SDA-(A+B)	SDA-(B+C)	SDA	TRIS+SDA-A	TRIS+SDA-(A+B)	District1
Total area(ha)	11239	1513	2240	3011	3753	5251	6764	12752	14992	18003
Rice area(ha)	8713	1177	1709	1972	2886	3681	4858	9890	11599	13571
Gross Inflow(m^3)	4.0E+08	1.1E+08	1.4E+08	1.3E+08	2.4E+08	1.5E+08	2.6E+08	4.1E+08	4.2E+08	4.4E+08
Irrigation	3.5E+08	1.1E+08	1.3E+08	1.1E+08	2.3E+08	1.3E+08	2.3E+08	3.6E+08	3.6E+08	3.6E+08
Rainfall	3.3E+07	3.3E+06	4.8E+06	8.8E+06	8.0E+06	1.4E+07	1.7E+07	3.6E+07	4.1E+07	5.0E+07
Pumping from Ground water/creeks	1.5E+07	1.8E+06	2.0E+06	8.6E+06	3.8E+06	1.1E+07	1.2E+07	1.7E+07	1.8E+07	2.7E+07
Storage Change(m^3)	-2.6E+06	-4.5E+05	-1.3E+06	-2.3E+06	-1.7E+06	-3.5E+06	-4.0E+06	-3.0E+06	-4.3E+06	-6.6E+06
Net Inflow(m^3)	4.1E+08	1.2E+08	1.4E+08	1.3E+08	2.4E+08	1.5E+08	2.6E+08	4.1E+08	4.2E+08	4.4E+08
Total Outflow(m^3)	3.3E+08	1.0E+08	1.2E+08	1.1E+08	2.2E+08	1.2E+08	2.1E+08	3.3E+08	3.2E+08	3.2E+08
Committed outflow	2.3E+08	9.5E+07	1.1E+08	9.8E+07	2.0E+08	1.0E+08	2.0E+08	2.4E+08	2.4E+08	2.5E+08
Uncommitted Outflow	4.9E+07	0.0E+00	0.0E+00	0.0E+00	0.0E+00	0.0E+00	0.0E+00	4.9E+07	4.9E+07	4.9E+07
Percolation	4.4E+07	5.9E+06	8.7E+06	1.2E+07	1.5E+07	2.0E+07	2.6E+07	5.0E+07	5.8E+07	7.0E+07
Total Depletion(m^3)	6.8E+07	9.9E+06	1.5E+07	2.0E+07	2.5E+07	3.4E+07	4.4E+07	7.8E+07	9.3E+07	1.1E+08
Process- ET_{rice}	5.7E+07	8.0E+06	1.2E+07	1.3E+07	2.0E+07	2.5E+07	3.3E+07	6.5E+07	7.7E+07	9.0E+07
Non Process $ET_{non-rice}$	1.1E+07	1.9E+06	3.2E+06	6.3E+06	5.2E+06	9.5E+06	1.1E+07	1.3E+07	1.6E+07	2.2E+07
Available Water(m^3)	1.6E+08	1.6E+07	2.5E+07	3.4E+07	4.1E+07	5.8E+07	7.5E+07	1.8E+08	2.0E+08	2.4E+08

Rice Yields Estimation The yield data were obtained from the weekly monitoring activities of NIA at all spatial scales of District 1. NIA has divided District 1 into different zones and these zones are again divided into farmer-irrigators association (FIA) level for better maintenance and operation of the irrigation system. It was observed that the NIA monitoring was not completely accurate due to a large number of discrepancies in the reported programmed and harvested rice areas during the dry

season 2001. One possible reason for this discrepancy is under reporting of area by farmers because the irrigation revenue is based on the yield of the rice grown area. The use of the biomass growth model for estimating rice yield data using remote sensing was not possible due to non-availability of any high-resolution satellite images at the peak of the cropping season during the dry season 2001.

The NIA-monitored yield data showed that TRIS-Lower area has the highest rice yield in District 1. It was decided to use the NIA-monitored average yield data for all scales of District 1 because it was not practically possible to validate these yield data in any other way. The average rice yield of the TRIS-L scale is 6.1 tons/ha as compared to 4.7 tons/ha (SDA-A), 5.6 tons/ha (SDA-B) and 4.8 tons/ha (SDA-C). The average rice yields of each FIA in District 1 are shown in Figure 5.11.

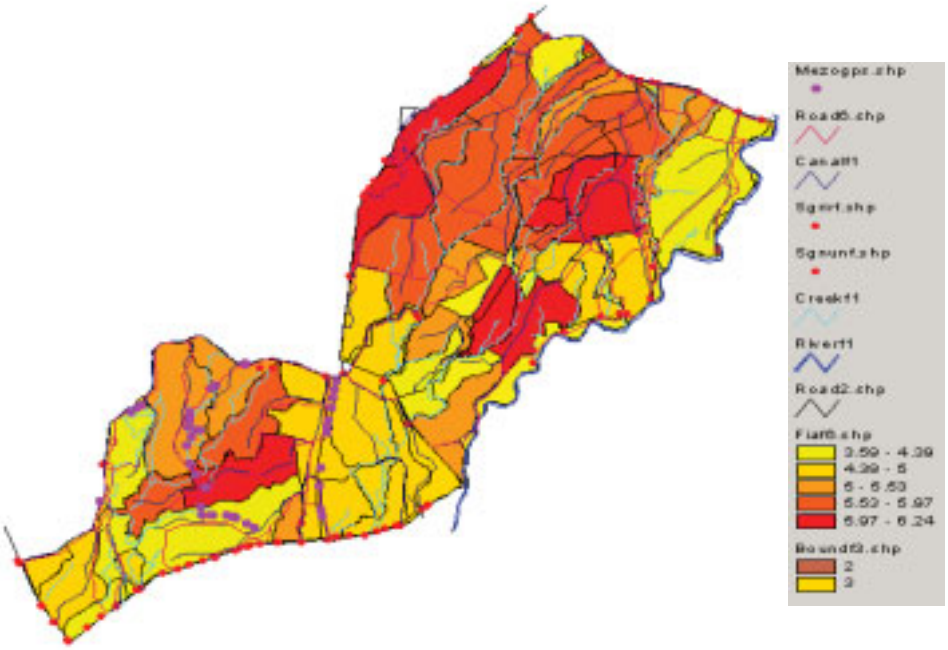

Figure 5.11: Average rice yield (tons/ha) at farmer-irrigators association (FIA) level in District 1.

5.1.3 Water accounting indicators

Molden and Sakthivadivel (1999) introduced 3 types of water accounting indicators: physically based indicators (depleted fractions), beneficial utilization indicators (process fraction) and water productivity indicators. The definition of water accounting indicators is given in Text Box 2. The depleted-fraction indicators reveal information

about the flow paths of water, how much water is being depleted and which use is depleting the water. These fractions do not provide a value judgement about the use of water and can be defined as gross inflow (DF_{gross}), net inflow (DF_{net}), and available water ($DF_{available}$). In this study, DF_{gross} and $DF_{available}$ are used only because DF_{net} is almost equal to DF_{gross}. Process depletion is the total amount of water transpired by the crop. In other words, the process fraction indicates the percentage of water that is depleted through ET_{rice} and can be defined as gross inflow (PF_{gross}), net inflow (PF_{net}), depleted water ($PF_{depleted}$), and available water ($PF_{available}$).

Text Box 2.Water Accounting Indicators (Molden 1997)

Depleted fraction (DF) is that amount of water, which is depleted through process and non-process depletion. In other words, it is the ratio of gross inflow or available water to total depleted water by both process and non-process uses (evapotranspiration of rice crop and swampy areas).
Process fraction (PF) is the ratio of process depletion (evapotranspiration of rice crop) to gross inflow or total depleted water or the amount of available water.
Water Productivity (WP) is expressed only in terms of yield per unit water supply (kg/m^3), while ignoring economics, and the domestic and industrial water needs. It is the ratio of physical mass production of rice measured against gross inflow, net inflow, irrigation inflow, or process depletion. Mathematically, it is represented as WP_{gross}, WP_{net}, $WP_{irrigation}$, and WP_{ETrice}.

The water productivity indicators provide information about how beneficial the water use is and can be defined in many ways, i.e., gross inflow (WP_{gross}), net inflow (WP_{net}), irrigation ($WP_{irrigation}$), or beneficial evapotranspiration (WP_{ETrice}). In agriculture, the productivity of water per unit evapotranspiration of rice crop is comparable to a water use efficiency term (Viets 1962; Howell et al. 1990). In this study, four productivity indicators are used for comparison at different spatial scales in District 1. These performance indicators are presented in the form of fractions in Table 5.2.

Table 5.2. Water accounting indicators for different spatial scales of District 1.

Items	Scales									
	TRIS-L	SDA-A	SDA-B	SDA-C	SDA-(A+B)	SDA-(B+C)	SDA	TRIS+SDA-A	TRIS+SDA-(A+B)	District 1
Total area (ha)	11239	1513	2240	3011	3753	5251	6764	12752	14992	18003
Rice area (ha)	8713	1177	1709	1972	2886	3681	4858	9890	11599	13571
Depleted Fraction (-)										
of gross inflow	0.17	0.09	0.11	0.15	0.10	0.23	0.17	0.19	0.22	0.26
of available water	0.42	0.61	0.60	0.58	0.60	0.59	0.59	0.43	0.45	0.47
Process Fraction (-)										
of gross inflow	0.14	0.07	0.09	0.10	0.08	0.16	0.13	0.16	0.18	0.21
of available water	0.35	0.49	0.47	0.40	0.48	0.43	0.44	0.36	0.38	0.38
of depleted water	0.84	0.81	0.78	0.68	0.79	0.72	0.74	0.84	0.83	0.80
Rice Yield (kg/ha)	6089	4734	5580	4826	5157	5203	5047	5412	5468	5307
Rice Production (kg)	5.3E+07	5.6E+06	9.5E+06	9.5E+06	1.5E+07	1.9E+07	2.5E+07	5.9E+07	6.8E+07	7.8E+07
Water Productivity (kg/m^3)										
Gross Inflow	0.13	0.05	0.07	0.07	0.06	0.13	0.10	0.14	0.16	0.18
Net Inflow	0.13	0.05	0.07	0.07	0.06	0.12	0.09	0.14	0.16	0.18
Irrigation	0.15	0.05	0.07	0.09	0.07	0.15	0.11	0.17	0.19	0.22
ET_{rice}	0.92	0.70	0.82	0.72	0.77	0.77	0.75	0.90	0.89	0.86

TRIS-Lower

The process fraction of gross inflow (PF_{gross}) indicates the amount of gross inflow, which is depleted by process depletion ET_{rice}. PF_{gross} indicates that only 14 % of the water is depleted through ET_{rice} in the TRIS-Lower area, while 78 % of the area is under rice crop. The possible reason for the low PF_{gross} value is that a large amount of water (57 % of gross inflow) is committed water for the Santo Domingo area and it simply passes from the TRIS-Lower area through the diversion canal. All the creeks discharging water into Talavera River are considered uncommitted flow because the irrigation water is specifically released for TRIS-Lower. The process fraction of the available water ($PF_{available}$) is 0.35, meaning that 35 % of available water is beneficially depleted, i.e., through ET_{rice}. The process fraction of depleted water ($PF_{depleted}$) is 0.84, meaning that 84 % of the depleted water is consumed by ET_{rice} in TRIS-Lower and the remaining 16 % evaporates from free water surfaces or non-crop vegetation. The depleted fraction of the gross inflow (DF_{gross}) is 0.17 meaning that 83% of the inflow water (irrigation, rainfall and pumps) is flowing out of the TRIS-lower system that can be used by downstream farmers of SDA-D. The depleted fraction of the available water ($DF_{available}$) is 0.42 (means 42 % of the available water is depleted).

The average rice yield of TRIS-L is very high as compared to the other areas of District 1. The water productivity per unit of irrigation water ($WP_{irrigation}$) is 0.15 kg/m^3, while the water productivity per unit of gross inflow (WP_{gross}) net inflow (WP_{net})

is 0.13 kg/m^3. The water productivity per unit of evapotranspiration (WP_{ETrice}) is 0.92 kg/m^3.

SDA-A

The PF_{gross} value is 0.07, which is very low as compared to the TRIS-L area even if the rice area (78 %) is the same for both cases. In SDA-A, 83 % of the gross inflow is leaving the system for SDA-D. All the outflow of SDA-A is considered as committed water for the downstream area of SDA-D. $PF_{available}$ is also 0.49, meaning that only 49% of the available water is beneficially depleted and $PF_{depleted}$ is 0.81, which indicates that 81 % of the depleted water is consumed by the evapotranspiration of the rice crop. The DF_{gross} value is 0.09, meaning that 9 % of the gross inflow is depleted, and the remaining 91 % is potentially available for the downstream area, i.e., SDA-D. The $DF_{available}$ is 0.61, meaning 61 % of the available water is depleted. The average rice yield of SDA-A is 22 % less than that of the TRIS-L area and the values of WP_{gross}, WP_{net} and $WP_{irrigation}$ are 0.05 kg/m^3, while WP_{ETrice} is 0.70 kg/m^3.

SDA-B

The PF_{gross} value is 0.09, almost the same as SDA-A; 76 % of the area is under rice crop. At the SDA-B scale, 89 % of the gross inflow is committed water for downstream areas of Santo Domingo. The $PF_{available}$ is 0.47, meaning that ET_{rice} depletes 47 % of the available water and the value of $PF_{depleted}$ is 0.78 %, which is almost the same as the other scales of District 1. The DF_{gross} value is 0.11, meaning 11% of the gross inflow is depleted, and the remaining 89 % is potentially available for the downstream area, i.e., SDA-C and SDA-D. $DF_{available}$ is 0.60, meaning 60% of the available water is depleted. The average rice yield of this scale is only 8 % lower than that of the TRIS-L area and all three water productivity indicators (WP_{gross}, WP_{net} and $WP_{irrigation}$) have a common value 0.07 kg/m^3. The water productivity per unit rice evapotranspiration is 0.82 kg/m^3.

SDA-C

This is the southernmost part (tail end) of District 1 and only 65 % of the area is under rice crop. The process fraction of gross inflow PF_{gross} is 0.10, which means that 10 % of the gross inflow is consumed by the rice. The $PF_{available}$ value is 0.40, which indicates

that 40 % of the available water is depleted by beneficial evapotranspiration. $PF_{depleted}$ is 0.68, meaning that 68 % of the depleted water is consumed by the rice crop and 32 % is lost through non-process depletion. The depleted fraction of gross inflow is 0.15, which shows that 85 % of the gross inflow is flowing out of SDA-C. The average rice yield is again 21 % lower than that of the TRIS-L scale, and the WP_{gross} value is 0.07 kg/m^3. The water productivity per unit of evapotranspiration is 0.72 kg/m^3. One reason for the low ET_{rice} is the very low rice yield of the SDA-C scale as compared to other scales.

SDA-(A+B)

Gross inflow is almost equal to net inflow, because the change in storage is very small as compared to the other components of the water balance for this scale. Only 8 % of the gross inflow is consumed by crop ET (PF_{gross} =0.08) and the process fraction of the available water is increased from 0.32 (weighted average of SDA-A and SDA-B) to 0.42. $PF_{depleted}$ is increased from 0.62 (weighted average) to 0.79, meaning that only 79 % of the depleted water is consumed by crop ET. The depleted fraction of the available water is increased enormously from 0.37 (weighted average) to 0.48 and DF_{gross} is slightly increased from 0.08 (weighted average) to 0.10. WP_{gross} is slightly increased from 0.05 kg/m^3 (weighted average) to 0.06 kg/m^3 and $WP_{irrigation}$ is increased from 0.05 kg/m^3 (weighted average) to 0.07 kg/m^3, which reflects the water re-use on that scale. The water productivity per unit evapotranspiration of rice is slightly increased from 0.61 kg/m^3 (weighted average) to 0.77 kg/m^3.

SDA-(B+C)

The water productivity per unit of gross inflow is 0.13 kg/m^3 (almost double that of the weighted average of SDA-B and SDA-C). $WP_{irrigation}$ increased double from 0.08 (weighted average) to 0.15, which reflects the high water re-use within the system. At the SDA-(B+C) scale, 70 % of the area is under rice crop. It was observed that all the drainage water from the rice field is captured through creeks and stored at three check dams for irrigating downstream areas. WP_{ETrice} remained the same (0.77 kg/m^3).

PF_{gross} increased from 0.09 (weighted average) to 0.16, which indicates that 15 % of the gross inflow is consumed by the rice crop and $PF_{depleted}$ decreased slightly from

0.73 (weighted average) to 0.72. DF_{gross} is increased from 0.13 (weighted average) to 0.23 (high gross inflow is depleted at this scale).

SDA-(A+B+C)

The boundaries of the SDA scale are taken as the TRIS-Lower north (upstream), the Santo Domingo main canal to the west, the Ilog Baliwag River to the south, and the SDA-D to the east. The average rice yield is 17 % lower than that of the TRIS-Lower scale where 72 % of the area is under rice crop. The PF_{gross} value is increased from 0.09 (weighted average of SDA-A, SDA-B and SDA-C) to 0.13 and the process fraction of depleted water decreased slightly from 0.75 (weighted average) to 0.74. It shows that other land uses (upland crops and perennial vegetation) deplete more water relative to the process depletion, i.e., rice evapotranspiration. DF_{gross} is increased from 0.12 (weighted average) to 0.17 and $DF_{available}$ remained the same from 0.59 (weighted average) to 0.59.

The water productivity of the gross inflow is 0.10 kg/m^3, a decrease compared to SDA-(B+C), but an increase compared to the weighted average of the SDA-A, SDA-B and SDA-C scales. $WP_{irrigation}$ is increased from 0.07 kg/m^3 (weighted average of SDA-A, SDA-B and SDA-C) to 0.11 kg/m^3, which reflects the water re-use within this scale. WP_{ETrice} remained the same (0.75 kg/m^3) as the weighted average of SDA-A, SDA-B and SDA-C.

TRIS-L + SDA-A

At this scale, the rice area is 78 % of the gross area. All the creeks discharging water into Talavera River are considered uncommitted flow because the water is specifically for the TRIS-Lower and different areas of Santo Domingo. A large amount of water (83 %) is flowing out from the SDA-A area through creeks and laterals, which is also considered as committed water for downstream of the SDA-D scale. In this study, it was not possible to measure the amount of water flowing out from the tail ends of SDA-D, which leads to an ambiguity concerning the actual productivity of District 1. WP_{gross} is slightly increased from 0.12 kg/m^3 (weighted average of TRIS-L and SDA-A) to 0.14 kg/m^3. $WP_{irrigation}$ is increased from 0.14 kg/m^3 (weighted average) to 0.17 kg/m^3, which reflects the high water re-use within the system through check dams. The water

productivity per unit of evapotranspiration remained the same at 0.90 kg/m^3 (weighted average).

The weighted average of PF_{gross} for TRIS-L and SDA-A is 0.13, while the PF_{gross} is 0.16, meaning that only 16 % of the gross inflow is consumed by rice ET. The $PF_{depleted}$ remained the same from 0.84 (weighted average) to 0.84, and the $PF_{available}$ is decreased slightly from 0.37 (weighted average) to 0.36. The depleted fraction of gross inflow is slightly increased from 0.16 (weighted average) to 0.19 and the $DF_{available}$ is decreased slightly from the weighted average of 0.44 to 0.43.

TRIS-L + SDA-(A+B)

The rice area is 77 % of the total area at this scale, which is similar to the TRIS-L+SDA-A scale. The process fraction of gross inflow is increased from 0.13 (weighted average of TRIS-L, SDA-A, and SDA-B) to 0.18, while the process fraction of depleted water remained similar 0.83 (weighted average) to 0.83. The depleted fraction of gross inflow increased from the weighted average of 0.15 to 0.22 for this scale. The water productivity per unit of rice evapotranspiration remained the same (0.89 kg/m^3) and WP_{gross} increased from 0.11 kg/m^3 (weighted average) to 0.16 kg/m^3. The water productivity of the irrigation increased from 0.13 kg/m^3 (weighted average) to 0. 19 kg/m^3. The water re-use on this scale is clearly reflected in the $WP_{irrigation}$ values that are almost 1.5 to 3 times higher than those of the TRIS-L and SDA-A scales, respectively.

District 1

This scale is aggregated by adding areas of TRIS-L, SDA-A, SDA-B, and SDA-C. The rice area is 75 % of the total rice area which is somewhat lower than that of the TRIS-L+SDA-(A+B) scale. The gross and net inflows are almost equal, because little change in the groundwater storage was observed over the dry season 2001. All creeks discharging water into Talavera River are considered uncommitted flow because the water is specifically for TRIS-Lower and different areas of Santo Domingo. The high outflow (74 %) from downstream of SDA that is considered as committed water for the SDA-D scale. As there is no information available about the actual water consumed for different purposes and finally the amount of water flowing out from the SDA-D scale, we cannot be sure about the actual productivity of District 1. WP_{gross} increased from

0.11 kg/m^3 (weighted average of TRIS-L, SDA-A, SDA-B and SDA-C) to 0.18 kg/m^3. Similarly, $WP_{irrigation}$ increased almost double from 0.12 kg/m^3 (weighted average) to 0.22 kg/m^3. This shows that the water productivity of irrigation is 4 times higher than SDA-A scale. The major reason for this very high increase in water productivity is the capture of drainage water by the 15 check dams located within this scale and its subsequent re-use. WP_{ETrice} slightly decreased from 0.89 kg/m^3 to 0.86 kg/m^3, which corresponds well with the 2 % reduction of the rice area (from 77 % to 75 %) at this scale.

The PF_{gross} increased double from 0.12 (weighted average) to 0.21, which means 21 % of the gross inflow is consumed by rice ET. The process fraction of available water also remained same from 0.38 (weighted average) to 0.38 at this scale. The process fraction of depleted water is 0.80, meaning that 80 % of the depleted water is consumed by rice ET and the remaining 20 % is non-process depletion, i.e., evapotranspiration from upland crops, fallow land, and water bodies. The DF_{gross} increased from 0.15 (weighted average) to 0.26, means that 74 % of the gross inflow (rainfall, irrigation, and groundwater) is flowing out of District 1. The $DF_{available}$ decreased slightly from a weighted average of 0.48 to 0.47 at this scale.

5.1.4 Water accounting indicator trends across scales

The results of 3 water accounting indicators across 10 different scales, i.e., SDA-A, SDA-B, SDA-C, SDA-(A+B), SDA-(B+C), SDA-(A+B+C), TRIS-Lower, TRIS-L+SDA-A, TRIS-L+SDA-(A+B) and District 1 are discussed in this section.

The process fraction trends over different spatial scales of District 1 are shown in Figure 5.12. The PF_{gross} at three downstream scales of SDA is very low because a high net inflow is flowing out for the SDA-D scale. Overall, the process fraction of gross inflow shows an upward trend with increasing scales. The $PF_{depleted}$ indicates how much of the depleted water is process-consumed (used for intended purposes). The $PF_{depleted}$ also shows upward trends across the scaling-up, except for SDA-C where the rice area is decreased 7 % of the total area as compared to other scales of District 1. The average value of $PF_{depleted}$ is 0.80 for District 1, meaning that 80 % of the water is depleted through evapotranspiration of the rice crop, and the remaining 20% by evaporation from fallow land, upland crops and perennial vegetation. The $PF_{available}$

indicates how much of the available water is consumed for intended purposes such as irrigation. The $PF_{available}$ shows a very low value at the TRIS-L scale because of the high outflow from the system. The process fraction of the available water also shows the downward trend from different scales of SDA to larger scales of District 1.

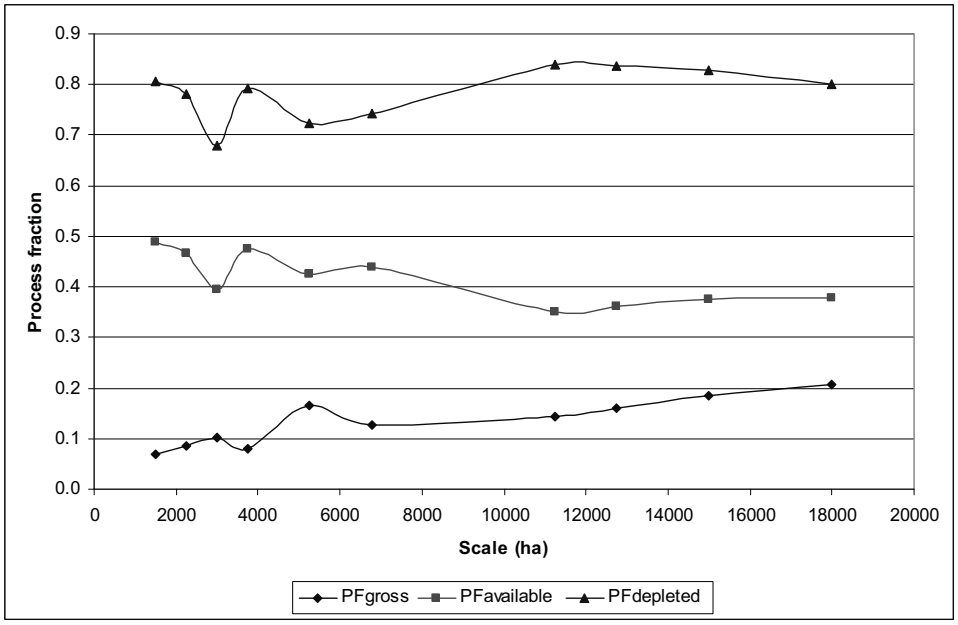

Figure 5.12: Process fraction trends over different spatial scales of District 1.

The depleted fraction trends over 10 different spatial scales of District 1 are shown in Figure 5.13. The DF_{gross} indicates how much water entering into the basin is depleted. The depleted water includes evaporation from open water bodies and soils, transpiration by beneficial and non-beneficial vegetation, process consumed, and water entering into sinks. The higher the fraction, the more water is depleted. The depleted fraction of gross inflow (DF_{gross}) again shows an upward trend from 0.09 (SDA-A scale) to 0.26 (District 1), which indicates the high water re-use through the small check dams in the system. At the SDA-A scale, the DF_{gross} shows a low value, which mean a high outflow is available for the downstream SDA-D scale. There is a decrease of the DF_{gross} at the SDA-(A+B) scale. At the SDA-(B+C) scale, 2 small check dams are working very well. At the District scale, the DF_{gross} is 0.26, means that 74 % of the inflow (irrigation, rainfall, and groundwater pumping) is flowing out of District 1. There is a wide scope for increasing water productivity by reducing the high outflow from the system. The second indicator, depleted fraction with respect to available water, gives an indication of

how much water is still available for further use, and can be interpreted as irrigation system efficiency. The $DF_{available}$ of 6 spatial scales of SDA (tail end) shows no strong variation, even though the value is much higher than that of the TRIS-L scales. This can be explained by the low outflow from all SD scales as compared to high committed outflow from the TRIS-L scales. That is why the $DF_{available}$ shows a downward trend when scaling up to the District 1 level. There are considerable opportunities for increasing the amount of available water within the system by reducing the high outflow through better water management of existing small check dams.

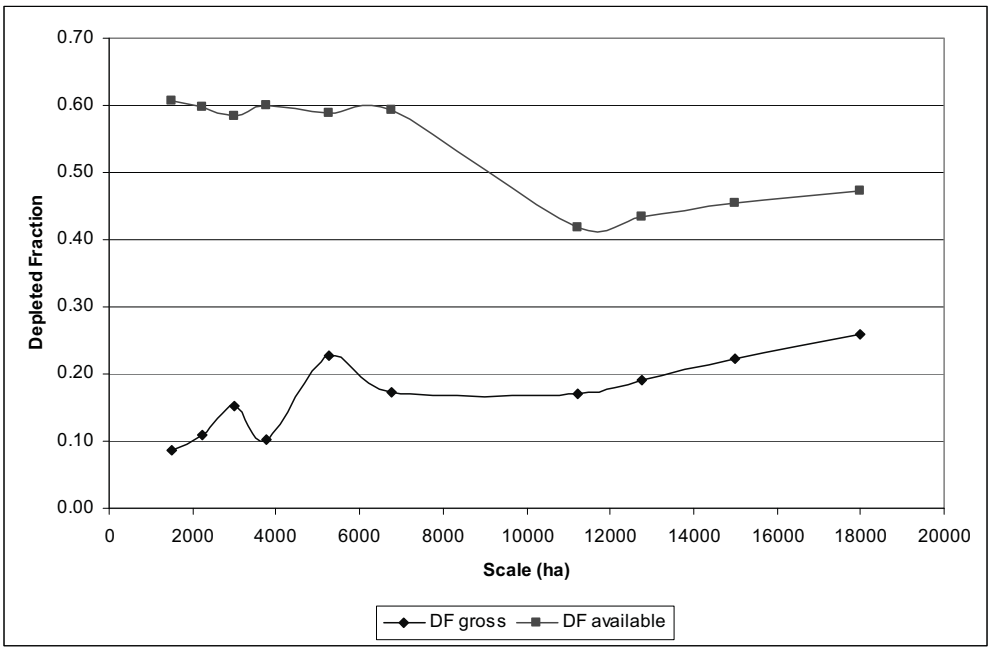

Figure 5.13: Depleted fraction trends over different scale of District 1.

The water productivity trends across different spatial scales of District 1 are shown in Figure 5.14. The difference in the water productivity at different scales is related to the rice yield variations between different areas. WP_{gross} shows an upward trend across the scale-up in District 1. The average rice yield of SDA-A, SDA-B, and SDA-C is 22 %, 21 % and 8 %, respectively, less than that of the TRIS-L scale, which leads to low WP_{gross} values at 3 SDA scales. The water productivity per unit of gross inflow is high at the TRIS-L scale. The WP_{gross} value rises abruptly at the SDA-(B+C) scale because the 3 check dams play an active role in capturing the re-used water from the farmers' fields through creeks and putting it to productive use. WP_{gross} of District 1 increased enormously from 0.11 kg/m^3 (weighted average of TRIS-L, SDA-A, SDA-B,

and SDA-C) to 0.18 kg/m^3, which can be explained by the large amount of water for re-use collected in 15 small check dams, hundreds of small farm ponds and through the 1451 pumps installed in different areas of District 1. The total water volume re-used by pumping is equivalent to 30 % of the water lost through rice evapotranspiration during the dry season 2001.

The water productivity per unit of irrigation ($WP_{irrigation}$) also shows an upward trend across the scale-up due to re-use of water. $WP_{irrigation}$ is highly dependent on the amount of rainfall. The total rainfall over the study area is equivalent to 14 % of the irrigation water releases through canals in District 1. The scaling-up effect can be checked through $WP_{irrigation}$ due to the high water re-use opportunities at the larger scale level. The water productivity per unit of irrigation increased enormously from 0.12 kg/m^3 (weighted average of TRIS-L, SDA-A, SDA-B, and SDA-B) to 0.22 kg/m^3 at the District 1 level.

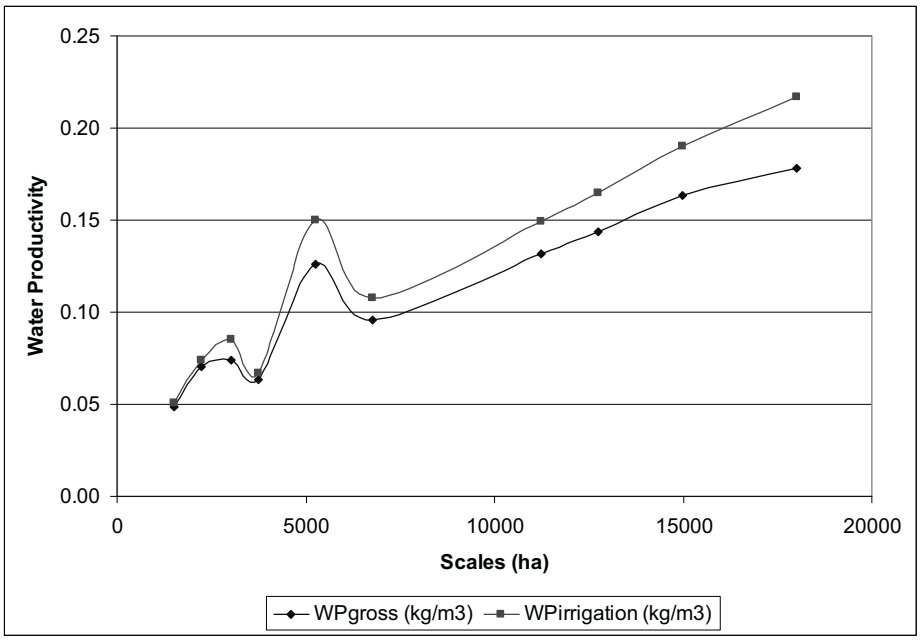

Figure 5.14 Water productivity trends over different spatial scales of District 1.

$WP_{irrigation}$ of District 1 is almost three to four times higher than that of the different spatial scales of SDA because the water from creeks is captured by the small check dams for re-use in downstream areas. The higher water productivity value indicates that the system is performing very well. It is also clear from Figure 5.4 that the water productivity decreases towards the tail end (SDA-A, SDA-B, and SDA-C scales) of the irrigation system.

The water productivity per unit of rice evapotranspiration (WP_{ETrice}) will not change too much with scaling-up because the production water required by the rice plant is the same at all locations in the irrigation system (Figure 5.15). WP_{ETrice} explains how well a specific crop is performing in terms of crop-water-use efficiency. WP_{ETrice} is around 0.75 kg/m^3 for the different areas of Santo Domingo, while it is around 0.90 kg/m^3 for the remaining scales of District 1. One reason for the low WP_{ETrice} of the different SD areas is the low rice yield of these scales as compared to the TRIS-Lower scales. The possible reasons for the low yields of the Santo Domingo scales are crop varieties, agronomic practices, on farm water management, and irrigation water availability. The WP_{ETrice} values are location specifics and have nothing to do with the scaling effect. At the District 1 scale, WP_{ETrice} is slightly decreased from 0.89 kg/m^3 to 0.86 kg/m^3, which is justified through the 2 % reduction of the rice area (from 77 % to 75 %).

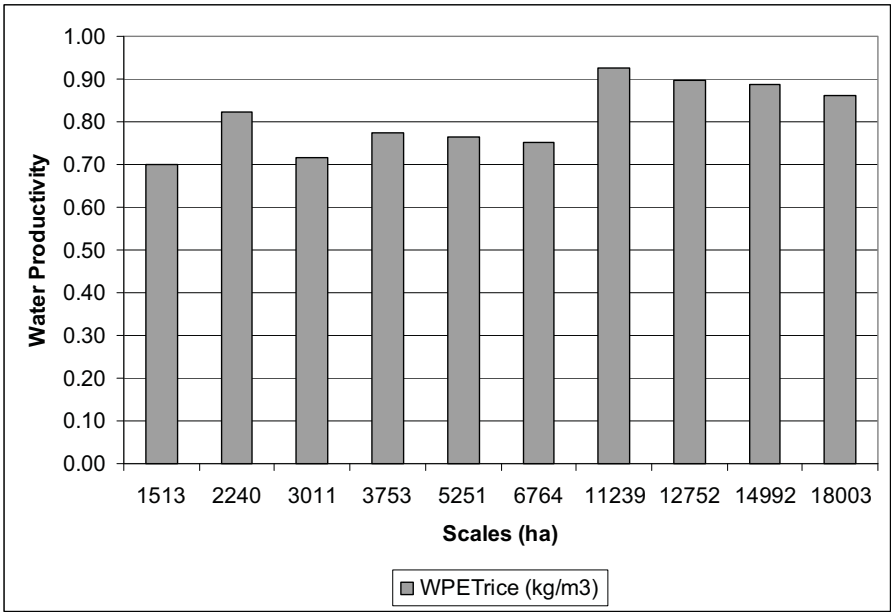

Figure 5.15: Water productivity per unit of evapotranspiration across different spatial scales in District 1

Water productivity can be increased in four ways: (i) increasing the productivity per unit of beneficial depletion, (ii) reduction of non-beneficial depletion, (iii) reduction of uncommitted outflows, and (iv) reallocation of water to higher valued crops (Molden and Sakthivadivel 1999). Reducing the high outflows of utilizable, uncommitted outflows through improved management of existing facilities in the study

area can increase the water productivity. The results show that there is high non-process depletion (32 %) of water at the SDA-C scale and that the water productivity can be improved by reducing these depletion losses. There is a wide scope of measures for additional water saving in the study area, because it was seen that 74 % of the rainfall, pumped groundwater and irrigation water releases flow out of the study area.

5.2 Accuracy analysis

Accuracy is defined as the degree of conformance of a measurement to a standard or true value. Bos (1989) reported three types of common errors that can occur while measuring the flow rate of any canal, i.e., spurious errors (human mistakes and instrument malfunctions), random errors (experimental and reading errors), and systematic errors (constant or variable). Accurate application of water measuring devices generally depends upon standard design or careful selection of devices, care of fabrication and installation, good calibration data and analyses, and proper user operation with sufficiently frequent inspection and maintenance procedures. This section deals with the accuracy analysis of different water balance components, surface flow measurement, rainfall, percolation, evapotranspiration, and groundwater fluctuation.

5.2.1 Surface flow measurement

The discharge value obtained through measurement is simply the best estimate of the true flow rate that can be obtained from the data collected; the true flow rate may be slightly higher or lower than this measured value. The usefulness of the flow rate measurement is greatly enhanced if a statement of possible error accompanies the result. The error may be defined as the difference between the true flow rate and the flow rate that is calculated from the measured water level with the aid of the appropriate head-discharge equations.

The periodic reading on a calibrated staff gauge may serve adequately when continuous information on the flow rate is not required or feasible. A total of 158 locations were selected along the boundary of all 4 spatial scales (TRIS-L, SDA-A, SDA-B, and SDA-C) for measuring surface inflow and outflow for each particular scale of District 1. The surface water flows (in/out) were measured on the 158 locations by

installing 119 wooden staff gauges, 4 parshall flumes and 35 using circular culverts at the boundaries of all spatial scales.

The wooden staff gauges were placed in such a manner that the water level can be easily read from the canal bank and non-visible wooden staff gauges were frequently replaced by new staff gauges in the study area. Care was taken that the staff gauge was firmly secured and did not interfere with the flow pattern in the canal. The four field assistants recorded the staff gauge readings twice a day (early morning and afternoon) at all locations of District 1. Randomly, independent staff gauge readings of a few selected points were taken and compared with the readings recorded by the field assistants to check whether they had taken the staff gauge readings in the field or had created data without visiting the staff gauge locations. All staff gauges installed on the big canals/drains/creeks were calibrated 7-9 times at different water levels using the current meter (Model D622 Digital Price Meter with a Model 1100 Flow Indicator). A pygmy current meter/v-notch weir was used along small canals/creeks and farm drainage ditches. The meter-stick technique was used as a flow-measuring device for the small farm ditches with circular culverts. The V-notch weir is one of the most precise discharge measuring devices as compared with other structures and suitable for a wide range of flow conditions (Bos, 1989). The rating curves having high R-squared values (0.95 or more) were selected among the linear, polynomial, exponential and power correlations for all calibrated staff gauges as shown in Table 1 (Appendix B).

Two staff gauges were also placed within 200 meter of each other at the same locations, i.e., the lateral B-4 and Santo Domingo main canal, to compare the discharge of both staff gauges. The purpose of installing the double staff gauge was to consider the slope effect for the estimation of discharge. The gauge datum was set so that a reading of zero was below the lowest anticipated stage to avoid negative readings and same staff gauge datum were maintained for the staff gauges at both locations. The results show that the discharge of one staff gauge varied only 1.5 % from that of the other during the entire dry season 2001. It can be concluded that a single staff gauge is accurate for the estimation of discharge areas like District 1.

All 35 culverts were regularly painted at the center of the circular structure, to make sure that the field assistant took the reading at the center. The actual water flow area was estimated with/without sediment deposit at the bed of every culvert in 2-month

intervals during the dry season 2001. The measured discharge from the staff gauge was compared with the estimated discharge of the culvert using the meter-stick technique at two selected locations, i.e., creek and farm ditch in the Santo Domingo area. The result of two locations showed that the average discharge measured by the culvert is 35 % less than that measured by the staff gauge at the same location. The possible reason for the under-estimation of the discharge is poor rating curves (R^2 = 0.51 and 0.11) of the culvert as compared to the rating curves (R^2 = 0.98 and 0.95) of staff gauges at both locations. The other possible reason is less accurate measurement of the culvert area due to sedimentation and a change in the hydraulic characteristic of the flow from free water surface flow to submerged flow. The measured discharge through the culverts is only 3 % of the total irrigation water supply to District 1 during dry season 2001, and thus did not affect the accuracy of flow measurement too much.

The water level measurement taken from the staff gauge provides the discharge value at the actual moment of measurement. In many systems, measurements are taken only once a day, and the average of two readings, morning and afternoon, is better for determining a uniform rise of water than a single reading. If the discharge in the canal/creek is increasing or decreasing rapidly, then multiple readings will be required. As this was the case in District 1, with its tropical climate where rainfall is frequent, it was decided to record the total variability of flow for one day. Therefore, 11 electronic D-divers were installed to monitor the water level fluctuation at 5-minute intervals at critical flow locations within District 1. The divers measure the height of the water column by measuring the water pressure with a built-in pressure transducer. The D-diver has a memory capable of storing 2 x 24,000 recordings, enabling measurements every 10 minutes for six months before the memory is full. The water level is measured by subtracting the barometric pressure from the water pressure of the D-diver; the discharge is obtained using calibrated rating curves of head-discharge relationship of that particular location. The discharge estimated from the automatic diver is considered as the true discharge of that location.

In this study, we attempted estimation of the flow measurement errors by comparing the water head measured through the staff gauges (see above) with the water head recorded by the electronic D-divers at 5-minute intervals for 11 locations within the study area during the different periods of the dry season. However, the electronic

diver at Bausao dam was stolen a week after installation. In addition, it was not possible to calibrate the discharge of the Pajo dam due to the low flow rate at the location of diver. The discharge variation during different periods of dry seasons is represented in Figure 5.16.

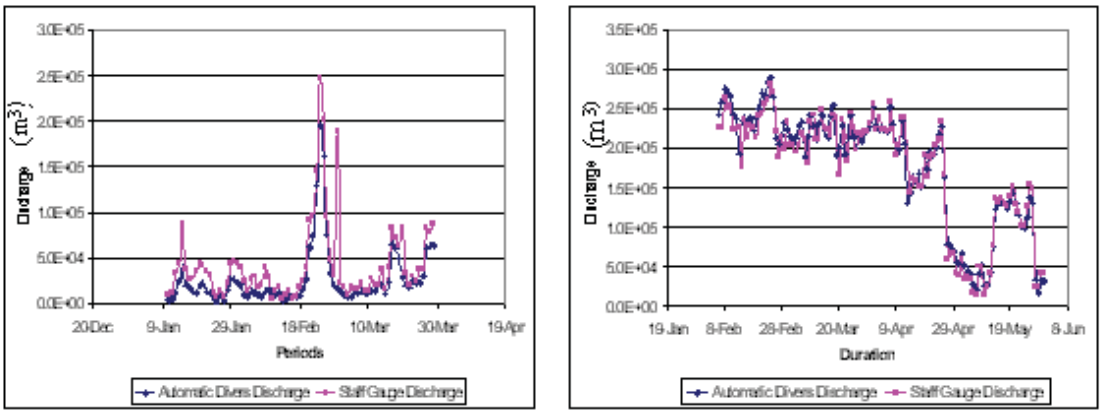

Figure 5.16: Comparison of discharge estimated from staff gauge and automatic divers for Lamboy creek (left) and Santa Rita Dam (right) in District 1.

Figure 5.16 shows that at some points, the staff gauge discharge is very close to the true discharge but most of the time it is either over-or underestimating the actual discharge. The best-known approach in determining the statistical difference of two group means (i.e., true discharge and staff gauge discharge) is the two-paired sample *t*-test. This analysis was done using SPSS 10.0 for Windows software.

Table 5.3: Mean percent error and descriptive statistics from paired-sample analysis

Locations	Mean percent error	Descriptive statistics from paired-sample analysis (m^3)				
		Mean	Standard deviation	Mean standard error	Confidence interval at 95 % level	
					Lower	Upper
Lamboy Creek	+55.0	-15519	21312	2413	-20325	-10714
Baloc Creek	+21.0	-7164286	7479386	1413471	-10064489	-4264082
Bridge 3 Creek	+12.0	-94351	134382	15314	-124852	-63850
Debabuyan Creek	-32.0	4805	2525	225	4360	5251
Deleon Canal	-17.0	28830	18834	2146	24555	33105
Ilog Baliwag Creek	0.01	-272	7698	1012	-2295	1751
Pajo Creek	-50.0	53983	27263	2564	48901	59065
SDA-supply canal	+21.0	-161738	72076	6472	-174550	-148925
Santa Rita Dam	+3.0	2947	15942	1486	2	5892

Table 5.3 shows how the two data groups means differ from each other. Mean percent error values showed that the discharge from the staff gauge is overestimated in the range of 3-55% relative to the true discharge for the 5 locations of divers, and underestimated in the range of 17-50% for 3 locations during the dry season 2001. In the case of Ilog Baliwag Creek, the mean estimated discharge from the staff gauge is only exactly equal to the mean of the true estimated discharge using automatic divers during the dry season 2001. The possible reasons for this high discrepancy in mean percent error are wrong location of staff gauge, observer's reading mistake, and high fluctuation in flow due to peak rainstorms in the evening.

The discharge estimated from the automatic divers and staff gauges were compared through the paired *t*-test. Results show (Table 5.4) that the staff gauge discharge is significantly different (t = 6.43) from the true discharge in the case of Lamboy creek. However, the two discharge data are highly positively correlated (0.88) even though they are totally different flow data sets. The same result is observed in six other locations except for Ilog Baliwag creek and Santa Rita dam. In these cases, the results show that the discharge using staff gauge is not significantly different (t = 0.27, and t = 1.98) from the true discharge and the two discharge data are highly positively correlated (0.99 and 0.98).

Table 5.4: Correlation and t-test of discharge measures (true and staff gauges)

Locations	Paired-sample *t*-test			Paired-correlation test		
	t	df	Sig.	N	Correlation	Sig.
Lamboy Creek	6.43	77	0.0001	78	0.88	0.0001
Baloc Creek	5.07	27	0.0001	28	0.93	0.0001
Bridge 3 Creek	6.161	76	0.0001	77	0.78	0.0001
Debabuyan Creek	21.36	125	0.0001	126	0.95	0.0001
Deleon Canal	13.43	76	0.0001	77	0.92	0.0001
Ilog Baliwag Creek	0.27	61	0.789	62	0.99	0.0001
Pajo Creek	21.05	112	0.0001	113	0.39	0.0001
SDA-supply canal	24.99	123	0.0001	124	0.97	0.0001
Santa Rita Dam	1.98	114	0.050	115	0.98	0.0001

Selecting a device that is not appropriate for the site conditions can result in reduced accuracy, sometimes greater than ± 10 %. Overall, the results proved that automatic divers are better than staff gauges because they capture the fluctuation of the

flow rate more accurately. Measurement methods are often selected based on the initial cost of the primary device with in sufficient regard for the additional cost associated with providing the desired records of flow over an extended period of time. The cost of the measurement method includes the cost of the device itself, the installation, secondary devices, and operation and maintenance. The initial primary cost of an electronic diver is 100 times higher than that of a wooden staff gauge, and the results of 9 electronic divers showed that the staff gauges over-estimated 13 % discharge from true discharge. However, it is difficult to maintain such high accuracies of discharge through staff gauges, which usually requires considerable expenses or effort (e.g., special construction, recalibration, maintenance, etc.) in the field. It can be concluded that the discharge estimated from staff gauges provides fairly good results for larger irrigation systems despite all the encountered problems.

5.2.2 Groundwater

The water shortage is a major restraining factor for growing high water consuming crops like rice during the dry season in District 1 of UPRIIS. Groundwater utilization to fully irrigate or supplement canal system deliveries can significantly alleviate the farmers' water scarcity problem. Certainly, a first step will be to determine the number of pumps and then to measure the discharge being pumped in order to manage the exact quantity of water at the irrigation system level, something that is rarely done at present.

A survey was carried out by NIA to determine the exact number of pumps, their respective sizes, and the irrigated area. A total number of 1154 pumps were recorded in the study area, pump sizes varying from 3 to 5 inches in diameter, while 95 % of the pumps were of 4-inch size. The total pump usage and irrigated area were obtained through monitoring 50 selected farmers for different farming activities in the dry season. The total pumping time per hectare for each pump size was obtained by dividing the total pumping time over the irrigated area in the dry season 2001. A total of 33 pumps of different sizes (2 for 2-inch, 8 for 3-inch, 22 for 4-inch, and 2 for 5-inch) was calibrated 5-7 times using a V-notch weir and Pitot tube for estimating the actual discharge of each pump size.

The regression analysis was done between the irrigated area and total pumping hours of 22 farmers with 4-inch pumps. The regression results show that 73 % of the

variation in pumping hours can be explained by variation in the irrigated area, which is found to be significant at the 99 % confidence level. The same trend was observed for other pump sizes in the study area. The total volume of pumped water was estimated by multiplying the actual discharge with the pumping hours per hectare. It was assumed that all farmers followed almost same pumping trends for different farming activities in the dry season 2001, and the total water pumped can be measured by multiplying the average pumped water for each pump size with the total number of pumps installed in the different areas of District 1. The total volume of water pumped in District 1 is equivalent to 30 % of the water lost through evapotranspiration of the rice crop.

5.2.3 Percolation

A small percentage of the water applied to the crops should move downward below the root zone. This deep percolation is needed to remove salts that would otherwise accumulate in the root zone. Poor irrigation management often causes excessive rates of deep percolation in many irrigation systems. DeDatta et al. (1973) reported that percolation losses are higher due to longer intervals of irrigation because of deeper and bigger cracks forming on the soils. It is often difficult to determine the exact amount of water losses through percolation because they vary from field to field and depend on many factors like soil texture, structure, longer irrigation intervals, and the height of water standing over the soil. In this study, the average percolation rate is estimated from 1512 readings using percolation drums in 10 rice fields during the dry season 2001. The descriptive statistics of the variation of percolation losses in the 10 rice fields is summarized in Table 5.5.

Table 5.5 Descriptive statistics of the percolation losses (mm/day) in 10 rice fields

Location	N	Mean	Standard deviation
Rice Field 1	165	2.95	1.35
Rice Field 2	165	1.35	0.98
Rice Field 3	132	3.79	2.28
Rice Field 4	165	3.08	1.83
Rice Field 5	165	2.35	0.45
Rice Field 6	150	1.39	0.70
Rice Field 7	150	1.53	0.85
Rice Field 8	150	1.46	0.65
Rice Field 9	150	0.73	0.33
Rice Field 10	120	0.45	0.22
Average	1512	2.15	1.53

The results show that the mean percolation losses varied from 0.68 to 3.68 mm/day (mean of 2.15 mm/day), which matches very well with the results of other percolation studies for District 1. In parallel studies for District 1, Sattar (1992) reported that average SP rate varied from 1-4 mm/day (mean 2 mm/day) during the dry season, and Lucero (1984) showed that it varied from 1.7-2.5 mm/day with a mean of 2.0 mm/day in District 1 (TRIS-L & SDA)

The percolation rate was also estimated from the water balance by solving the other components of the water balance except percolation losses for 10 different spatial scales of District 1. The percolation rate found in the range of 2.0 to 3.5 mm/day with a mean of 2.80 mm/day which is very close to the mean (2.15 mm/day) estimated from independent percolation study in District 1.

5.2.4 Rainfall

The ideal rain gauge would catch all the precipitation falling in the surrounding area. The main source of error is the use of inaccurate measures and spilling water when transferring it to the measure. The errors involved in measuring the catch collected in a gauge are small compared with the uncertainty due to the effect of the exposure of the instruments, provided reasonable care is taken in the readings. The daily rain gauges should be read to the nearest 0.1-0.2 mm. In this study, the two rain gauges, i.e., Tandod and Radial gate, were found to be installed under trees and near a building. They were shifted to open fields where permanent concrete structures were built.

The number of rainfall stations determines the accuracy of measurement, whereby the larger the area under consideration, the lower the network density required for determining the area's average rainfall. The minimum recommended density of a precipitation network for flat regions of tropical zones like District 1 of UPRIIS is 60,000-90,000 per hectare (WMO, 1981). In this study, 8 rain gauge stations with an average density of 2500 per ha were installed to obtain better spatial variation within the different areas of District 1. The Thiessen Polygon method is the most appropriate method for determining areal rainfall from point rainfall data when the stations are not evenly distributed over the flat areas (Ritzema, 1994). As the locations of the 8 rain gauges were not evenly distributed in District 1, which is relatively flat with altitudes

from 30-80 m, the point values of rainfall data were interpolated using the Thiessen Polygon method to determine the representative rainfall of the area.

5.2.5 Evapotranspiration

The Landsat image of 18 May 2001 of District 1 of UPRIIS was processed to estimate the broadband surface albedo, NDVI, surface emissivity, surface temperature and daily incoming surface net radiation. One of the most complex components of SEBAL is the iteration system, which leads to the refinement of the values of the sensible heat flux. The new method developed by Tasumi et al. (2000) was advised for five successive iterations in order to reach stabilization of the result H values. An experiment was setup in order to properly examine this allegation. The protocol did not include the recommended Slope and Aspect Modification, while all other parameterizations were followed. The difference of soil to air temperature ($dTair_h$) for the "Hot pixel" (Bastiaanssen and Sakthivadivel, 1999) is the critical parameter in the fine-tuning of the sensible heat flux. A set of successive iterations was set up in order to show the $dTair_h$ evolution (Figure 5.17). The iteration system was subsequently repeated until the difference between the new value and the old one reaches a range lower than 1 K, which was considered to be a completely stable condition. The initial set-up of the values of H (H0) for two pixels, the "hot" pixel where sensible heat flux takes all [net radiation – soil heat flux], and the "cold" pixel where sensible heat flux is null. After that, iterations result in sensible heat flux maps numbered from H1 for iteration 0 to H10 for iteration 9.

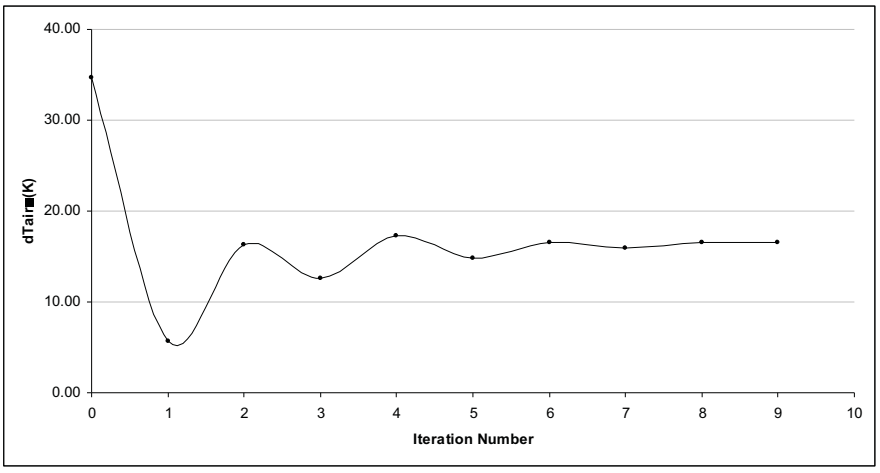

Figure 5.17: Evolution of dTair with the iteration number

As can be observed, the number of iterations that meet the criterion for stability is 9, ($dTair_{h9}$ - $dTair_{h8}$ < 1K). Further implications are shown by the variations of the H results at different iteration stages as in Figure 5.18 and 5.19.

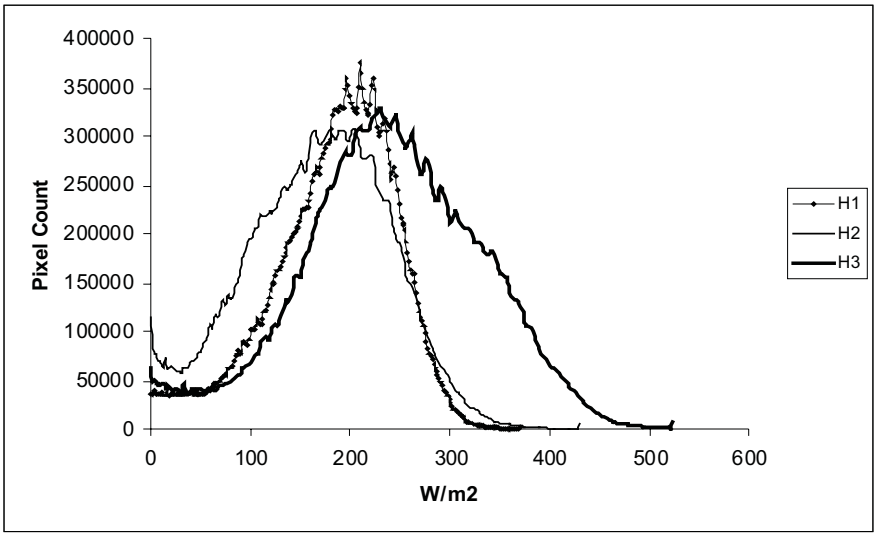

Figure 5.18: Histograms of H1, H2 and H3.

Iterations 0, 1 and 2 are shown in Figure 5.18, with respective values of H1, H2 and H3. The high variation in the starting $dTair_h$ values is reflected in the shift of the histograms of H. It can be noted that the base the height ratio is also variable; this can be accounted for by the values of the R_{ah} curves that simultaneously change in spreading.

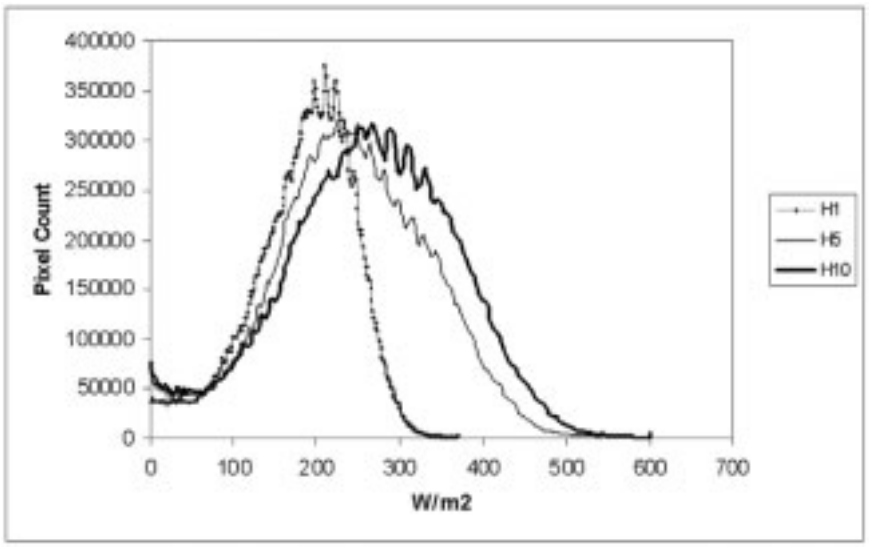

Figure 5.19: Histograms of H1, H5 and H10

Iterations 0, 4 and 9, representing H1, H5 and H10, respectively, show a high level of variation. The skew ness is less for the higher iteration numbers, as the mean and standard deviations in Figure 5.20 demonstrate.

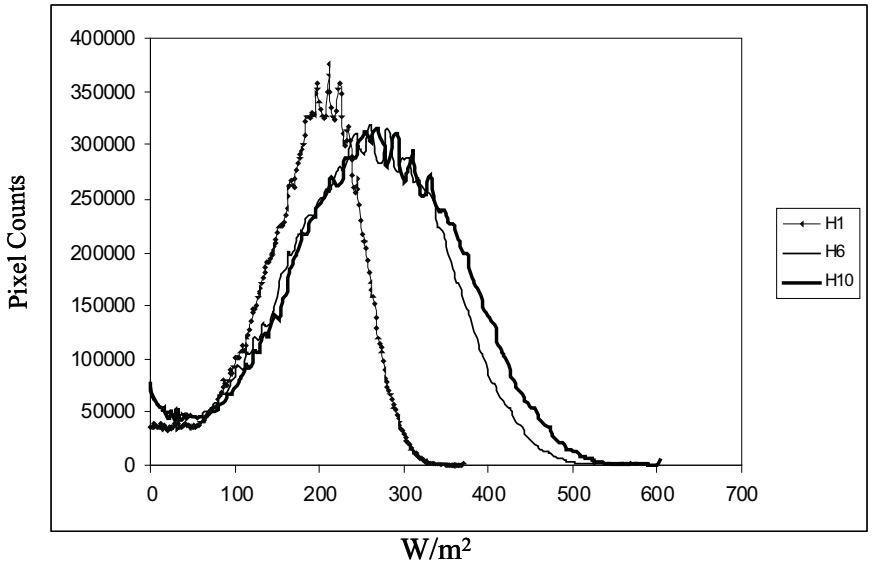

Figure 5.20: Histograms of H1, H6 and H10

Iterations 0, 5 and 9 are respectively the initial condition of H, the recommended iteration result by Tasumi et al. (2000), and the maximum iteration calculated in this experiment. It can be seen that there is a real difference between initial conditions and the results after 5 or more iteration cycles. In addition, iteration 5 (H6) and iteration 9 (H10) do not fit entirely, and peaks around the modes are estimating areas in sinusoidal patterns that are not in same phase, eventually leading to inaccuracy in the resulting estimations. The right sides of the curves are also shifted from one another.

Mean and standard deviation (SD) of H1 to H3 are highly variable (as shown in Figure 5.21); the set-up of the iteration cycles strongly influences image distribution. This is especially because of the introduction of the psychometric parameter correction for heat and momentum transport in computation of the sensible heat flux.

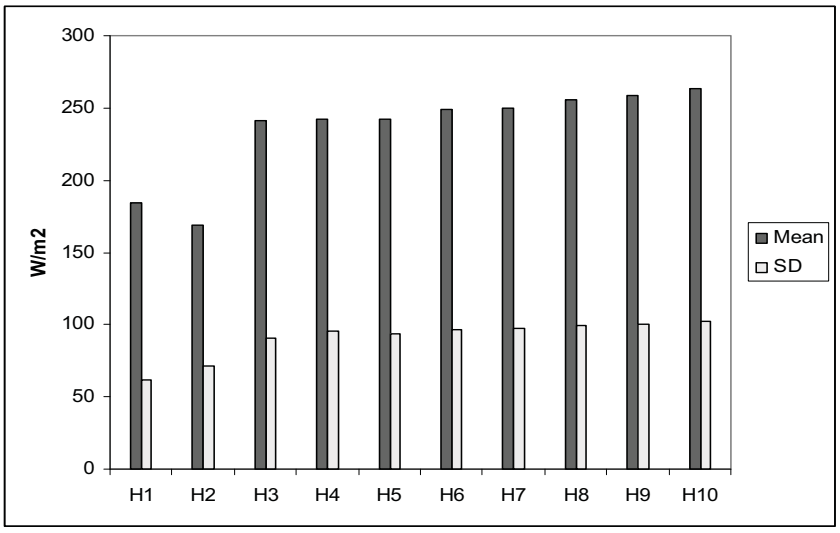

Figure 5.21: Mean and standard deviations of the H histograms

The difference of iterations of H means from H10 is shown in Figure 5.22.

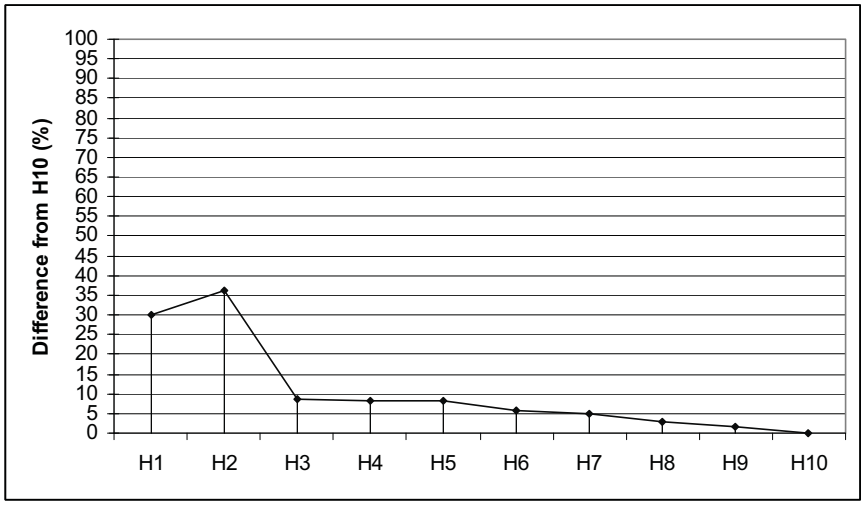

Figure 5.22: Difference of H means from H10 mean

Iteration 2 resulting in H3 is a first step in determining the accuracy of the maximum mean (H10) by reaching below 10 %. This has a great interest for heavy computations restricted users, which can easily reach a sensible level of accuracy of the mean H10. However, to reach a difference below 5 % of the H10 mean, iteration cycles have to be repeated 7 times (H8). One can see that the recommended iteration cycle of 5 times does not fit the requirement for this image (H6 = 93% of H10). The accuracy is increased if more than 5 iterations are performed, despite the fact that there is a high hardware requirement constraint involved in such number of iterations.

6. GENERAL DISCUSSION AND CONCLUSIONS

6.1 General Discussion

The growing water scarcity is a major motivation for many Asian countries to manage water resources, particularly for the agriculture sector, in a sustainable and efficient way without compromising crop yields. This is particularly true for irrigated rice in Asia where consumption of total diverted fresh water for irrigated agriculture is high but water-use efficiency is low. In this regard, efforts should be placed on increasing the productivity or value of every drop of water. An important means to achieve such a goal is to reallocate water from lower to higher-valued uses. But this is only possible when the management decisions are based on the analysis of accurate information at any scale. Unfortunately, water resource managers are often tackling the problem amid a paucity of reliable information and a lack of adequate and appropriate tools for analysis, especially at the irrigation system and basin level. The use of appropriate, reliable and consistent information at the irrigation system level can improve water management by indicating the necessary changes required for managing the water more beneficially and minimizing the negative impacts in downstream areas. An important challenge in the field of water resources is to get the timely, objective and accurate information at each spatial scale in the system.

This study aimed to measure water productivity at ten (10) different spatial scales in District 1 of UPRIIS through the water accounting procedure. In particular, it quantified the current water use, water re-use, and water productivity; and estimated seasonal actual evapotranspiration using different sensors (Landsat 7 ETM+, TERRA/ASTER and TERRA/MODIS) for the dry season 2001.

Water accounting at ten different spatial scales (877 ha to 18,000 ha) was applied to measure water use and water productivity in the irrigated rice system of District 1. District 1 is divided into 10 different spatial scales, i.e., SDA-A, SDA-B, SDA-C, SDA-(A+B), SDA-(B+C), SDA-(A+B+C), TRIS-Lower, TRIS-L+SDA-A, TRIS-L+SDA-(A+B) and TRIS-L+SDA (District 1) for measuring all water accounting components.

6.1.1 Evapotranspiration

An important component of the water balance is evapotranspiration (ET), since this water is lost to the system and cannot be recycled. In this study, the seasonal actual evapotranspiration (ET_s) is estimated at different spatial scales in District 1 for the dry season 2001 through SEBAL using different sensors (Landsat 7 ETM+, TERRA/ASTER and TERRA/MODIS).

SEBAL is a thermodynamically based remote sensing model, which partitions between sensible heat flux and latent heat of vaporization flux. The daily ET_a is calculated from the daily average net radiation and the instantaneous evaporative fraction, which is computed from the instantaneous surface energy balance at the moment of satellite overpass for each pixel. Many researchers have applied SEBAL for irrigation systems in many countries like Argentine, China, India, Egypt, Kenya, Pakistan, Spain, and Sri Lanka. However, SEBAL has not yet been tested for rice-based cropping areas in tropical countries like the Philippines.

The main constraint in using remote a sensing-based model, is that ET_a is calculated only on the satellite overpass days. Temporal integration strategies have to be used in order to fill in the missing satellite data and get the integrated ET_a information for a season. However, in tropical countries it is practically impossible to get well-distributed cloud-free images over the entire cropping season from one sensor, e.g., 1 out of 92 cloud-free images from TERRA/ASTER L1B, 3 of 12 from Landsat 7 ETM +, and 7 out of 110 MODIS L1B images were available in the study area over the entire dry season of 2001. This limit to the availability of cloud-free images was overcome by using the combination of high spatial resolution sensors (3 Landsat 7 ETM+, and 1 ASTER images), with a high temporal resolution sensor (6 MODIS images) covering different time periods of the dry season in the study area.

All essential meteorological data for calibration through SEBAL, like air temperature, relative humidity, wind speed, solar radiation, and various vegetation properties at the day of satellite overpass were collected from the two weather stations in District 1. To validate the remote sensing results, ET_a values for the whole dry season 2001, calculated through SEBAL, were compared with the measured evaporation through Class A Pan (E_{pan}), estimated ET_o and crop evapotranspiration (ET_c) from the PAGASA and PhilRice meteorological stations using the modified Penman-Monteith

method. Since no instruments were available for measuring the Bowen ratio or other potential indicators, point data at both meteorological stations were used for comparison, because they show same trends in ET for dry season 2001, i.e., 18 November 2000 to 18 May 2001.

The first task was to estimate ET_a using 6 MODIS images (spatial resolution of 250-1000 m), acquired on different dates during the dry season. The E_{pan} results of both meteorological stations differ strongly from the ET_a results of the MODIS images, which might be attributed to the thermal bands of MODIS because they provide surface temperature information of larger than a 1-km pixel size, which is larger than the small water ponds in District 1. In the early part of the cropping season (16 November and 20 December 2000, and 03 January 2001), calculated ET_o values from both weather stations were higher than the ET_a of rice fields because the vegetation cover was not fully developed in the fields. During the crop maturity stage (26 January, 1 March and 24 March 2001), calculated ET_o values were always lower than ET_a because the rice crop was actively transpiring at this stage. Results proved that calculated ET_a from MODIS data is within a good range in comparison to ET_o and ET_c calculations from the weather data.

Secondly, a high spatial resolution ASTER (15-90 m) image of 2 February 2001 was used to determine the feasibility of SEBAL estimation in irrigated rice systems. The E_{pan} results of the 2 meteorological stations coincide almost perfectly with the highest ET_a rates practically found from the ASTER image. The ET_a results calculated from the ASTER image are lower than the ET_o values (7 %) and ET_c values (2.5 %) from the meteorological stations. Validation from meteorological data found accurate matching with remotely sensed daily ET_a.

Three Landsat 7 ETM+ images (spatial resolution of 30-60 m) were used to compute the spatial variation in ET_a within a large-scale surface irrigation system in the second part of the dry season 2001 (16 April, 2 May, and 18 May 2001). For pixels assumed to be under (ripening) rice, the estimated ET_a was on average 6 % lower than the ET_c calculated at the nearby weather stations. This can be explained by the fact that during the ripening of rice, farmers drain the fields (to promote ripening) so that the crop experiences drought conditions and closes its stomata, thereby reducing its transpiration rate. Moreover, the evaporation from the underlying, drying soil surface is

lower than that from a ponded water layer under potential evapotranspiration conditions. The difference in ET_a values among sub-regions of the irrigation district was significant at the end of the growing season only when the rice was harvested and new crops were planted. The differences were caused by differences in crop scheduling. Results showed that SEBAL provides realistic ET_a estimates for irrigated rice over spatially extended areas in the tropics.

The seasonal actual evapotranspiration (ET_s) was estimated by merging 6 MODIS and 3 Landsat images (degraded to get MODIS pixel size), while the missing ET_a values were obtained by daily calculation of ET_o as proposed by Tasumi et al. (2000). Due to the large pixel size of MODIS (250 m), it is difficult to absolutely compare such information with the classical point data from meteorological data. Comparison of ET_a values estimated through SEBAL with E_{pan}, ET_o, and ET_c measurements indicates relatively good accuracy and potential for use in the water balance studies for the dry season of 2001.

In addition, the unique combination and inter-relationship of ASTER and Landsat images with the MODIS images for water consumption were examined and results showed a non-significant variation. Comparison with other meteorological data showed close relationship with daily ET estimated by different sensors as predicted by SEBAL. The interchangeability between Landsat 7 and ASTER images was explored, as well as the early study of the convergence of MODIS data to the high-resolution accuracy in terms of water consumption. The comparison shows that high spatial resolution sensors (ASTER vs. Landsat) can be used for ET studies even at smaller scale irrigation systems like District 1.

Finally, this study addresses the assessment of the crop water deficit of an irrigation system in terms of spatial homogeneity. It deals with two different images (MODIS and Landsat) of different processing levels on the same overpass day (18 May 2001) in the dry season. Volumes of water consumption and deficit were compared at different pixel sizes, which showed that 59.4% (11,800 ha) out of 20,000 ha command areas was in best condition (water deficit of -0.75 to +0.75mm/day) in District 1 on 18 May 2001.

6.1.2 Water accounting and productivity

Data for water accounting indicators were measured at 10 different spatial scales for better understanding of the performance of the irrigation system. Surface inflow and outflow were measured across 10 different spatial scales through staff gauges, parshall flumes and culverts at 158 locations. The flow (inflow and outflow) measurement errors were estimated by comparing the water head measured from staff gauges (twice a day) with the recorded water head from electronic divers (5-minute intervals) for 11 locations which shows that the staff gauge over-estimated 13 % discharge from the true discharge in the study area. The amount of rainfall at each scale was estimated using 8 rain gauges, and groundwater fluctuation was estimated by monitoring 50 observation wells within District 1. The percolation rate was measured at 1512 locations within the rice fields of the study area and considered as outflow from the system. The total amount of re-used water was estimated by measuring the actual discharge of 1154 pumps installed in District 1. Remote sensing estimates provided spatially distributed seasonal actual evapotranspiration and different land uses in District 1. The yield data were obtained from the weekly monitoring activity of the NIA at all spatial scales of District 1.

In this study, the system boundary lies between the bottom of the crop root zone and top canopy of the crop. All the water going out from these boundaries is treated as either depleted or as outflow from that particular scale. The amount of water carried through laterals and canals is treated as committed water for downstream areas, while the quantity of water directly discharging into Talavera River is treated as uncommitted outflow from District 1. The amount of water required for environmental purposes in downstream areas of UPRIIS is considered zero due to lack of information about these areas.

Three types of water accounting indicators, alternative to the classical irrigation efficiencies, were used in this study: physically based indicators (depleted fractions), beneficial utilization indicators (process fraction), and water productivity indicators (Molden and Sakthivadivel 1999). In agriculture, the water-use efficiency term is similar to the productivity of water per unit evapotranspiration of rice crop (Viets 1962; Howell et al. 1990).

Overall, the PF_{gross} value ranges from 0.07 at the SDA-A to 0.21 at the District 1 level, showing an upward trend from the lower to the higher scales. The PF_{gross} at the

three downstream scales of SDA is very low because a very high proportion of the net inflow is flowing out of the SDA-D scale. $PF_{depleted}$ indicates how much of the depleted water is consumed for intended purposes, and also shows an upward trend except for the SDA-C scale, where the rice area is decreased by 7 % of the total area as compared to other scales of District 1. The average value of $PF_{depleted}$ is 0.80 for District 1, meaning that 80 % of the water is depleted through ET_{rice}, and the remaining 20 % is depleted by evaporation from fallow land, upland crops, and perennial vegetation. $PF_{available}$ indicates how much of the available water is consumed for intended purposes such as irrigation, and shows a downward trend from the SDA to the District 1 scale. The value is very low at the TRIS-L scale, because the outflow from the system is very high.

DF_{gross} shows an upward trend across scales ranging from 0.09 (SDA-A scale) to 0.26 (District 1) indicating a high water re-use through small check dams within the system. At the SDA-A scale, the DF_{gross} value is low, indicating a high outflow available for the downstream SDA-D scale. At the District scale, DF_{gross} is 0.26, which means that 74 % of the inflow (irrigation, rainfall, and groundwater pumping) is flowing out of District 1, there thus being a wide scope for increasing water productivity by reducing the high outflow from the system. Meanwhile, the second indicator, $DF_{available}$, can be interpreted as irrigation system efficiency. $DF_{available}$ of 6 spatial scales for SDA (tail end) shows no large variation, even though the value is much higher than that for the TRIS-L scales. This explains the low outflow from all SD spatial scales as compared to high committed outflow from the TRIS-L scales. This is why the $DF_{available}$ shows a downward trend as the scales increase to the District 1 level. There are a number of opportunities for increasing the irrigation system efficiency by reducing the high outflow through better water management of existing small check dams.

WP_{gross} shows an upward trend across the scales in District 1. The average rice yields of SDA-A, SDA-B, and SDA-C are 22 %, 21 % and 8 %, respectively, less than that of the TRIS-L scales, and lead to low WP_{gross} values at the 3 SDA scales. WP_{gross} in District 1 increased from 0.11 kg/m^3 (weighted average) to 0.18 kg/m^3, which can be explained by high volume of re-used water provided by the 15 small check dams, hundreds of small farm ponds and 1451 pumps installed in different areas of District 1. The total amount of water re-used by pumping is equivalent to 30 % of the water lost through rice evapotranspiration during the dry season of 2001.

$WP_{irrigation}$ also shows an upward trend across scales. The scaling-up effect on productivity can be checked through $WP_{irrigation}$ due to numerous water re-use opportunities at larger scale levels. $WP_{irrigation}$ of District 1 is almost three to four times higher than that of the different scales of SDA due to re-captured water at 15 check dams and hundreds of small farm ponds. WP_{ETrice} (crop water use efficiency) is around 0.75 kg/m^3 for different areas of Santo Domingo, while it is around 0.90 kg/m^3 for the remaining scales of District 1. One reason for the low WP_{ETrice} of different the SD areas is the low rice yield of these scales as compared to the TRIS-Lower scales. The possible reasons for the low yields at the Santo Domingo scales are crop varieties, agronomic practices, on-farm water management, and irrigation water availability. The WP_{ETrice} values are location-specific and have nothing to do with the scaling effect. At the District 1 scale, WP_{ETrice} slightly decreased from 0.89 kg/m^3 to 0.86 kg/m^3, which is justified as the rice area is reduced by 2 % (from 77 % to 75 %).

6.2 Conclusions

This study found that the SEBAL algorithm using the high spatial resolution satellites, Landsat 7 ETM and ASTER, provided realistic ET_a estimates for irrigated rice in the tropics. Results from MODIS in combination with higher resolution satellites are found encouraging, but the issue still needs further empirical research. Validation from meteorological data gave accurate matching with remotely-sensed daily ET_a, thus proving possible the use of SEBAL in combination with high spatial and temporal resolution satellites for accurate and spatially distributed seasonal actual evapotranspiration (ET_s) in tropical countries like the Philippines, where the cloud coverage is a big constraint in getting satellite images from one sensor.

The water accounting technique, as used in this study, has provided relevant information on water productivity. The estimated total amount of water re-used through pumping, which is equivalent to 30 % of the water lost through rice evapotranspiration during the dry season of 2001, shows that a lot of farmers are depending on water re-use in the system. The water can be saved at the SDA-C scale by reducing the high losses (32 %) through non-process depletion. There is also a high outflow of utilizable uncommitted water (12 % of gross inflow) going out from the TRIS-L scale, which can be saved by better management of the De-Leon check dam. In the whole District 1, 74

% of the water inflow leaves this area. These findings prove that there is a wide scope for additional water saving in the study area through improved water management and rehabilitation of existing structures. Overall, the findings of the study showed that water productivity (e.g., $WP_{irrigation}$) increases (e.g., almost three to four times in District 1) across scales from small irrigation systems (SDA-A) to the large-scale level (District 1) due to increased water re-use opportunities.

7. REFERENCES

Ahmad MD and Chemin Y (2000) Evaporation calculation from an energy balance model (SEBAL) A manual. IIMI-Pakistan Blue Report No. 102, Lahore, Pakistan, July 2000, 27p

Alexandridis T and Chemin Y (2001) Irrigation water consumption through remote sensing. Comparison at different scales in Zhanghe irrigation system, China. Water Resources Management Conference, September 2001, Halkidiki, Greece, 10p

Allen RG, Pereira LS, Raes D and Smith M (1998) Crop Evapotranspiration. Guidelines for computing crop water requirements. FAO Irrigation and Drainage Paper 56. Food and Agricultural Organization of the United Nations, Rome, Italy, 300p

Alley RE (1999) Algorithm Theoretical Basis Document for Brightness Temperature. Version 3.0. April 5, 1999. Jet Propulsion Laboratory, Pasadena, CA, USA, 14p

Bandara KMPS (1998) Water needs and water use of agro-ecosystems in the Kirindi Oya watershed, Sri Lanka. A remote sensing approach. M.Sc. Thesis, ITC, Enschede, The Netherlands.

Barker R Dawe D, Tuong TP, Bhuiyan SI, Guerra LC (1999) The outlook for water resources in the year 2020: challenges for research on water management in rice production. In "Assessment and orientation towards the 21st century", Proceedings of 19th session of the International Rice Commission, Cairo, Egypt, 7-9 September 1998. FAO, pp 96 – 109.

Brent MS, Dennis PG, and Meine VN (2001) The effect of scales, flows and filters on property rights and collective action in watershed management. Paper submitted to Journal Water Policy

Bos MG (1979) Der Einfluss der Groesse der Bewaesserungs einheiten auf die verschiedenen Bewaesserungswirkungsgrade. Zeitschrift für Bewaesserungs-wirtschaft, Bonn 14 (1), pp139-155

Bos MG (1989) Discharge Measurement Structures, Publication No. 20, International Institute for Land Reclamation and Improvement, Wageningen, The Netherlands.

Bos MG and Wolters W (1989) Project or overall irrigation efficiency. In irrigation theory and practice, 499-506 Proceedings of the International Conference held at the University of Southhampton, 12-15 September 1989. London, UK.

Bhuiyan SI (1990) Technical farm-level issues in irrigation for rice-based farming systems: An intercountry synthesis. Miranda S.M. and Maglinao, A.R. editors. Irrigation management for rice-based farming systems in Bangladesh, Indonesia and the Philippines. Proceedings of the Tri-Country Workshop held in Colombo, Sri Lanka, 12-14 Nov. 1990. Colombo, Sri Lanka, IIMI, xi + 357 p.

Bouman BAM and Tuong TP (2001) Field water management to save water and increase its productivity in irrigated lowland rice. Journal of Agricultural Water Management; 49, pp11-30.

Bagley JM (1965) Effects of competition on efficiency of water use. Journal of Irrigation and Drainage Division of the American Society of Civil Engineers 91 (IR 1), pp 69-77.

Bastiaanssen WGM (1995) Regionalization of surface flux densities and moisture indicators in composite terrain, A remote sensing approach under clear skies in Mediterranean climates. Report 109, Agricultural Research Department, Wageningen, The Netherlands.

Bastiaanssen WGM, Ahmad MD, Chemin Y (2001) Satellite surveillance of water use across the Indus Basin. Journal for Water Resources Research (Accepted)

Bastiaanssen WGM, Menenti M, Feddes RA, Holtslag AAM (1998) A remote sensing surface energy balance algorithm for land (SEBAL): 1. Formulation. Journal of Hydrology, 212/213, pp198-212.

Bastiaanssen WGM, Chemin Y, Ahmad MD, Ali S, Asif S and Prathapar SA (1999) Patterns of crop evaporation in the Indus Basin recognized from NOAA-AVHRR satellite. 17th International Conference on Irrigation and Drainage (ICID), Lausanne, Switzerland, September 1999, 9p.

Bastiaanssen WGM, Sakthivadivel R, and Van Dellen A (1999) Spatially delineating actual and relative evapotranspiration from remote sensing to assist spatial modeling of non-point source pollutants. Assessment of non-point source pollutants, American Geophysical Union, Geophysical Monograph 108, pp 179-196.

Brutsaert W (1982) Evaporation into the atmosphere, theory, history and applications, Dordrecht, 229 p.

Brutsaert W and Sugita M (1992) Application of self-preservation in the diurnal evolution of the surface energy budget to determine daily evaporation. J. of Geophysical Res., 97, D17: 18,322-18,377.

Bussieres N and Goita K (1997) Evaluation of strategies to deal with cloudy situation in satellite evapotranspiration algorithm. Proceedings of the Third International Workshop NHRI Symposium 17, 16-18 October 1996, NASA, Goodard Space Flight Center, Greenbelt, Maryland, USA, pp 33-43

Castaẻda AR and Bhuiyan SI (1993) Sediment pollution in a gravity irrigation system and its effects on rice production. Agriculture, Ecosystems and Environment, 45, pp 195-202.

Carlson TN and Buffmen MJ (1989) On estimating total daily evapotranspiration from remote surface temperature measurements, Remote Sensing of Environments, 29, pp 197-207.

Carlson TN, Taconet O, Vidal A, Gillies RR, Olioso A and Humes K (1995) An overview of the workshop on thermal remote sensing held at La Londe Les Maures, France, September 20-24, 1993, Agriculture and Forest Meteorology, 77, pp141-151.

Chandrapala L and Wimalasuriya M (2001) Satellite measurements supplemented with meteorological data to operationally estimate actual evapotranspiration over Sri Lanka. Special issue, Agricultural Water Management. Submitted.

Chemin Y and Alexandridis T (2001) Improving spatial resolution of ET seasonal for irrigated rice in Zhanghe, China. 22nd Asian Conference of Remote Sensing, November 5-9, 2001, National University of Singapore, Singapore, 6p.

Chemin Y and Alexandridis T (2001) Using remote sensing for deriving water productivity indicators in low data environments. A case study for different irrigation unit sizes in Zhanghe Irrigation District, China.

Choudhury BJ (1994) Synergism of multispectral satellite observations for estimating regional land surface evaporation. Remote Sensing of Environment 49, pp 264-274.

Department of Agriculture (2002) Metro Manila, Philippines http://www.da.gov.ph/welcome.html

De Bruin HAR, Nieveen JP, De Wekker SFJ and Heusinkveld BG (1996) Large Aperture Scintillometry over a 4.8 km path for measuring areally-average sensible heat flux: a case study. Proceedings of the 22nd AMS Symposium on Agricultural and Forest Meteorology, 28-January-2 February, Georgia, USA.

Diak G and MS Whipple (1993) Improvements to models and methods for evaluating land-surface energy balance and effective roughness using radiosonde reports and satellite measured skin temperature data, Agriculture and Forest Meteorology 65, pp 21-45

Dong B, Loeve R, Li YH, Chen CD, Deng L and Molden D (2001) Water productivity in Zhanghe Irrigation System: Issues of scale. In: Barker R, Loeve R, Li YH, Tuong TP (Eds.). 2001. Water-saving irrigation for rice: Proceedings of an International Workshop held in Wuhan, China, 23-25 March 2001, Colombo, Sri Lanka. IWMI, pp 97-115.

DeDatta SK, Krupp HK, Alvarez EI and Modgal, SC (1973) Water management in the Philippines, Irrigation system: Research and Operations, pp 1-8

Doorenbos J and Pruitt WO (1977) Guidelines for Predicting Crop Water Requirements. FAO Irrigation and Drainage Paper No. 24, Rome, Italy.

Droogers P (2000) Estimating actual evapotranspiration using a detailed agro-hydrological model. Journal of Hydrology 229, Elsevier, Netherlands, pp 50-58

Farah HO (2001) Estimation of regional evaporation under different weather conditions from satellite and meteorological data: A case study of the Navaisha Basin. Doctoral thesis Wageningen University and ITC, CIP-Data Koninklijke Bibliotheek, Den Haag, 170p.

Gillespie A, Rokugawa S, Matsunaga T, Cothern JS, Hook S, and Kahle AB (1998) A temperature and emissivity separation algorithm for Advanced Spaceborne Thermal Emission and Reflection Radiometer (ASTER) images. IEEE Transcations on Geoscience and Remote Sensing 36,1998, pp 1113-1126.

Gleick PH (1993) Water crisis: a guide to the world's fresh water resources. Pacific Institute for Studies in Development, Environment, and Security. Stockholm Environment Institute. Oxford University Press. New York, 473 p.

Granger RJ (1997) Comparison of surface and satellite-derived estimates of evapotranspiration using a feedback algorithm. Applications of remote sensing in hydrology: Proceedings of the Third International Workshop NHRI Symposium 17, 16-18 October 1996, NASA, Goodard Space Flight Center, Greenbelt, Maryland, USA.

Guerra LC, Bhuiyan SI, Tuong TP and Barker R (1998) Producing more rice with less water from irrigated systems. SWIM Paper 5. IWMI-IRRI, Colombo, Sri Lanka, 24 p.

Hafeez MM, Chemin Y, N Van De Giesen and Bouman BAM (2002) "Field evapotranspiration estimation in Central Luzon, Philippines, using different Sensors: Landsat 7 ETM+, TERRA MODIS and ASTER" Proceedings of joint conference on "Geospatial Theory, Processing, & Applications" organized by ISPRS/Canadian Institute of Geomatics Conference, Ottawa, Canada, 8-12 July 2002, 7p.

Hafeez MM and Chemin Y (2003) Evapotranspiration estimation using TERRA/ASTER sensor: A case study in District 1 of UPRIIS, Central Luzon, Philippines. Canadian Journal of Remote Sensing (in press).

Hossain SMI (2001) Ground water utilization for irrigation in the Upper Pumpanga river basin. Ph.D. thesis, Central Luzon State University, Munoz, Nueva Ecija, Philippines

IRRI (1997) Rice Almanac, second edition. International Rice Research Institute (IRRI), Los Baños, Philippines, 181 pp

IRRI (2001) Annual Report 2000-2001 Rice research: the way forward. International Rice Research Institute (IRRI), Los Banos, Philippines, 71 pp.

Jackson RD, Reginato RJ, and Idso SB (1977) Wheat canopy temperatures: a practical tool for evaluating water requirements Water Resources Research Journal, 13, pp 651-656

Jensen (1990) Evapotranspiration and irrigation water requirements, ASCE Manual Reports on Engineering Practice No. 70. New York: ASCE

Jha KP, Dinesh C and Challaiah (1981) Irrigation requirement of high yielding rice varieties grown on soils having shallow water table Indian Journal of Agricultural Sciences, 51, pp 732-737

Keller A, Keller J, and Seckler D (1996) Integrated water resources systems: Theory and policy implications. Research Report 3, Colombo, Sri Lanka: International Water Management Institute, 15 pp.

Klemm (1999) Water saving in rice cultivation. In assessment and orientation towards the 21st century, Proceedings of 19th session of the International Rice Commission, Cairo, Egypt, 7-9 September 1998. FAO, pp 110–117.

Kustas WP and Norman JM (1996) Use of remote sensing for evapotranspiration monitoring over land surfaces IAHS, Hydrological Sciences Journal, 41(4), pp 495-516.

Loeve R, Dong B, and Molden D (2002) Field level water savings in Zhanghe irrigation system and the impact on system level. In: Bouman, Hengsdijk, Hardy, Bindraban, Tuong, Lafitte and Ladha (Eds.), Water-Wise Rice Production, IRRI, Los Baños, Philippines (in prep).

Liang S, Strahler AH and Walthall CW (1999) Retrieval of land surface albedo from satellite observations: A simulation study. Journal of Applied Meteorology.

Lucero LC (1984) Improved project water management in irrigated rice. Ph.D. thesis, Utah State University, Logon, Utah, USA.

Maglinao AR (1992) Irrigation management for rice-based farming systems in the Philippines. Philippine Council for Agriculture, Forestry and Natural Resources Research and Development and International Rice Research Institute, Los Banos, Philippines.

Molden D (1997) Accounting for water use and productivity. SWIM Paper 1. Colombo, Sri Lanka: International Water Management Institute.

Molden D and Sakthivadivel R (1999) Water accounting to assess use and productivity of water. Water Resources Development 15, 55–71.

Moran MS, Clarke TR, Inoue Y and Vidal A (1994) Estimating crop water deficit using the relations between surface-air temperature and spectral vegetation index Remote Sensing of the Environment, 49(2), pp 246-263.

NIA (1977) Upper Pampanga River project Completion Report 1977. National Irrigation Administration (NIA), Manila, Philippines, 39 pp.

NIA (1996) Annual Report 1996. National Irrigation Administration (NIA), Manila, Philippines, 46 pp.

Palacios-Velez, E. (1994) Water Use efficiency in irrigation districts. In Efficient wateruse, Montevideo: UNESCO/ROSTLAC.

Pingali PL, Hossain M and Gerpacio RV (1997) Asian rice bowls; the returning crisis? CAB International, Oxon, UK (in association with IRRI, Los Baños, Philippines). 341 pp.

Petehercych S, Goodison B, Swaill V and Saulesleja A (1983) Clouds: A fundamental limitation to satellite remote sensing in the visible spectral region. Proceedings of Eighth Canadian Symposium on Remote Sensing. Sherbrooke, Quebec, 1983, pp 223-228

Postel S (1997) Last Oasis. Facing water scarcity. Norton and Company, New York, USA, 239 pp.

Ramos EP (1986) Evaluation of soil parameters for irrigation planning and design for upland crops. M.Sc. thesis, Central Luzon State University, Munoz, Nueva Ecija, Philippines.

Roerink GJ, Bastiaanssen WGM, Chambouleyron J and Menenti M (1997) Relating crop water consumption to irrigation water supply by remote sensing. Water Resources Management 11, pp 445-465

Rosegrant MW, Gonzales LA, Bouis HE and Sison JF (1986) Price and investment policies for food crop sector growth in the Philippines. International Food Policy Research Institute. Washington DC. Final report submitted to Asian Development Bank (ADB) for the project Study of food demand/supply prospect and related strategies for developing countries of ADB.

Rosegrant MW (1997) Water resources in the twenty-first century: challenges and implications for action. Food, Agriculture, and the Environment Discussion Paper 20. IFPRI, Washington D.C., USA, 27 pp.

Sattar MA (1992) Water management and technology adoption for direct seeded rice in an irrigation system. Ph.D. thesis, Central Luzon State University, Munoz, Nueva Ecija, Philippines.

Seckler D (1996) The new era of water resources management: From “dry” to “wet” water savings. Research Report 1, Colombo, Sri Lanka: International Water Management Institute, 15 pp.

Seguin B and Itier B (1983), Using midday surface temperature to estimate daily evaporation from satellite thermal IR data. International Journal of Remote Sensing, 4, pp 371-383

Sellers PJ, Heiser MD, and Hall FG (1992) Relationship between surface conductance and spectral vegetation indices at intermediate length scales. Journal of Geophysical Research 97(D17), pp 19033-19059

Shafique MS, Bukhari MS and Hafeez MM (1998) Development of a modified low-cost pitot tube for measuring pump discharges. International Water Management Institute (IWMI), Pakistan National Program, Lahore Pakistan. Research Report # 55, p 62

Solomon KH and Davidoff B (1999) Relating Unit and Sub-unit Irrigation Performance. American Society of Agricultural Engineers 42 (1), pp 115-122.

Tabbal DF, Bouman BAM, Bhuiyan SI, Sibayan Eb and Sattar MA (2002) On-farm strategies for reducing water input in irrigated rice; case studies in the Philippines. Agricultural Water Management, 56/2, pp 93-112.

Tasumi M, Bastiaanssen WGM, Allen RG (2000) Application of the SEBAL methodology for estimating consumptive use of water and stream flow depletion in the Bear River Basin of Idaho through Remote Sensing. Appendix C: A step-by-step guide to running SEBAL. EOSDIS Project Final Report, The Raytheon Systems Company and the University of Idaho, USA.

Timmermans WJ and Meijerink AMJ (1999) Remotely sensed actual evapotranspiration: implications for groundwater management in Botzwana. Journal of Applied Geohydrology 1(3/4), pp 222-233.

Tuong TP and Bouman BAM (2002) Rice production in water-scarce environments. To be published in proceedings of the Water productivity Workshop, 12-14 November 2001, IWMI, Sri Lanka.

Undan RC, Tabago JL and Ringor OF (1992) Water augmentation and drainage srudies in crop-diversified areas. Maglinao A.R. (Ed.) Irrigation management for rice-based farming systems in the Philippines. Los Baños, Laguna: Philippine Council for Agriculture, Forestry and Natural Resources Research and Development, 1992, 357 pages (Book series No.122).

Vidal A and Perrier A (1989) Analysis of a simplified relation used to estimate daily evapotranspiration from satellite thermal IR data. International Journal of Remote Sensing 10(8), pp 1327-1337.

Van Vuren Geritt (1993) Constraints in the use of irrigation efficiency coefficients. ICID Fifteenth Congress. The Hague. The Netherlands: International Commission on Irrigation and Drainage (ICID).

Van de Griend AA and Owe M (1993) On the relationship between thermal emissivity and the normalized difference vegetation index for natural surfaces International Journal of Remote Sensing 14(6), pp 1119-1131.

Wan, Z. 1999. MODIS Land-surface Temperature algorithm theoretical basis document (LST ATBD). University of California, Santa Barbara.

Wickham TH and Singh VP (1978) Water movement through wet soils. In: Soils and Rice. IRRI, Los Banos, Philippines, pp 337-358

Yudelman M (1993) Demand supply of foodstuffs up to 2050 with special reference to irrigation. Draft report prepared for the International Irrigation Management Institute, Colombo, Sri Lanka.

Zulu G, Toyota M, and Misawa S (1996) Characteristics of water reuse and its effects on paddy irrigation system water balance and the rice land ecosystem. Agricultural Water Management 31, pp 269-283.

APPENDIX

Table 1. The rating curve of inflow/outflow locations in District 1.

No	Location	Staff Gage Reading									Equation	R^2
		1	2	3	4	5	6	7	8	9		
1	T.o Lacub	50.00	57.00	38.00	45.00	61.50	46.00	25.00			Q=0.0045x- 0.1064	0.9325
2	Labut A	27.00	91.00	100.00	130.00	19.00					Q=0.0003x^2 + 0.0193x - 0.425	0.9934
3	D3 Ha	149.00	140.00	162.00	176.00	115.00					Q = 0.0002x2 - 0.0011x + 0.224	0.9912
	Hb	139.00	135.00	145.00	148.00	104.00						
4	Labut B	3.00	97.00	32.00	50.00	100.00	22.50				Q=0.0002x^2 + 0.0027x + 0.0157	0.9437
5	D4 Ha	250.00	170.00	222.00	234.00							
	Hb	170.00	150.00	150.00	180.00							
6	D5 Ha	165.00	210.00	200.00								
	Hb	150.00	190.00									
7	D.C. UP	10.00	257.50	30.00	233.00	160.50	192.00	217.00	250.00		Q=0.0003x^2 + 0.0113x + 0.287	0.8698
8	F-up Ha	187.00	200.00	195.00	173.00						Q = 0.0005x2 - 0.1002x + 5.3412	0.9417
	Hb	172.00	173.00	93.00	119.00							
9	F1 Ha	75.00	220.00	210.00	160.00							
	Hb		161.00	152.00	125.00							
10	F1a Ha	130.00	160.00	153.00	110.00							
	Hb	175.00	78.00	80.00	65.00							
11	SDA 2	66.00	6.00	44.00	104.00	94.00	132.00	158.00	170.00		Q=0.0002x^2 + 0.0639x + 0.0433	0.9526
12	1	12.00	102.50	51.00							Q = 0.0429x - 0.3919	0.9893
13	DC end	157.00	169.00	124.50	97.50	170.00	170.50	192.00			Q=0.0714x - 6.3605	0.9688
14	TRIS	37.00	144.00	116.50	131.00	46.00					Q = 0.0025x - 0.0146	0.9128
15	F3	73.00	53.00	15.00	25.50	76.00	82.00				Q=0.004x^1.2173	0.9259
16	F-mid	70.00	43.00	59.00	176.00	36.50	80.00	88.00			Q=0.0007x^2 - 0.0491x + 1.1506	0.986
17	F4	43.00	17.00	38.00	30.00	58.00	35.00	46.50			Q=0.009x - 0.0686	0.8746
18	F5-UP	41.00	18.00	29.00	35.00	31.50	48.00	55.00			Q=0.0103x - 0.0403	0.8329
19	F6	63.00	53.00	42.00	45.00	55.00	69.50				Q=0.0077x - 0.2667	0.9831
20	F down	70.00	55.00	67.00	81.50						Q = 0.0162x - 0.16	0.9232
21	Viernes A	45.00	59.00	21.00							Q = 0.0146x - 0.5317	0.9048
22	Basang H.	14.00	45.00	60.00	117.00	51.00					Q = 0.0122x - 0.06	0.9217
23	Tabacao	55.00	40.00	25.00	65.00	48.00	87.00				Q = 0.0004x2 - 0.0198x + 0.3215	0.9304
24	Tabacao X Ha	27.00	23.00	13.00								
	Hb	17.50	16.00	10.00								
25	P. Balbido	8.00	17.50	21.00	10.00	30.00	15.00				Q = 0.0033x - 0.0251	0.8239
26	Tagaytay	92.00	63.00	93.00	85.00	53.00	75.00	53.00	250.00	124.00	Q = 0.0193x - 1.1025	0.9346
27	Pantoc A	114.00	149.00	127.00	14.00						Q = 0.0005x^1.3177	0.944
28	Pantoc B	31.00	39.00	45.00	54.00	61.50					Q = 1E-07x^3.7288	0.9735
29	F-5 end	74.00	48.00	55.00							Q = 0.0026x - 0.0933	0.9681
30	De Leon C	150.00	173.00	120.50	135.00	205.00					Q = 0.0011x^2 - 0.1442x + 3.5061	1
31	Spillway Deleon	133.50	118.00	156.00	290.00	164.00					Q = 0.0005x2 - 0.0453x - 0.6047	0.9999
32	De Leon B	128.00	105.00	119.00	52.00	75.00					Q = 0.0108x - 0.5625	0.9797
33	A	61.50	6.00	99.00	20.00	80.00					Q = 0.0338x - 0.2196	0.9327
1	SG	42.0	43.0	32.0	25.0	38.0					Q = 0.0002x2 - 0.0098x + 0.1466	0.9944

No	Location	Staff Gage Reading									Equation	R^2
		1	2	3	4	5	6	7	8	9		
2	C2 Ha	No Flow										
	Hb											
3	SDA MC end	104.0	80.0	120.0	69.0	128.5	147.0				Q= 0.0004x^2 - 0.059x + 2.5301	0.9278
4	CASSA A Ha	36.0	57.0									
	Hb	38.0	59.0									
5	CASSA B Ha	33.0	52.0	48.0	65.0						Q= 0.0204x - 0.4176	0.744
	Hb	34.0	51.0	48.0	65.0							
6	SDA LAT.G	118.0	106.5	77.0	137.0	125.0	142.0	146.0			Q= 0.0001x^2 - 0.0102x + 0.2229	0.9753
7	OSMEÑA A Ha	81.0	72.0	75.0								
	Hb											
7a	OSMEÑA X Ha	31.0	21.5	35.0	33.0	totally blocked						
	Hb	16.0		32.0	43.0							
8	OSMEÑA B Ha	78.0	109.0	195.0	104.0	89.0					Q= 0.0013x + 0.0126	0.6173
	Hb	76.0	107.0	93.0	101.0	77.5						
9	JUNCTION Ha	78.0	97.0	105.0	105.0	91.0	100.0				Q= 0.002x - 0.0917	0.7446
	Hb	75.0	94.0	105.0	101.0	87.0	98.0					
10	C10 Ha	No Flow										
	Hb											
11	C11 Ha	17.0	19.0									
	Hb	17.0	19.0									
12	SDA LAT F1	101.0	88.0	41.0	16.0	70.0	107.0	97.0			Q= 0.0117x - 0.1384	0.9948
13	C13 Ha	No Flow										
	Hb											
14	C14 Ha	10.0	19.0	22.0	16.0						Q= 0.0002x^2 - 0.0016X+.0084	0.9937
	Hb	3.5	12.0	12.0	8.0							
14a	14a	15.0	20.0	9.0	20.0	12.0					Q = 0.0011x^2 - 0.02x + 0.1228	0.9814
15	SDA LAT F	83.0	60.0	79.0	69.0	43.0	86.0	92.0	101.0		Q= 0.0076x - 0.1855	0.9486
16	ILOG BALIWAG	130.0	13.0	173.5	213.0	47.0	98.5	135.0	138.0		Q= 0.0002x^2 + 0.0156x-0.4813	0.9862
17	C17 Ha	No Flow										
	Hb											
18	C18 Ha	No Flow										
	Hb											
19	C19 Ha	53.0	58.0									
	Hb	60.0	40.0									
20	C20 Ha	8.0	17.5	30.0								
	Hb	15.0	20.0	36.0								
21	SDA LAT B-5	28.0	15.0	48.0	67.0	33.0					Q= 0.00007x^2 + 0.0018x - 0.0239	0.9590
22	C22 Ha	27.0	39.0	21.0								
	Hb	38.0	39.0	26.0								
23	C23 Ha	14.5	41.0									
	Hb	25.0	58.0									
24	C24 Ha	44.0	68.0	40.0	52.0	55.5					Q= 0.0039x- 0.1476	0.9856
	Hb	44.0	78.5	57.0	62.0	62.0						
25	C25 Ha	14.5	43.0	42.0								
	Hb	25.0	46.0	41.0								
26	C26 Ha	No Flow										
	Hb											

No	Location	Staff Gage Reading									Equation	R^2
		1	2	3	4	5	6	7	8	9		
27	C27 Ha	No Flow	14.0									
	Hb		15.0									
28	C28 Ha	40.0	20.0									
	Hb	53.0	18.0									
29	C29 Ha	43.0	80.0	51.0	62.0							
	Hb	46.0	79.0	53.0	61.0							
30	C30 Ha	11.0										
	Hb	13.5										
31	SDA LAT B	75.0	28.0	63.0	115.0	42.0	128.0	106.0			Q = 0.0159x - 0.2036	0.9141
32	SDA LAT B-4	30.0	15.0	77.0	57.0	83.0	69.0				Q = 5E - 05x^2 + 0.0049x - 0.0701	0.9968
33	C33 Ha	No Flow										
	Hb											
34	BRIDGE 1	81.0	53.0	108.0	106.0	120.0					Q = 8E-05x^2 - 0.0059x + 0.222	0.9128
35	BRIDGE 2	59.0	65.0	72.0	80.0	87.0					Q = 0.0003x2 - 0.0283x + 0.894	0.8288
36	BRIDGE 3	60.0	82.0	200.5	23.0	135.0	94.0				Q = 0.1324x - 2.0243	0.984
37	BRIDGE 4											
38	C38 Ha	8.5										
	Hb	8.0										
39	C39 Ha	No Flow										
	Hb											
40	SDA LAT A-X	40.0	25.0	75.5	17.5	84.0	50.0	98.0			Q=0.0001x^2 - 0.0015x + 0.0034	0.9921
40a	SDA LAT A-X1	20.0	15.0	10.0	22.5	27.5						
40b	SDA LAT A-X2	20.0	17.0	14.0	10.0	12.0					Q=0.007x - 0.0018	0.9593
41	SDA LAT A	36.0	17.0									
42	C42 Ha	40.0										
	Hb											
43	C43 Ha	No Flow										
	Hb											
44	LOMBOY	42.0	74.0	53.0	5.0	125.0	108.0				Q = 0.0004x^2 - 0.0057x - 0.0049	0.9992
45	BALOC	150.0	112.0	160.0	243.5	179.0	20.0				Q = 0.0004x^2 - 0.0291x - 0.474	0.9812
46	SDA SPILLWAY	50.0	120.0	252.0	143.0	170.0	195.0	18.0	36.0		Q = 0.000009x^2.5269	0.9396
47	SDA MC	164.0	58.0	45.0	92.0	160.0	118.0	16.0	166.0		Q = 0.0785x - 0.5393	0.9735
48	LAT G-3B	53.0	27.0	60.0	47.0	67.0	40.0				Q = 0.0002x^2 - 0.0133x + 0.2492	0.9113
49	LAT G-2	45.0	14.5	77.0	57.0	53.0	70.0	25.0			Q = 0.0107x - 0.1511	0.9781
50	BOUNDARY BACAL I & II	30.0	24.0	36.0	32.0	18.0					Q = 0.0119x - 0.2445	0.9719
51	BACAL A	42.0	31.0	36.0	18.0	20.0	62.5				Q = 0.0002x^2 - 0.0026x + 0.0233	0.9993
52	BACAL B	41.0	45.0	50.0	53.0	57.0					Q = 0.0088x - 0.3078	0.9975
53	LAT. G	39.0	25.0	32.5	45.0	35.0	55.0				Q = 0.0006x^2 - 0.0251x + 0.5567	0.8255
54	BANTUG A	25.0	35.0									
55	BANTUG B	20.0	16.0	22.0	18.0						Q = 0.0117x - 0.1304	0.8194
56	INC. BEFORE	20.0	15.0									
57	INC. AFTER	15.0	11.5									
58	DEBABUYAN C.	35.0	19.0	28.0							Q = 0.0076x - 0.0912	0.9932
59	LAT FX - A	64.0	44.0	51.0	73.0	86.0	15.0				Q = 0.0145x - 0.3936	0.9007
60	LAT FX - B											
61	SDA LAT. A Ha	80.0	85.0									

No	Location	Staff Gage Reading									Equation	R^2
		1	2	3	4	5	6	7	8	9		
	Hb	79.0	90.0									
62	SDA MC. MID	16.0	28.0	50.0	91.0	114.0	63.5	130.0			Q = 0.0901x - 0.938	0.9721
63	SDA LAT B Ha	69.0										
	Hb	No flow										
64	TABON PARE	31.0	36.0	68.0	132.0	24.0					Q = 0.0001x^2 - 0.0042x + 0.0685	1
65	PAJO	70.0	63.0	154.0	101.0	81.0					Q = 0.0001x^2 - 0.0102x + 0.3153	0.9924
66	LABONG SDA MC	74.0	57.0	96.0	128.0	138.0	146.0				Q = 0.0003x^2 - 0.0066x - 0.0708	0.9598
67	LAT F-Xc	25.0	18.0	40.0	30.0	9.0	36.0	27.0			Q = 0.0002x^2 + 0.0012x - 0.02	0.9574
68	LAT FX - D	20.0	16.0	22.0								
Z1	Farm Ditch Ha	32.0	41.0	46.0	50.0						$Q = 0.0004h^2-0.0128h+0.0904$	0.7736
	Hb	22.0	31.0	36.0	40.0							
Z2	Farm Ditch Ha	21.0	33.0	35.0	35.0	37.0					$Q = 0.00008h^2-0.0009h-0.0161$	0.9963
	Hb	1.5	13.0	15.0	15.0	17.0						
Z3	Farm Ditch Ha	29.0	30.5	34.0	35.0	39.0					$Q = 0.0001e^{0.2044h}$	0.9788
	Hb	28.0	30.0	32.0	33.0	38.0						
Z4A	Lateral B-4 S.G	46.0	50.3	58.0	60.0	63.5	80.5	84.8	90.0	94.5	$Q = 0.0001h^2-0.0095h+0.3289$	0.9639
Z4B	Lateral B-4 S.G	38.5	41.0	46.5	51.0	52.0	75.0	77.0	79.0	87.0	$Q = 0.00008h^2-0.0095h+0.1375$	0.9487
Z5	Farm Ditch S.G	11.0	23.5	27.0	32.0	33.5	34.5	42.5	43.00		$Q = 0.00001h^{2.3347}$	0.9535
Z6	Farm Ditch S.G	13.8	20.0	30.0	33.5	37.0	43.0				$Q = 0.00001h^{2.4908}$	0.9483
Z7	Farm Ditch Ha	46.0	51.0	58.0	63.0	70.0					Q = 0.0012h-0.0379	0.1138
	Hb	50.0	52.5	56.0	60.0	79.0						
Z8	Farm Ditch Ha	40.0	41.0	42.0							$Q = 0.000003h^{2.552}$	0.9853
	Hb	24.0	25.0	26.0								
Z9	Farm Ditch Ha	6.0	8.0	9.0	14.0	15.0	18.0	48.0			$Q = 0.0002h^2-0.0118h+0.1873$	0.9609
	Hb	6.5	8.0	8.0	14.0	15.5	18.5	48.0				
Z10	Farm Ditch S.G	8.5	14.0	20.5	21.5	25.0	27.0					0.3345
Z11	Farm Ditch S.G	18.5	23.5	24.5	33.5						$Q = 0.0001h^2+0.0064h+0.08$	0.9999
Z12	Farm Ditch S.G	14.0	17.5	20.3	14.0						$Q = 0.00005h^{1.9851}$	0.4682
Z13	Drainage S.G Ha	52.3	58.0	62.0	62.0	64.5	77.0				$Q = -0.000009h^2+0.0021h+0.0223$	1
	Hb	46.5	50.5	55.0	59.5	54.5	77.0					
Z14A	SD Canal S.G	20.0	44.3	53.0	77.5	97.0	99.0	108.5	114.0	142.0	$Q = 0.0056h^{1.464}$	0.9918
Z14B	SD Canal S.G	23.5	53.5	61.0	87.0	114.0	129.5	119.0	124.0	155.5	$Q = 0.0033h^{1.5539}$	0.9829
Z15	Farm Ditch S.G	21.3	27.5	33.0	36.5	42.0	46.0				$Q = 0.0001h^2-0.0033h+0.0367$	0.9944
Z16	Drainage Culvert H1a	20.0	27.0	27.0	30.0	33.5	40.0				$Q = 0.0001h^2-0.0164h+0.5519$	0.6552
	H1b	12.0	19.0	19.0	22.0	24.0	32.0					
	Drainage Culvert H2a	18.0	26.0	26.0	28.0	31.0	39.0					
	H2b	13.0	21.0	22.0	23.0	26.0	24.0					
	Drainage Culvert H3a	15.0	23.0	23.0	25.0	36.0	36.0					
	H3b	14.0	21.0	22.0	24.0	37.0	35.0					
Z17A	Farm Ditch S.G	19.0	24.5	29.0							$Q = -0.00007h^2 +0.0037h-0.0377$	0.65
Z17	Drain Ditch S.G	22.5	28.3	33.0	37.0	41.0	46.5	49.8	51.0		$Q = 0.00007h^2+0.0037h-0.0377$	0.751
Z18	Farm Ditch S.G	21.0	24.0	26.0	28.0	29.5	33.5	38.0			$Q = 0.0006h^2-0.0227h+0.2365$	0.9961
Z19	Farm Ditch S.G	3.5	6.5	6.8	9.0	11.0					$Q = 0.00004h^2 - 0.0004h+0.0021$	0.85
Z20	Farm Ditch S.G	7.0	11.0	16.5	20.0	23.0	27.0	31.0			$Q = 0.00008h^2 -0.002h+0.0198$	0.86
Z21	Farm Ditch S.G	5.5	8.0	10.5	12.0	14.8	17.5	20.0	67.0		$Q = -0.00002h^2 +0.0008h-0.0008$	0.88

No	Location	Staff Gage Reading									Equation	R^2
		1	2	3	4	5	6	7	8	9		
Z22	Drainage Creek S.G	29.0	30.5	39.5	48.0	53.0	79.5				$Q = 0.0002h^2-0.0104h+0.2098$	0.9974
Z22A	Drain F.Ditch S.G	9.3	12.5	15.0	17.0						$Q = 0.00001h^2 -0.0004h+0.0059$	0.9000
Z22B	Creek S.G	27.5	37.0	43.0	57.0	65.5					$Q = 0.00003h^{2.3518}$	0.8514
Z23	Drainage Culvert H1a	8.0	12.0	17.0	18.0	22.0	33.0				$Q = 0.00001h^{2.3139}$	0.5102
	H1b	15.0	15.0	20.0	26.0	30.0	41.0					
	Drainage Culvert H2a	13.0	9.0	14.0	25.0	27.0	39.0					
	H2b	12.0	12.0	22.0	24.0	24.0	38.0					
Z24	Creek S.G (2Culvert)	16.5	20.5	22.5	31.5	39.5	41.3	46.0	52.0		$Q = 0.00009h^2+0.0151h+0.203$	0.9767
Z25	Creek S.G (3Culvert)	39.0	42.0	46.5	55.0	61.3	68.5	71.3			$Q = 0.0002h^2-0.0115h+0.1821$	0.9965
Z26	Farm Ditch S.G	8.3	9.3	11.5	13.0						$Q = -0.0007h^2 +0.0162h-0.0853$	0.95
Z27	Farm Ditch S.G	4.0	9.5	11.0	12.5	16.5					$Q = 0.00001h^{2.8583}$	0.9787
Z28	PAJO Creek S.G	51.0	113.0	115.0	128.5	138.5					$Q = 0.005h^{1.1382}$	0.6577
Z29	Farm Ditch S.G	17.8	27.0	29.0	34.5	39.5	44.0				$Q = 0.000002h^{2.8438}$	0.7299
Z30	Lateral B-3 S.G	24.5	40.5	46.3	53.5	61.0	68.0	75.0			$Q = 0.0001h^{1.9198}$	0.9683
Z31	Drainage Canal S.G	26.5	33.0	40.0	55.0	67.8	75.0				$Q = 0.0001h^2-0.00264h+0.071$	0.9837
Z32	Farm Ditch S.G	12.5	22.5	27.0							No Equation	
Z33	Farm Ditch S.G	11.5	18.5	19.0	24.5	29.8					$Q = 0.0001h^2-0.0022h+0.0159$	0.9948
Z34	Farm Ditch S.G	19.5	28.5								No Equation	
Z35	Farm Ditch S.G	11.0	19.0	21.5							No Equation	
Z36	Farm Ditch S.G	25.5	27.5	32.0	33.0	36.5	37.0				$Q = 0.0000003h^{3.324}$	0.7314
Z37	Farm Ditch S.G	24.5	25.5	29.0	34.5						$Q = 0.0009h^2-0.0446h+0.5829$	0.9847
Z38	Farm Ditch S.G	27.5	29.5	32.0	36.5	39.0					No Equation	
Z39	Farm Ditch S.G Ha	31.5	37.0	38.0	39.0	42.0	43.5	44.5	46.0	46.8	$Q = 0.0003h^2-0.0203h+0.3149$	0.9837
	Farm Ditch S.G Hb	30.5	34.0	39.5	39.5							
Z40	Lateral B-5 S.G	22.0	32.0	45.3	50.3	78.0	85.0	102.0	117.0	119.5	$Q = 0.0003h^{1.7599}$	0.9245
Z41	SD Canal S.G	42.5	83.5	152.0	156.0	162.0	193.0				$Q = 0.1941e^{0.0211h}$	0.9862
Z42	SD Canal S.G	69.0	96.0	149.5	154.5	204.0	205.0	214.0	219.0		$Q = 0.0838e^{0.0187h}$	0.9338
Z43	Creek S.G	11.0	20.5	31.5	35.8	49.0					$Q = 0.000004h^{2.8774}$	0.95
Z44	Lateral E-X S.G	30.5	39.0	45.0	52.0	65.0	68.0				$Q = 0.0001h^2-0.0073h+0.1624$	0.9243
Z45	SWA Dam Outlet1 S.G	35.5	43.0	53.0	60.0	67.0	89.0				$Q = 0.0001h^2-0.0069h+0.1957$	0.964
Z46	SWA Dam Outlet2 S.G	55.0	59.8	65.0	71.5							
Z47	SWA Dam Outlet3 S.G	29.5	43.0	49.8	52.8	54.5	62.0	69.0			$Q = 0.000002h^{2.7677}$	0.9625
Z48	Santa Rita Dam S.G	24.0	111.0	119.0	124.5	130.5					$Q = 0.0016h^{1.5354}$	0.9956
Z49	Buasao Dam S.G	102.5	124.0	138.5	140.0						$Q = 0.0006h^2-0.1401h+8.2002$	0.956

Figure 1. Overflowing of Santo Domingo main Canal in SDA-C scale

Figure 2. Staff gauge calibration using a current meter in the irrigation system

Figure 3 Staff gauge installed for measuring water level in the canal

Figure 4 V-notch weirs for calibration of staff gauges along the small canals/creeks

Figure 5. Meter-stick technique for measuring water level in small farm ditches with circular culverts

Figure 6. Pitot tube for calibration of the actual pump discharges.

This work is dedicated to my father; Hafeez Ahmad Choudhary who always encouraged me to pursue Doctoral degree since I was studying in high school

ACKNOWLEDGEMENT

I would like to thank the following people and organizations whose invaluable help and assistance have made the completion of this study possible:

My former supervisors at International Water Management Institute (IWMI) Pakistan, Prof. G.V. Skogerboe, Dr. M. S. Shafique, and Dr. S. Ejaz for recommending me for the doctoral study at ZEF. Dr. M. Latif, Director of Centre of Excellence in Water Resources Engineering (CEWRE) Pakistan, and Mr. Gul Muhammad Shah, Regional Director of Pakistan Council of Research in Water Resources (PCRWR), for their help and recommendation to pursue the Ph.D. study at ZEF;

Prof. Dr. Helmut Eggers, my first supervisor, for his encouragement, perpetual guidance, thoughtful suggestions and constructive criticism during the entire dissertation period;

Prof. Dr. Paul Vlek, my second supervisor, for sharing his ideas on the study, providing generous support to pursue trainings for professional development and for ensuring that I finish each phase of research and writing-up according to the schedule;

Dr. Nick van de Giesen, my tutor at ZEF, for all his unselfish assistance on any matter but most especially for the regular guidance on my dissertation. His ideas during data collection, data analysis and write-up enabled me to refine my work. His continual willingness to listen, discuss and render critical judgments helped me to produce this dissertation in its present shape;

Dr. Bas Bouman of IRRI, my supervisor in the Philippines, for giving valuable technical, administrative and professional advice, especially during my field work in the Philippines. He was a constant source of inspiration and encouragement throughout my research;

The International Rice Research Institute (IRRI) for giving me the opportunity to conduct my field work, with its staff (Crop Soil and Water Division) support and facilities. Mr. Doming Tabbal, Dr. Ruben Lampayan, Mr. Lucio Caramihan, Ms. Liezzel Llorca and Ms. Lou Herrero for their technical support during data collection, for the enjoyable discussions and for the friendship;

Mr. Yan Chemin, for sharing his ideas in the applications of remote sensing for hydrology. His help in solving SEBAL algorithm problems for different sensors through electronic messages is highly appreciated;

Dr. Rodolfo Undan, President of Central Luzon State University (CLSU) in Munoz, for providing me with house in the university campus. Staff of engineering faculty of CLSU for providing office space during the field data collection. Mr. Jimmy Quilang of Phil Rice, for his cooperation in meteorological data collection for remote sensing analysis. National Irrigation Administration (NIA) staff of District 1 for their help and kind cooperation during the field data collection;

Mr. Jan Friesen and Mr. Jens Liebe of ZEF, for their support in purchasing meteorological instruments. Dr. Mathias Brown of ZFL, for his friendly cooperation and ever welcoming help in solving remote sensing software problems. Dr. Günther Manske and Ms. Hanna Peters of ZEF-doctoral program, for their kind assistance during the last 3 years;

Mr. Ian Makin, Director of IWMI Sri Lanka, for his help in building database for the study area, and his cooperation during my stay in IWMI Sri Lanka. Dr. Hugh Turral of IWMI for sharing a part of vegetation dataset;

Ms. Margaret Jend for the quick and careful editing of this thesis;

Mr. Paul Beder, Dr. Altaf Bhatti, Mr. Fumitisho Ishino, Dr. Arif & family, Dr. Shamsal Alam & family, Mr. Hameed Solangi, Dr. Faiz Ahmad, Dr. Zahid Hafeez, and Dr. Jauhar Ali & family for the camaraderie and friendship during my stay in the Philippines;

My ZEF colleagues, especially Dr. Li Zhaohua, Dr. Rahayu Widyastuti, Mr. Tadasse Gole, Dr. Kaizzi Kayuki, and Ms. Racquel Lopez, for the memorable happy times during the daily coffee and lunch breaks;

Dr. W. Jehangir, Dr. M. Aslam, and Mr. N. H. Bukhari, my former colleagues at IWMI-Pakistan, for their help, and guidance throughout my job at IWMI-Pakistan;

My parents, brothers and sisters for their unconditional love and never-ending prayers during the period of my studies. Their moral support was always a continuous source of inspiration for me. I could not achieve my desire to finish Ph.D. without their kindness and help; and

Ms. Maria C. Carambas, for the caring, love, patience, valuable help and moral support I badly needed especially during the critical write-up stage of my dissertation. This work would never be realized without her presence in Bonn and continuous encouragement.